NTNU – Trondheim
Norwegian University of
Science and Technology

Removal of boron from silicon by slag treatment and by evaporation of boron from slag in hydrogen atmosphere

Helene Bjerke

Chemical Engineering and Biotechnology
Submission date: June 2012
Supervisor: Merete Tangstad, IMTE

Norwegian University of Science and Technology
Department of Materials Science and Engineering

Declaration

I declare that the work has been performed independently and in accordance with the rules and regulations of the Norwegian University of Science and Technology (NTNU).

Helene Bjerke

Trondheim, June 15th 2012

Preface

This Master Thesis has been carried out at the Department of Material Science and Engineering, NTNU, during the spring 2012. Several persons have contributed to the project, and I wish to express my sincere gratitude to:

- My supervisor professor Merete Tangstad who introduced me for the research group and solar cell material science. She has been a very proficient teacher showing a great enthusiasm to my work. I have learned a lot about research on silicon refining, and the process of performing a scientific report. It has been a valuable learning experience to work with her.

- Research Fellow Lars Klemet Jakobsson for the many instructive discussions during the project and useful advices during laboratory work.

- Trine Naalsund Andreassen for valuable help with the ICP-MS analysis.

- Delphine Leroy for assistance and support with the laboratory equipment.

Trondheim, June 2012
Helene Bjerke

Abstract

Background and objective: Removal of boron is one of the main challenges in the purification of metallurgical grade silicon (MG-Si) for solar cells and a simple low cost method is therefore needed. Boron removal by slag treatment is today regarded as the most promising method, but the efficiency of the refining method is relatively low. Slag refining as a method for boron removal can be improved by optimization of the slag composition by changing the components and/or the composition of the slag. Another method for improving the slag refining efficiency is to remove boron containing species from the slag by evaporation. The aim of this work is to study the refining properties of the Al_2O_3-MgO-SiO_2 slag and the CaO-SiO_2-TiO_2 slag, respectively. Furthermore, the possibility of evaporating boron from a CaO-SiO_2 slag when refined in a hydrogen containing atmosphere will be investigated.

Methods: In all, 12 experiments were performed at 1600˚C for determination of the distribution- and mass transfer coefficient of boron in the Al_2O_3-MgO-SiO_2 and CaO-SiO_2-TiO_2 slag, respectively. In the study of boron evaporation from CaO-SiO_2 slag in hydrogen atmosphere 14 experiments were performed. Boron evaporation was investigated in the temperature range 1500-1600˚C, the refining time was 0-6 hours and the slag/silicon mass ratio was varied between 0.25 and 1.5.

Results: The distribution- and mass transfer coefficient of boron in the Al_2O_3-MgO-SiO_2 (29%-23%-48%) slag was found to be 1.9 and $2.3x10^{-6}$ m/s, respectively. The amount of TiO_2 in the CaO-SiO_2-TiO_2 slag was found to rapidly decrease due to reduction of TiO_2 by Si. The distribution- and mass transfer coefficients found for the system were therefore not the same as for the original system. A decrease in the boron content in the slag was observed with increasing refining time in a hydrogen atmosphere at 1600˚C. This indicated that boron evaporated from the system, but the evaporation rate was found to be low. Temperature was not found to significantly influence the evaporation rate of boron in the temperature range 1500-1600˚C. When varying the slag/silicon mass ratio, a considerable increase in the refining efficiency compared to conventional slag refining was observed for the lower slag/silicon mass ratios. The effect diminished for the higher slag/silicon mass ratios.

Conclusion: The kinetic and thermodynamic properties of the Al_2O_3-MgO-SiO_2 slag evaluated in this thesis were shown to be in the same range as comparable slags in previous studies. In the CaO-SiO_2-TiO_2 slag most of the TiO_2 was reduced during the refining process which makes it difficult to use this compound as a part of a slag for refining of silicon. When slag refining was performed in a hydrogen atmosphere the refining efficiency compared to conventional slag refining was shown to increase.

Sammendrag

Bakgrunn og formål: En av hovedutfordringene innen oppgradering av metallurgisk silisium til solcelle silisium er å fjerne tilstrekkelige mengder bor. En av de mest lovende metodene er i dag å fjerne bor ved bruk av slagg, men effektiviteten til raffineringsmetoden er relativt dårlig. Slagg raffinering kan forbedres ved å endre komponentene og/eller sammensetningen til slaggen. En annen metode for å øke effektiviteten er å fordampe bor fra slaggen. Målet med denne oppgaven er å undersøke raffineringsegenskapene til slagg bestående av henholdsvis Al_2O_3-MgO-SiO_2 og CaO-SiO_2-TiO_2. Videre vil det bli undersøkt om bor kan fordampes fra CaO-SiO_2 slagg når raffineringsprosessen blir utført i hydrogen atmosfære.
Metoder: Til sammen ble det utført 12 forsøk ved 1600˚C for å bestemme fordelings- og masseoverføringskoeffisienten til bor i henholdsvis Al_2O_3-MgO-SiO_2 and CaO-SiO_2-TiO_2 slagg. Fordampning av bor fra CaO-SiO_2 slagg ble undersøkt med til sammen 14 forsøk. Fordampning ble undersøkt i temperaturområdet 1500-1600˚C, raffineringstiden var 0-6 timer og slagg/silisium masse ratioen ble variert mellom 0.25 og 1.5.
Resultater: Fordelings- og masseoverføringskoeffisienten til bor i Al_2O_3-MgO-SiO_2 (29%-23%-48%) slaggen viste seg å være henholdsvis 1.9 og $2.3x10^{-6}$ m/s. Mesteparten av TiO_2 i CaO-SiO_2-TiO_2 slaggen reagerte med silisium og ble redusert. Fordelings- og masseoverføringskoeffisientene som ble funnet for systemet var derfor forskjellig fra koeffisientene i det opprinnelige systemet. Det ble observert en avtagende mengde bor i slaggen med økende raffineringstid for raffinering i hydrogen atmosfære ved 1600˚C. Dette indikerte at bor hadde fordampet, men fordampningshastigheten var lav. Det ble ikke funnet noen signifikante forskjeller i fordampningshastigheten av bor fra slagg i temperaturområdet 1500-1600˚C. Der mengden slagg var liten i forhold til silisium ble det funnet en betydelig bedring i raffineringseffekten sammenlignet med tradisjonell slagg raffinering. Denne effekten avtok for økende mengde slagg i forhold til silisium.
Konklusjon: De kinetiske og termodynamiske egenskapene til Al_2O_3-MgO-SiO_2 slaggen i denne studien viste seg å være i samme område som liknende systemer undersøkt i tidligere studier. For CaO-SiO_2-TiO_2 slagg vil mesteparten av TiO_2 reduseres under raffineringsprosessen noe som gjør det vanskelig å benytte denne komponenten som en del av slagg for raffinering av silisium. For slagg raffinering utført i hydrogen atmosfære ble det funnet en økning i raffineringseffekten sammenlignet med tradisjonell slagg raffinering.

Table of contents

Nomenclature

P_i	Partial pressure of i
G	Gibbs energy
Q	Reaction coefficient
K	Equilibrium constant
a_i	Activity of i
η_0	Viscosity at any reference temperature
E_η	Activation energy for viscous flow.
η_e	Effective viscosity
L_M	Distribution coefficient
γ_i	Activity coefficient of i
ΔG^0	Standard Gibbs energy change
R	Gas constant
T	Temperature (measured in Kelvin)
Q	Reaction quotient
Ø	Volume fraction of solid particles
T_m	Melting temperature
σ	Surface tension
θ	Contact angle
S	Spreading coefficient
J	Flux
D	Diffusion coefficient
μ	(dynamic) Viscosity
r_B	Effective radius of boron in the metal
k_B	Boltzmann constant
$\dot{n}$	Molar flux (of boron)
B	Basicity
E	Activation energy
L_B	Distribution coefficient of boron
(%B)	Concentration of boron in the bulk slag
[%B]	Concentration of boron in the bulk metal
ρ	Density
n_i	Evaporation rate of i
N_i	Concentration of i in bulk liquid metal
A	Area
V	Volume
γ_i^0	Activity coefficient of i at infinite dilution
X_i	Molar fraction of i
k	Mass transfer coefficient

ε_j^i	First order interaction coefficient
ρ_j^i	Second order interaction coefficient
RSD	Relative standard deviation
ICP-MS	Inductively Coupled Plasma Mass Spectrometry
XRF	X-ray fluorescence

List of figures

List of tables

1. Introduction

The importance of solar energy is assumed to increase substantially in the years ahead due to the increase in the energy prices and as a result of the increased awareness set to the global warming problem. In recent years the solar industry has expanded worldwide, and in the fast growing Asian countries in particular, but the costs of producing solar cells are still too high to compete with low cost energy sources. New advances in the production of solar cell feedstock have made it possible to use relatively cheap metallurgical grade silicon (MG-Si) as a starting material for making solar grade silicon (SoG-Si), as an alternative to the traditional Siemens process [1]. Refining of MG-Si has been proven to be cheaper and less energy consuming than the former process, but proper methods for removal of impurities are required to maintain the solar cell efficiency. The boron content in MG-Si range from 5-70 mass ppm, while a boron content below 0.3 mass ppm is required for SoG-Si. Since boron is used as a dopant to control the conductivity of a solar cell it is of major importance to control the concentration of this element. However, efficient boron removal has been shown to be one of the greatest challenges in the refining of MG-Si for solar cells [2].

One of the most promising methods for boron removal from MG-Si today is by slag treatment. With this method boron is oxidized and extracted from silicon by a second phase; this phase is later removed from the silicon melt. Since the efficiency of the slags tried so far is relatively low, large amounts of slag are required for boron removal and the total costs of the refining process are high. The amount of boron extracted from silicon is determined by the composition and the properties of the slag used. One important purpose of this thesis is to study the distribution of boron between slag and silicon at equilibrium. The distribution of boron will be measured for different slags, and compared with previous studies. Another interesting method for improving the slag refining efficiency is to remove boron containing species from the slag by evaporation. By evaporating boron less slag will be needed for refining and a higher refining rate can be obtained. As a result, both the cost of the process as well as the waste slag after refining will be reduced. The possibility of evaporating boron containing species from the slag in a hydrogen atmosphere will also be investigated through this work. More specific, the aim of this work is to:

- Determine the distribution- and mass transfer coefficient of boron in the Al_2O_3-MgO-SiO_2 slag and the CaO-SiO_2-TiO_2 slag, respectively.
- Determine the activity coefficients of aluminum and magnesium in silicon at infinite dilution
- Investigate if boron can be evaporated from the CaO-SiO_2 slag when refined in an atmosphere containing 50% hydrogen, and investigate the effect of temperature on the boron evaporation rate
- Determine the evaporation rate of boron from the slag.
- Investigate the effect of hydrogen on a system containing both slag and metal.

2. Theory

Boron is one of the most demanding impurities to remove when making solar grade silicon. Because of the high segregation coefficient in silicon, leaching and directional solidification is not suitable for removal of boron. Furthermore, the vapor pressure of elemental boron is not high enough to be removed by vaporization. One solution is to remove boron by plasma refining, but this method requires a large initial investment for the plasma equipment and operation [3]. Slag refining has shown to be a proper method for boron removal, but improvements are desired. In this report two ways of improving the method are discussed;

1. Optimization of the slag composition:
In slag refining boron is distributed between slag and silicon until equilibrium is achieved. By changing the components and/or the composition of the slag more boron can possibly be extracted by the slag.

2. Evaporation of boron from the slag:
Slag refining as a method for boron removal can be improved by removing oxidized boron from the slag through an evaporation process. The evaporation process is illustrated in Figure 2.1 for a liquid slag. Oxidized boron is transported through the slag phase, transferred through the boundary layer and evaporated at the interphase between slag and gas. As long as boron is removed from the slag through evaporation, more boron will be transported from silicon to slag since the system aims for equilibrium between the two phases.

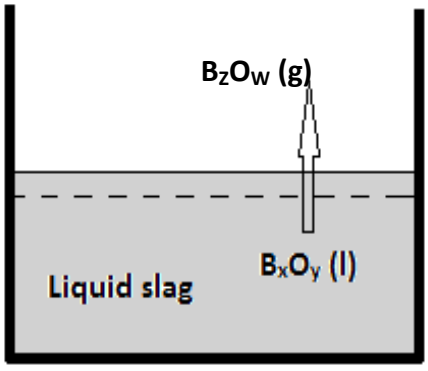

Figure 2.1: Evaporation of boron from slag

In the first part of this chapter general slag refining is described as it is used in the industry today, that is, no evaporation is involved in the process. In the second part general theory of vacuum refining is presented. While the third part focuses on combining these two refining techniques to produce a more efficient and cheaper method for removal of boron from solar grade silicon.

2.1 Slag refining

Slag refining is a process involving oxidation and absorption of impurities from the molten metal to a second slag phase [2]. This slag phase needs to be easy separable from the metal and it is important that it do not supply impurities to the silicon that cannot be removed at a later stage. The slag refining methods used in the silicon industry today are based on oxidation of impurities, and further absorption into a slag, this is shown in Figure 2.2. Slag can be both lighter and heavier than the silicon, depending on the slag composition. The slag refining process will not take place unless the species formed are more stable in the slag phase than in the silicon phase. Slag refining in the solar industry is mainly focused on the removal of boron. This is due to difficulties in removal of boron by other established refining processes.

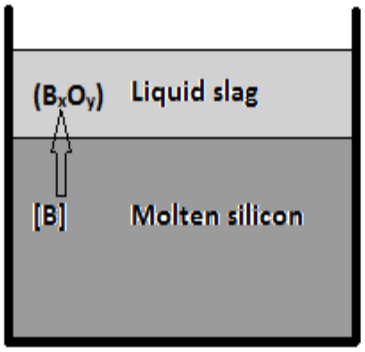

Figure 2.2: Slag purification of silicon

The effectiveness of a slag to extract impurities is determined by the thermodynamics and the kinetics of the system. The thermodynamics determines the potential of a slag to remove impurities and can be evaluated by the distribution coefficient given by Equation (2.1):

$$L_M = \frac{(\%M)}{[\%M]} \tag{2.1}$$

Where *(%M)* represents the concentration of impurity M in the slag phase, and *[%M]* is the concentration of the impurity in the molten silicon. The distribution coefficient should be as high as possible to minimize the amount of slag needed for refining, and thus the cost. Typical values of the distribution coefficient of boron range between 1 and 2 which means that large amounts of slag are needed to refine silicon. The kinetics determines the time for equilibrium to be reached, and is of major importance for large scale production [2].

2.1.1 Thermodynamics

As previously mentioned, the amount of slag should be as small as possible to minimize the cost of the refining process. To evaluate the ability of a slag to extract impurities the equilibrium constant should be considered, from this we can derive an expression for the distribution coefficient of boron (L_B). For a reaction, the change in Gibbs energy is given by Equation (2.2):

$$\Delta G = \Delta G^0 + RTlnQ \quad (2.2)$$

Here ΔG^0 represents the standard Gibbs energy for the reaction, R is the gas constant, T is the temperature measured in Kelvin, and Q is the reaction quotient. For a system in equilibrium $\Delta G=0$ and the equilibrium constant, K, can be expressed as

$$K = exp\left(\frac{-\Delta G^0}{RT}\right) \quad (2.3)$$

When the system has reached equilibrium no more purification will take place. The equilibrium composition is dependent on the temperature as can be seen in Equation (2.3).

The oxidation reaction of boron at the interface between metal and slag can be given by Equation (2.4):

$$2[B] + \frac{3}{2}O_2 = (B_2O_3) \quad (2.4)$$

The parentheses denote an oxide in the slag phase, while the brackets denote dissolved element in the metal phase. For a slag containing silica, the oxygen in Equation (2.4) can be provided by the reaction in Equation (2.5):

$$(SiO_2) = Si + O_2 \quad (2.5)$$

Equation (2.4) and (2.5) can be combined given the same oxygen partial pressure or if they both are at local equilibrium at the interface, giving Equation (2.6):

$$\frac{3}{4}(SiO_2) + [B] = (BO_{1.5}) + \frac{3}{4}Si \quad (2.6)$$

The equilibrium constant for this reaction can be defined by the activities, a, of the components:

$$K = \frac{a_{BO_{1.5}} a_{Si}^{3/4}}{a_{SiO_2}^{3/4} a_B} \quad (2.7)$$

For a liquid this activity can be expressed by the molar fraction of the respective substances, x_i, and the activity coefficient, γ_i:

$$a_i = \gamma_i x_i \quad (2.8)$$

With this inserted in Equation (2.7) we get:

$$K = \left(\frac{a_{Si}}{a_{SiO_2}}\right)^{3/4} * \frac{\gamma_{BO_{1.5}} x_{BO_{1.5}}}{\gamma_B x_B} \quad (2.9)$$

Due to the very low concentration of boron in molten silicon, the activity of silicon, a_{Si}, is assumed to be unity. For boron, the distribution coefficient given by Equation (2.1), can be rewritten into Equation (2.10). In this equation $k_{\%\rightarrow x}$ is a constant factor for conversion from mass percentage to molar fraction.

$$L_B = \frac{x_{BO_{1.5}}}{x_B} k_{\%\rightarrow x} \quad (2.10)$$

With this inserted into Equation (2.9), an expression for L_B is obtained:

$$L_B = \frac{K \gamma_B a_{SiO_2}^{3/4}}{\gamma_{BO_{1.5}}} k_{\%\rightarrow x} \quad (2.11)$$

From Equation (2.11) we can see that the distribution coefficient of boron is dependent on the temperature, slag composition and metallic impurities in the melt [2].

In Figure 2.3 Ellingham's diagram is shown. The diagram shows the Gibbs energy change of oxides formation as a function of temperature, and can be used to predict the stability of an oxide. The elements lying bellow silicon in the diagram are more likely to be oxidized than silicon and therefore potential components of a slag. If the slag contains an oxide with much higher Gibbs energy of change for oxidation, it will be reduced by silicon and enter the metal phase. The diagram is a thermodynamic evaluation of the process, no considerations are taken on the reaction kinetics [2].

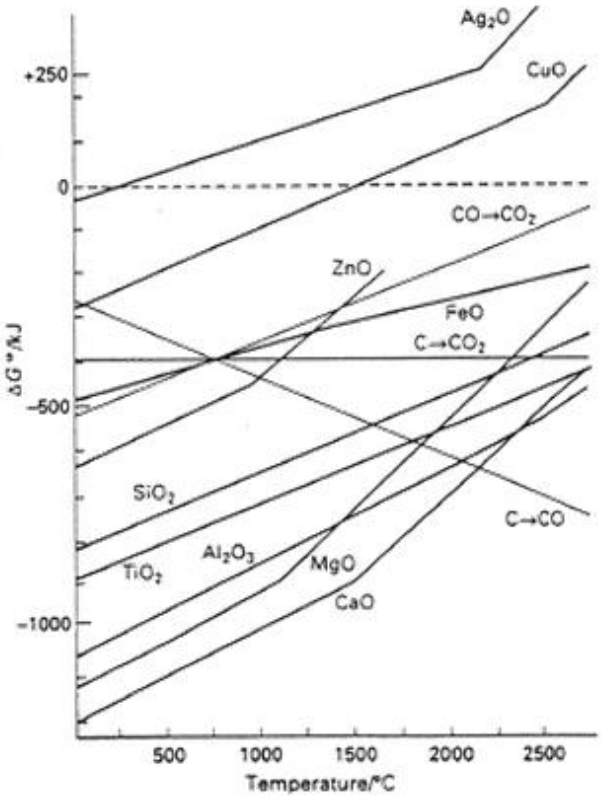

Figure 2.3: Ellingham's diagram [4]

2.1.2 Slag properties

In order to describe and understand the slag behavior in a refining process, properties of the slag must be considered. These properties, except for the activity coefficient, will affect the kinetics and not the thermodynamics of the system. In the following, the most important among them will be discussed. These are the viscosity, density, interfacial tension between slag and silicon melts and the diffusion coefficient of boron.

Viscosity

Viscosity is important for flow and mixing in the system. A lower viscosity will give better mixing properties and thinner boundary layers. As a result the rate of transportation of impurities from the bulk silicon to the bulk slag will be correspondingly increased. The viscosity decreases with increasing temperature and this dependency can be represented by an Arrhenius-type equation:

$$\eta = \eta_0 \exp\left(\frac{E_\eta}{RT}\right) \tag{2.12}$$

In Equation (2.12) η_0 represents the viscosity at some reference temperature and E_η represents the activation energy for viscous flow. Polymeric melts, including slags, will usually not obey Equation (2.12). The deviation is largest for acidic slags because they have the largest E_η values.

Acidic slags contain a large amount of network formers and have therefore high viscosity which results in low mass transfer rates. The dependency of the composition of the slag on the viscosity is shown Figure 2.4a and b. The figures show the viscosity diagrams for the Al_2O_3-MgO-SiO_2 slag and the CaO-SiO_2-TiO_2 slag, respectively, at 1600˚C [5].

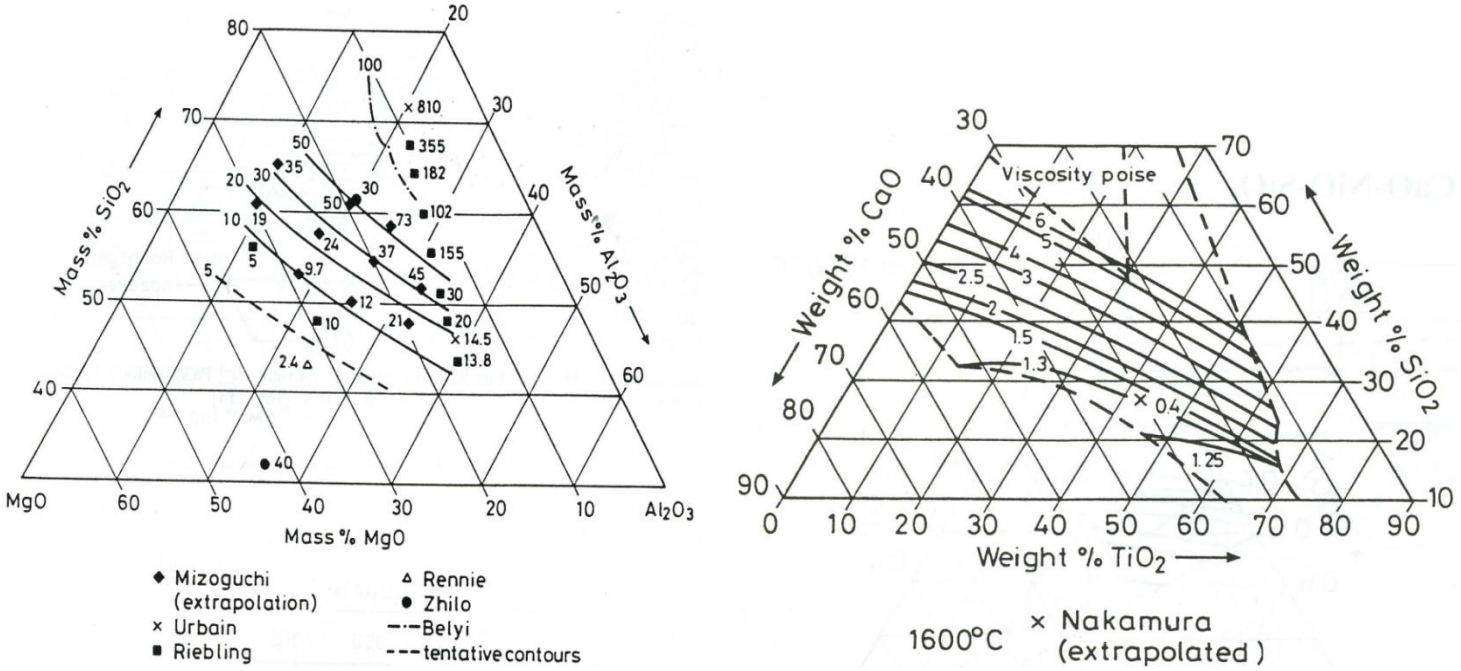

(a) (b)

Figure 2.4: Viscosity diagram at 1600 ˚C for the a) Al_2O_3-MgO-SiO_2 slag b) Viscosity of the CaO-SiO_2-TiO_2 slag [6]

Density

The temperature dependence of the density of silicon metal can be expressed by:

$$\rho_{Si} = 2533 - 0.45(T - T_m)\ \left[\frac{kg}{m^3}\right], \tag{2.13}$$

where T_m represents the melting temperature of silicon [2]. In Figure 2.5 the density of silicon at different temperatures is shown. From the figure it is found that the density of liquid silicon at 1600 ˚C is about 2.53 g/cm^3.

To prevent mixing between slag and metal, the density of the slag should be different from that of the metal. Figure 2.6 shows the effect of the SiO_2 content on the density in a CaO-SiO_2 melt for various temperatures. For instance, if the mass percent of SiO_2 in the slag is 46%, the density of the slag is about 2.65 g/cm^3, this means that the slag will sink to the bottom of the ladle at this composition.

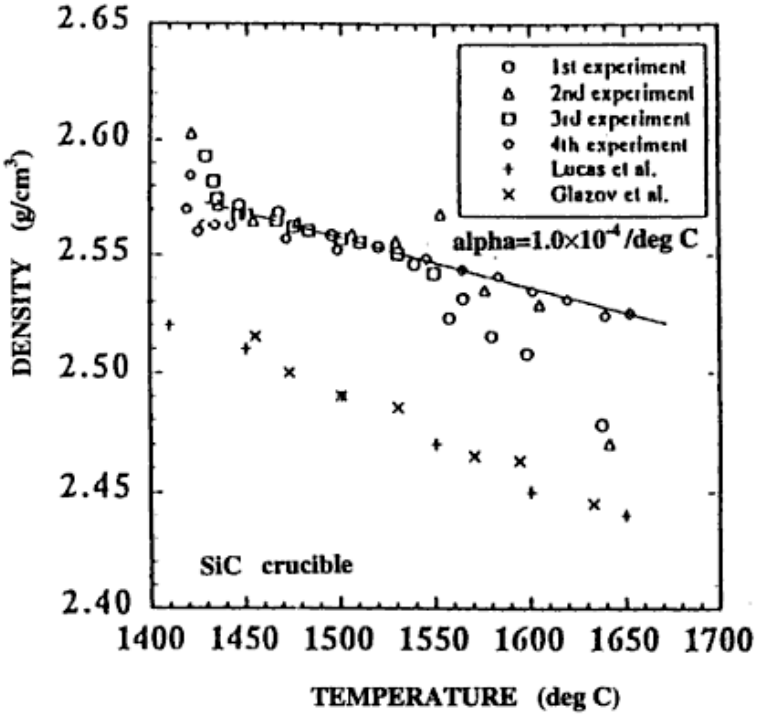

Figure 2.5: Density of liquid silicon at different temperatures [7]

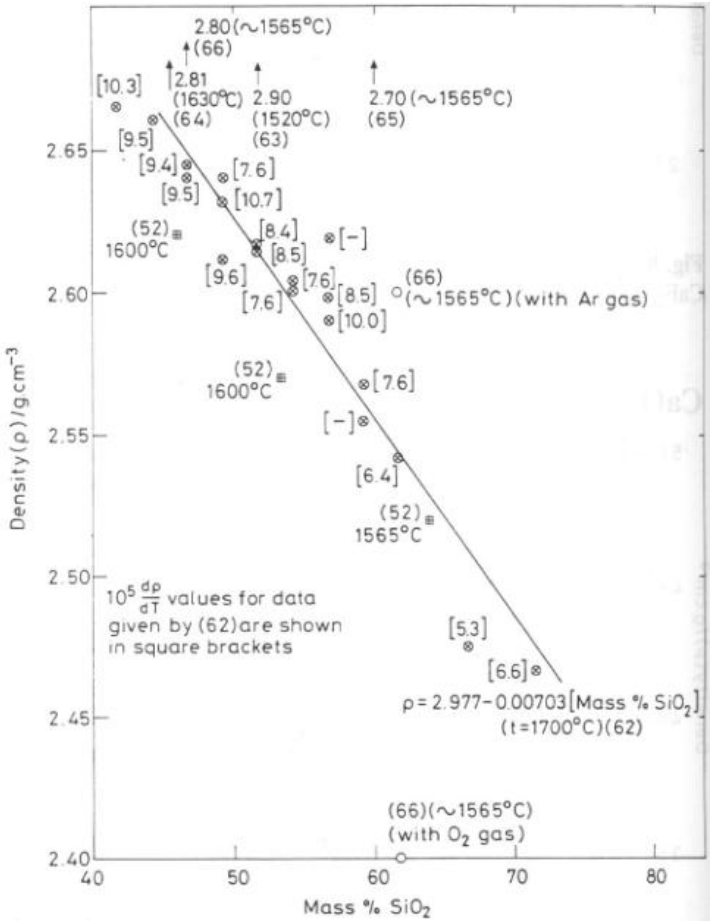

Figure 2.6: Effect of SiO_2 content on the density in the CaO-SiO_2 system [8]

Interfacial properties

The interfacial properties are important for reaction kinetics, nucleation, and the formation of suspension of liquid droplets in molten slags. Interfacial tension is defined as the work required to increase the area of an interface by a unit area [5]. The interface is called a surface if the second phase is a gas. Generally, the surface tension of liquids decrease with increasing temperature and can often be described by a linear relation over a limited temperature range. For liquid silicon, an equation for the surface tension has been derived from sessile drop measurements in the temperature range 1415-1600˚C:

$$\sigma = 885 - 0.28(T - T_m)\ [mNm^{-1}], \tag{2.14}$$

with an uncertainty in the gradient of ±0.004 mN(mK)$^{-1}$.

It is shown experimentally that the interface tension decreases when reactants are transferred across the interface due to chemical reactions between the two phases [5]. The interfacial tension can drop to zero at high transfer rates and even negative values have been measured in some cases.

The spreading coefficient, *S*, determines the tendency of a slag to spread across the metal surface. The spreading coefficient is given by:

$$S_{s/m} = \sigma_{g/m} - (\sigma_{\underline{g}\,\underline{s}} + \sigma_{\underline{s}\,\underline{m}}), \tag{2.15}$$

In Equation (2.15) g/m and g/s indicate surface energies for the gas/metal- and gas/slag surfaces, respectively. The slag/metal interfacial energy is given by s/m. The relation between the surface, interfacial tension and the contact angle is illustrated in Figure 2.7. The contact angle, θ, which is the angle between the tension vectors represented by the two terms in the parenthesis, is drawn in Figure 2.7a for a drop of slag (s) in gaseous environments laying at the surface of liquid metal (m). If the contact angle is < 90° the value of S is positive and the droplet tends to spread out over the metal surface. For a contact angle > 90° the value of *S* is negative and a slag/metal separation is then favorable. In Figure 2.7b a drop is laying on a solid surface in a gaseous environment. In this case the angle is called the wetting angle and is given by Equation (2.16):

$$cos\theta = \frac{\sigma_{g/ss} - \sigma_{l/ss}}{\sigma_{g/l}}, \tag{2.16}$$

where g/ss indicates the gas/solid interface and l/ss indicates the liquid/solid interface [5].

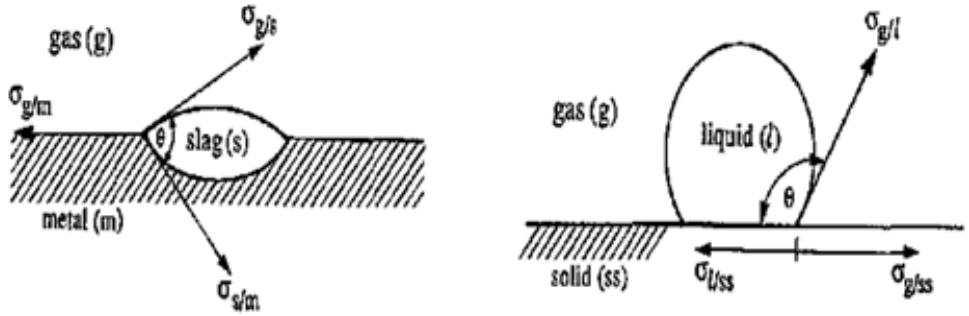

(a) (b)

Figure 2.7: Interfacial tension for a) slag on liquid metal, S > 0 and b) liquid on a solid surface [5]

Diffusion coefficient of boron

Diffusion is the spontaneous mixing of atoms and molecules due to random motions and is caused by concentration gradients in the melt [9]. The diffusion process is important for mass transfer of reactants, and is often the limiting factor for the overall rate of a reaction. The phenomenon can be described by Fick's law:

$$J = -D\frac{dc}{dx}, \tag{2.17}$$

where *J* represents the flux, *D* is the diffusion coefficient, and *dc/dx* is the concentration gradient. Equation (2.17) shows that the flux is proportional to the concentration gradient. Diffusion can occur even when no concentration gradients are present; this is due to a thermal energy process called self-diffusion. The self-diffusion coefficient of boron is found from the Stoke-Einstein equation:

$$D_B = \frac{k_B T}{4\pi\mu r_B}, \tag{2.18}$$

where μ represents the dynamic viscosity, r_B is the effective radius of boron in the metal and k_B is the Boltzmann constant. The effective radius of boron in silicon metal remains unknown and the diffusion coefficient is therefore found experimentally. In Figure 2.8 experimental values for the diffusion coefficient of boron in silicon are shown.

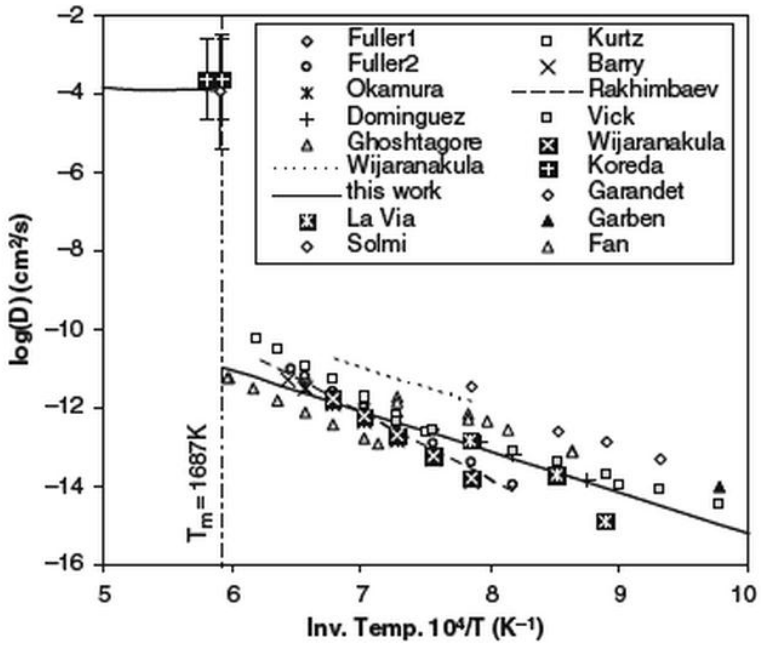

Figure 2.8: Diffusion coefficient of boron in silicon at various temperatures [10]

The abovementioned principles are also true for diffusion in the slag. However, since boron is oxidized the effective radius will be larger than for elemental boron. In addition the viscosity is higher, and consequently a lower diffusion coefficient is obtained in the slag phase. For most slags the diffusivity of boron is unknown [2].

2.1.3 Slag composition

The slag composition will affect the above mentioned properties such as viscosity, density, interfacial tensions and diffusivities. When it comes to the structure of the slag, the slag composition is usually divided into basic oxides, acid oxides and amphoteric oxides. The ratio between the basic and acid oxides will hence explain the above mentioned properties. The basic oxides donate oxygen. They have network breaking properties since they can bind themselves to oxides and therefore break up bonds between other oxides; this is illustrated in Figure 2.9.

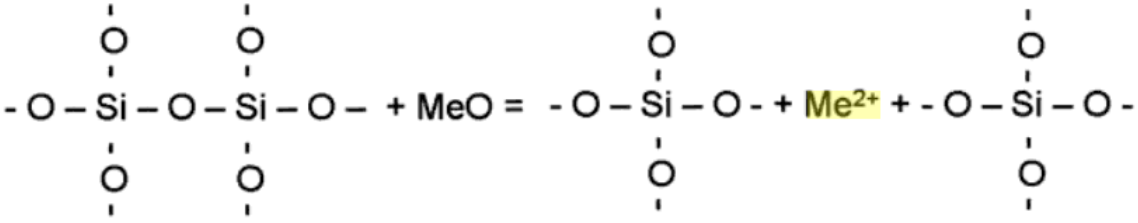

Figure 2.9: Addition of a network breaking oxide, MeO, to a silicate network [11]

As the slag becomes more basic the network breaking leads to a decrease in the viscosity. For the basic oxide CaO, oxygen ions are provided by Equation (2.19):

$$CaO = Ca^{2+} + O^{2-} \quad (2.19)$$

The acidic oxides are oxygen acceptors and will therefore form chemical bonds with other oxides and thereby increase the viscosity of the slag. An acid oxide such as SiO_2 is characterized by Equation (2.20):

$$SiO_2 + 2O^{2-} = SiO_4^{4-} \quad (2.20)$$

The last group, amphoteric oxides, act as a basic or acidic oxide depending on the other oxides present; Al_2O_3 is an example of an amphoteric oxide.

The basicity is defined as the sum of the basic oxides divided by the acidic oxides [2]:

$$B = \frac{\sum(\%\text{Basic oxides})}{\sum(\%\text{Acidic oxides})} \quad (2.21)$$

For the CaO-SiO_2 slag system, the basicity is the mass ratio CaO/SiO_2.

Control of the slag chemistry is important to optimize the extraction effect of the impurities from molten silicon. The impurities are absorbed into the slag as oxidized species and the reactivity of different elements with oxygen is therefore important. Silicon will be oxidized to SiO_2 when oxygen is present. To avoid high losses of silicon into the slag phase it usually contains SiO_2 as one of the components [2].

When silica is present in the slag it is most likely to act as an oxidizing agent. The reaction can be described by Equation (2.22):

$$(SiO_2) = Si + O_2 \quad (2.22)$$

The oxygen produced from Equation (2.22) is the oxygen partial pressure, P_{O_2}.

Because basic oxides reduces the viscosity of the slag, melts based on alkali and alkali-earth oxides are therefore expected to be the most appropriate for effective absorption into the slag phase [12]. A proper slag could therefore be the binary CaO-SiO_2 system which also acts as a base for other slag systems.

A section of the CaO-SiO_2 phase diagram is shown in Figure 2.10. For a CaO/SiO_2 mass ratio of 1.2 the mass percent of SiO_2 in the slag is 46%, and the slag is in liquid phase at 1600 ˚C. However, as can be seen from Figure 2.10, a small change in the slag composition can have a large impact of the slag properties. For instance, a decrease in the SiO_2 mass percent to about 43% will give an increase in the melting temperature of the slag of almost 150 ˚C. Examples of

two other slag systems are the Al_2O_3-MgO-SiO_2 and the CaO-SiO_2-TiO_2 slags, shown in Figure 2.11 and 2.12.

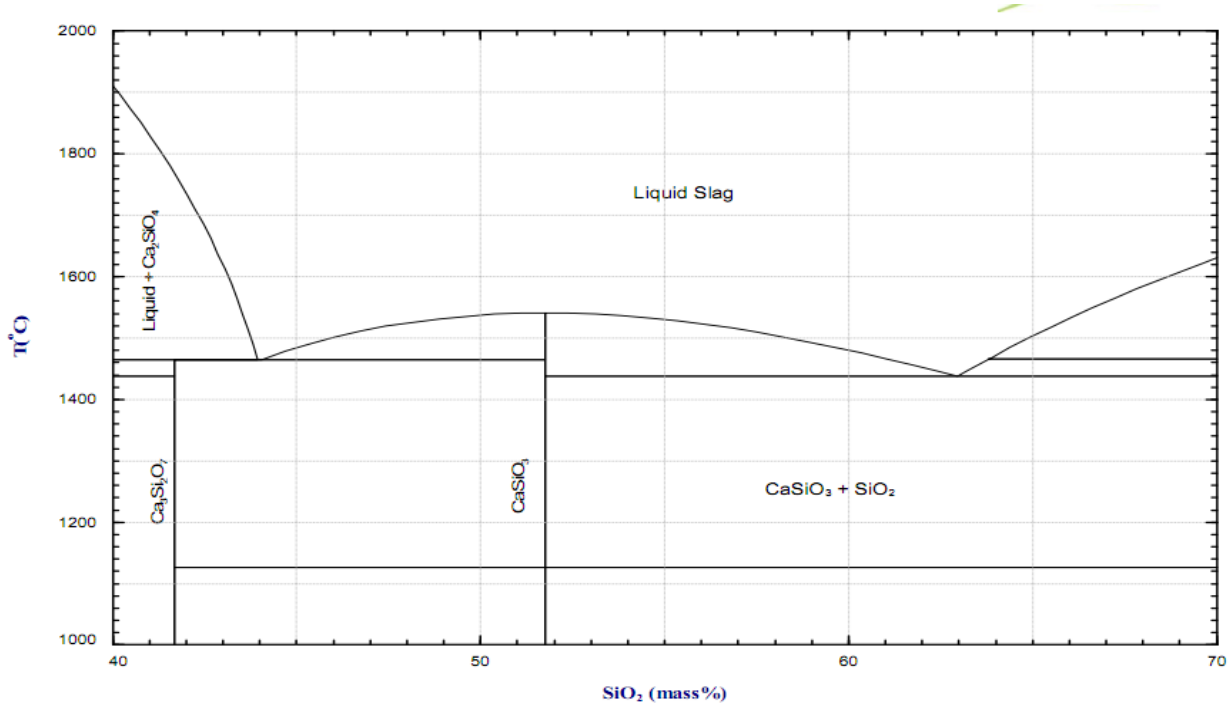

Figure 2.10: CaO-SiO_2 phase diagram [12]

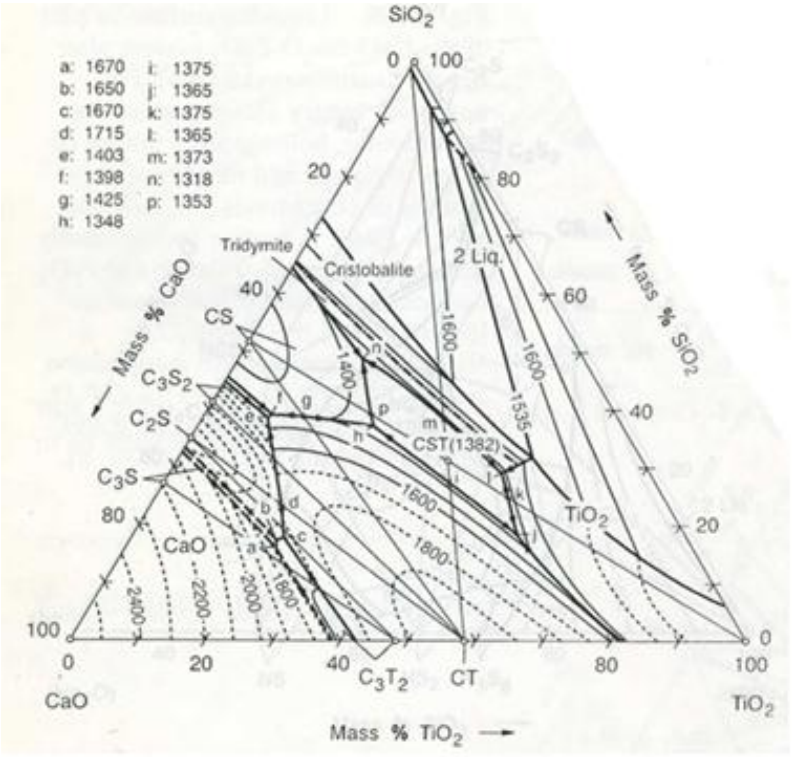

Figure 2.11: CaO-SiO_2-TiO_2phase diagram [6]

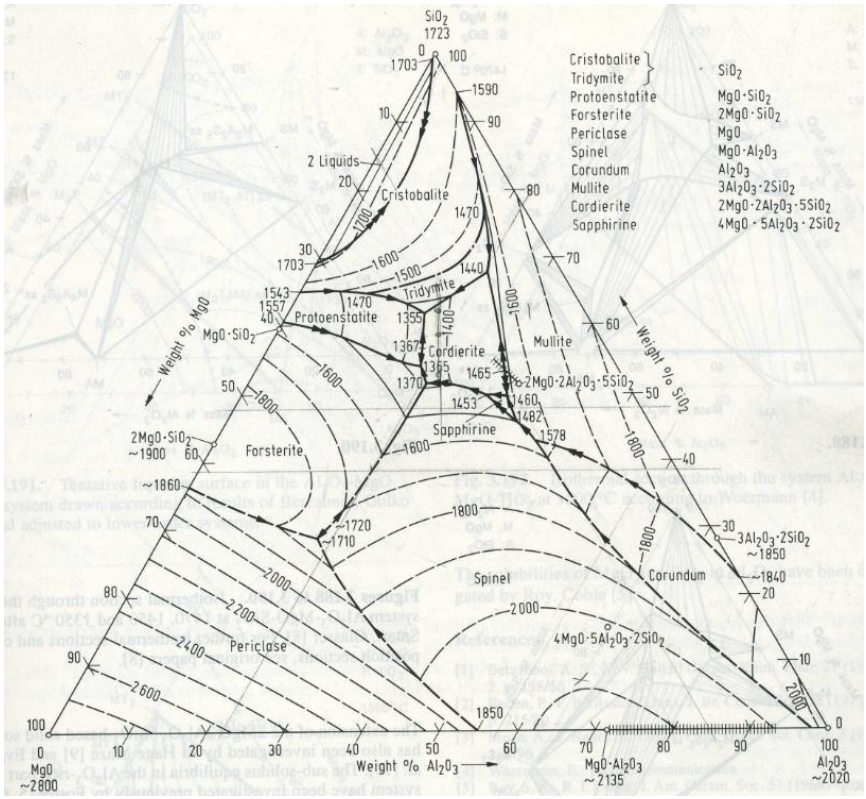

Figure 2.12: Al_2O_3-MgO-SiO_2 phase diagram [6]

2.1.4 Kinetics

During slag refining the dissolved boron goes through 5 steps described by Øverlid et al. [13]:

1. Transportation of the dissolved boron from the bulk metallic phase to the metal boundary layer.
2. Diffusion of boron through the metal boundary layer
3. Oxidation of boron at the interphase between metal and slag
4. Diffusion of boron through the slag boundary layer
5. Transportation from the slag boundary layer to the slag bulk phase

Figure 2.13 is a schematic illustration of slag refining in a ladle. A typical velocity profile at the boundary between metal and slag is shown to the right.

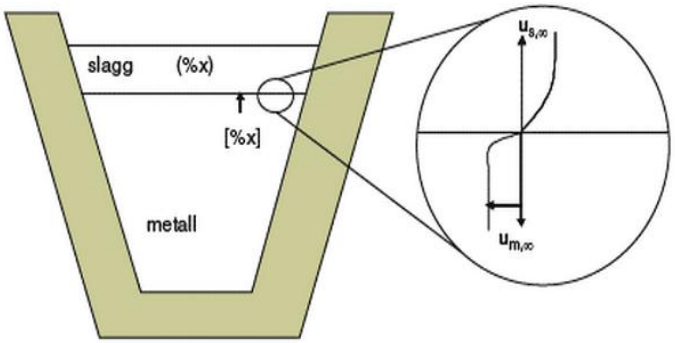

Figure 2.13: Slag refining in a ladle [13]

1. Transport in the bulk metallic phase

Transport of boron in the bulk metallic phase occurs by a combination of diffusion and convection. The latter could be either forced convection or natural convection. Diffusion is often a slow process and the mass transfer is therefore dependent on stirring and mixing.

Natural convection is movement of molecules in the fluid and occurs due to temperature differences in the metal. Different temperatures means different densities of the metal and the metal will rise and fall in the ladle due to heat gradients. Natural convection is dependent on the viscosity and the thermal conductivity of the metal.

Forced convection is dependent of the viscosity of the metal, and can for instance be performed using mechanical stirrers, gas stirring or pumping.

2. Diffusion of boron through the metal boundary layer

When a component enters the interface between metal and slag, a thin viscous sub layer film will give resistance to the flow on each side of the interface. The transport through this layer is mainly dependent of diffusion. Fix law for diffusion was given in Equation (2.17), for boron in silicon it can be written as:

$$J_B = -D_B \frac{\rho}{100} \nabla[\%B] \quad [\mathrm{kg/m^2 s}] \tag{2.23}$$

Where D_B is the diffusion coefficient of boron and ρ is the density of liquid silicon. To describe the mass transfer of boron through the boundary layer, a mass transfer coefficient, *k*, is used. This coefficient is dependent on the diffusion coefficient and the thickness of the boundary layer. The molar flux, ṅ , of boron through the metal boundary layer is then given by:

$$\dot{n} = \frac{k\rho}{100 M_B} ([\%B]\text{-}[\%B]_i) \tag{2.24}$$

where *k* represents the mass transfer coefficient, M_B is the molar weight of boron, ρ is the density of the metal, [%B] is the concentration of boron in the bulk metal, and $[\%B]_i$ is the concentration of boron dissolved in the metal at the slag-metal interface [14].

3. Oxidation of boron at the interface between metal and slag

For a chemical reaction aA + bB → cC + dD the reaction rate law is written as:

$$r = k(T)[A]^x[B]^y \tag{2.25}$$

where *k(T)* is the reaction rate constant and *x* and *y* are the reactions orders [15]. The temperature dependence of the reaction rate constant is given by the Arrhenius relation in Equation (2.26):

$$\mathrm{k(T)} = \mathrm{k_0 exp(-\frac{E_a}{RT})}, \tag{2.26}$$

where E_A represents the activation energy, *R* is the gas constant and *T* is the absolute temperature. Since the reaction rate is strongly dependent on the temperature, the chemical reaction rates are not assumed to be the limiting step when molten metal is involved. Hence, due to the high chemical reaction rate at high temperatures, the metal and slag at the interphase are assumed to be in equilibrium. The equilibrium constant is given by Equation (2.27):

$$K = \frac{(\%B)_i \gamma_B}{[\%B]_i f_B}, \tag{2.27}$$

Here $(\%B)_i$ is the concentration of boron in the slag phase at the slag metal interface, f_B represents the activity coefficient of boron in the metal phase, and γ_B is the activity coefficient of boron oxide in the slag. It is assumed that the concentration of silica in the slag and of silicon in the silicon metal is unity [14].

4. Diffusion of boron through the slag boundary layer

An equation similar to Equation (2.24) can be written for the molar flux through the slag boundary layer:

$$\dot{\mathrm{n}} = \frac{k_{slag}\rho_{slag}}{100M_B}\left((\%B)_i) - (\%B)\right), \tag{2.28}$$

where *(%B)* represents the concentration of boron in the bulk slag phase. This molar flux is different from the flux through the metal boundary layer due to the fact that boron is oxidized and due to the different physical properties of metal and slag [14].

5. Transport in the bulk slag

Transport of boron in the slag phase is very similar to the transport in the metal phase. Also here, the differences in the transport properties are due to the different properties of the slag.

2.1.5 Mass transfer

The slag phase can often be relatively viscous and therefore difficult to mix properly [2]. If we assume complete mixing in the slag phase, the diffusion through the metal and slag boundary layers can be assumed to be the rate limiting steps. For highly viscous slags however, this could be difficult to obtain. If we replace $(\%B)_i$ in Equation (2.28) with the expression in Equation (2.27), we obtain:

$$[\%B]_i = \frac{\dot{n}100M_B\gamma_B}{k_{slag}\rho_{slag}K'f_B} + \frac{(\%B)\gamma_B}{K'f_B} \tag{2.29}$$

The expression in Equation (2.29) for $[\%B]_i$ can be placed into Equation (2.24) for the molar flux in the metal boundary layer, Equation (2.30) is then obtained:

$$[\%B] - \frac{(\%B)\gamma_B}{K'f_B} = \dot{n}100M_B\left(\frac{1}{\rho k} + \frac{\gamma_B}{\rho_{slag}k_{slag}K'f_B}\right) \tag{2.30}$$

From Equation (2.30) an expression for the total mass transfer coefficient, k_t, can be defined:

$$k_t = \left(\frac{1}{\rho k} + \frac{\gamma_B}{\rho_{slag}k_{slag}K'f_B}\right)^{-1} \tag{2.31}$$

Based on Equation (2.31), the expression in Equation (2.32) for the change in boron concentration with time can be derived:

$$-\mathrm{M}\frac{\mathrm{d}[\%\mathrm{B}]}{\mathrm{dt}} = \mathrm{k_t}\rho\mathrm{A_s}\left([\%\mathrm{B}] - \frac{(\%\mathrm{B})\gamma_\mathrm{B}}{\mathrm{Kf_B}}\right) \tag{2.32}$$

where *M* represents the total mass of the metal and *As* is the area of the slag metal interface.

From Equation (2.32) an equation for the change in boron concentration over time can be derived, assuming no other parameters than the boron concentration changes with time, and that the total boron concentration in the system is constant. This equation is given by:

$$\frac{[\%\mathrm{B}]-[\%\mathrm{B}]_\infty}{[\%\mathrm{B}]_{\mathrm{in}}-[\%\mathrm{B}]_\infty} = \exp\left(-\frac{\mathrm{k_t}\rho\mathrm{A_s}\mathrm{t}}{\mathrm{M}}\left(1 + \frac{\mathrm{M}\gamma_\mathrm{B}}{\mathrm{M_s}\mathrm{K'f_B}}\right)\right) = \exp\left(-\frac{\mathrm{t}}{\tau}\right) \tag{2.33}$$

Where $\tau = \frac{M}{k_t \rho A_s}\left(1 + \frac{M\gamma_B}{M_s K' f_B}\right)^{-1}$ (2.34)

In Equation (2.33) $[\%B]_\infty$ represents the boron concentration in the metal at total equilibrium and $[\%B]_{in}$ is the initial amount of boron in the bulk metal. M_s represents the total mass of the slag and $K' = \frac{(\%B)_\infty \gamma_B}{[\%B]_\infty f_B}$.

A plot of Equation (2.33) as a function of [%B] is shown in Figure 2.14.

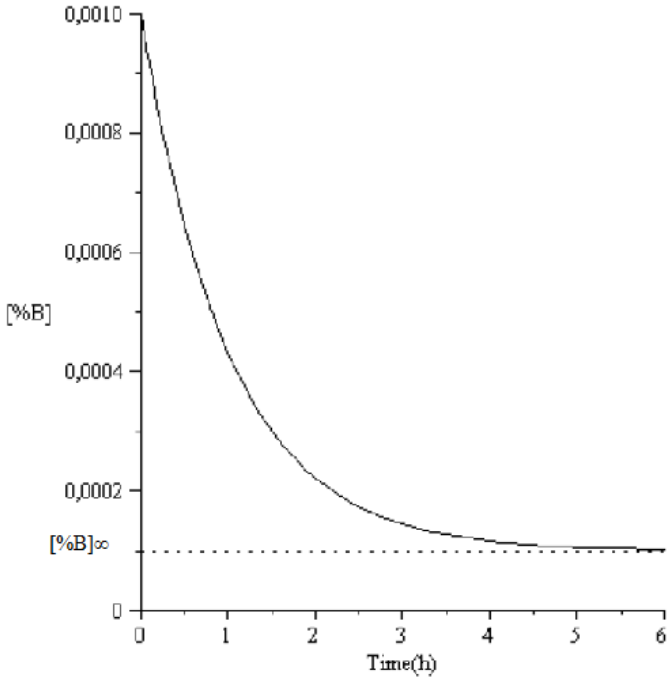

Figure 2.14: Decrease in the boron concentration in the silicon melt from an initial boron concentration of 0.001% to a final concentration of 0.0001%, τ =1 [2]

2.1.6 Literature: Distribution coefficient of boron

In this section relevant theory regarding the distribution coefficient of boron (L_B) in different slag systems are presented as well as background data on how to optimize these systems. The main focus has been on similar systems as those explored in this study. Knowledge of thermodynamic properties of impurities in silicon are important when considering the potential and efficiency of a silicon-refining method, some values for the activity coefficients of impurities in molten silicon are therefore also presented.

Teixeira et al. investigated the equilibrium distribution of boron between slag and metal using $CaO\text{-}SiO_2$ slags [3]. The silicon used was high purity electronic grade silicon doped with 150 ppm boron. They studied the system in an argon atmosphere. Three grams of silicon was melted in an electric resistance furnace together with 6.7 grams of the slag in a graphite crucible at

1823K. The composition range investigated was CaO/SiO_2 between 0.55-1.21. They found a parabolic trend when plotting the distribution coefficient as a function of the CaO/SiO_2 mass ratio (basicity) as shown in Figure 2.15. The highest distribution coefficient on 5.5 was obtained for a CaO/SiO_2 mass ratio of 1.2. Since an increased CaO/SiO_2 mass ratio will lead to a reduced oxygen partial pressure, the results suggested that L_B was strongly affected by both the basicity and the oxygen partial pressure.

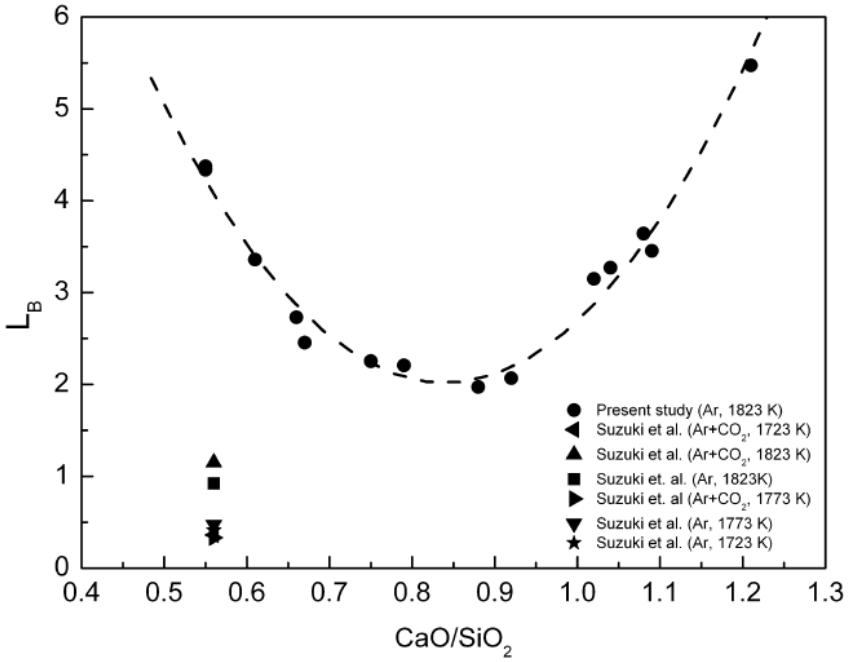

Figure 2.15: The distribution coefficient of boron in the $CaO-SiO_2$ system [3]

Johnston et al. studied the importance of slag basicity and oxygen potential on the distribution coefficient of boron [16]. Metallurgical silicon was doped with 0.19 wt% boron. A slag consisting of Al_2O_3-CaO-MgO-SiO_2 was equilibrated with doped Si at 1500˚C in an inert atmosphere. For each experiment 5.5 g of doped Si and 7.5 g of slag were used.

The effect of basicity was investigated by varying the CaO/SiO_2 ratio of the slag. The amount of Al_2O_3 and MgO was fixed at 35 and 3 wt%, respectively, and the experiments were performed in alumina crucibles. The results are illustrated in Figure 2.16a. For boron the distribution coefficient was found to increase until a CaO/SiO_2 ratio of about 0.6. The highest value obtained was about 1.6 indicating a slight preference for the slag. Since the value of L_B then started to decrease the oxygen partial pressure was expected to be an important influencing factor as well. This results is in accordance with the findings by Teixeira et al.[3].

Johnston et al. investigated further the effect of the oxygen partial pressure (p_{O2}) by varying the SiO_2/Al_2O_3 ratio of the CaO-MgO-Al_2O_3-SiO_2 slag, while CaO and MgO was held constant at 42 and 10 wt%, respectively. The amounts of CaO and MgO were fixed at 42 and 10 wt%

respectively, and the experiments were performed in magnesia crucibles. The distribution coefficient of boron was found to increase slightly with increasing SiO_2/Al_2O_3 ratio (Figure 2.16b). All the L_B values were found to lie in the range $1< L_B <2$. The highest L_B value was found in the slag with the highest SiO_2/Al_2O_3 ratio. From this Johnston et al. suggested that p_{O2}, and not the basicity was the major influencing parameter for removal of boron.

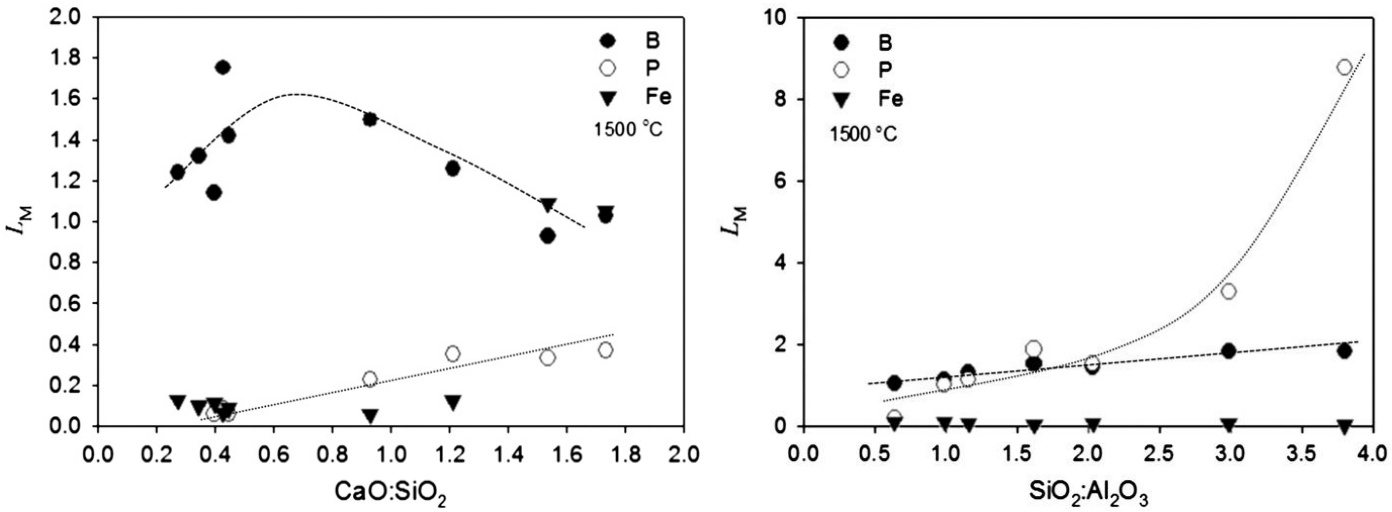

(a) (b)

Figure 2.16: L_B as a function of a) CaO/SiO_2 mass ratio (35% Al_2O_3, 3% MgO) and b) SiO_2/Al_2O_3 mass ratio (42% CaO, 10% MgO) [16]

Jakobsson et al. investigated the effect of the composition of $CaO\text{-}SiO_2$ slag on the distribution coefficient of boron [17]. Fifteen grams of $CaO\text{-}SiO_2$ slag was melted in a graphite crucible together with 15 grams of silicon at 1873 K. The CaO/SiO_2 mass ratios varied between 0.65 and 1.3. The silicon had a boron concentration of 111 ± 29 ppm, and the melting lasted for 3-6 hours. The systems with the highest calcium content were found to reach equilibrium with respect to boron after 3 hours. The distribution coefficient of boron is plotted as a function of CaO/SiO_2 mass ratio in Figure 2.17. They found L_B to follow a linear trend with respect to the slag composition, but the effect was small.

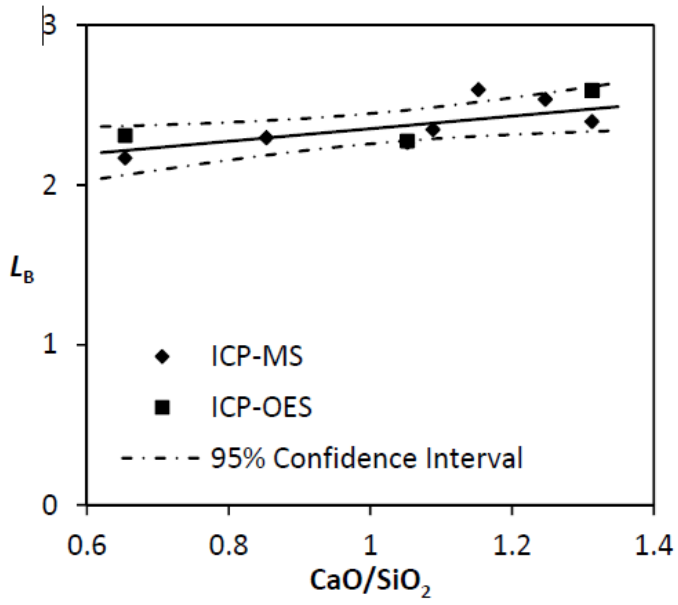

Figure 2.17: Distribution coefficient of boron as a function of CaO/SiO_2 mass ratio [17]

Luo et al studied the distribution of boron between different $CaO\text{-}SiO_2\text{-}Al_2O_3$ slags and silicon using electromagnetic induction slag melting (EISM) [18]. The mass ratio of CaO/SiO_2 was 1.21. For the binary $CaO\text{-}SiO_2$ system they found L_B to be 2.2, when 10% Al_2O_3 was added to the system L_B was found to be 4.2. The results were obtained after 1 hour at 1773 K.

When an increased amount of Al_2O_3 was added to the system, a higher L_B was obtained which is illustrated in Figure 2.18a. It was further shown that the addition of Al_2O_3 to the $CaO\text{-}SiO_2$ slag could greatly increase the basicity and the oxygen partial pressure of the slag, leading to an increase in L_B. From a kinetic point of view Al_2O_3 might reduce the melting temperature of the slag, and consequently the viscosity will be reduced at a certain temperature.

Luo et al. also investigated the effect of refining temperature for the $CaO\text{-}SiO_2\text{-}Al_2O_3$ slag. For a given refining time the value of L_B increased with increasing temperature, as illustrated in Figure 2.18b. As shown in Equation (9), a higher temperature leads to reduced slag viscosity, and thereby increased mass transfer rate of boron in the slag.

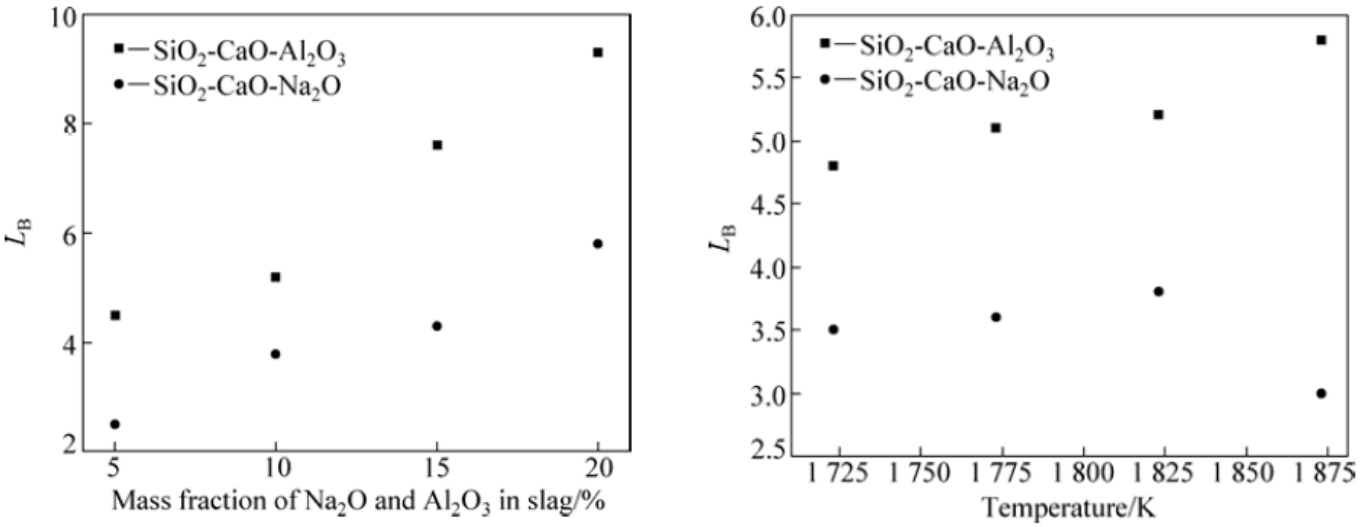

(a) **(b)**

Figure 2.18: L_B as a function of a) Al_2O_3 content, refining time 1 h at 1823 K b) temperature, refining time 1 h [18]

The kinetics of boron removal during slag refining was investigated by Krystad et al [19]. The mass transfer of boron was measured for a CaO-SiO_2 slag containing 50% CaO and 50% SiO_2 , and for a CaO-SiO_2 based slag containing 19% MgO. The experiments were performed in graphite crucibles at 1600 ˚C. Slag was melted together with crushed EG-silicon doped with approximately 250 ppm boron. During melting the silicon phase took a sphere like shape, this because the wetting properties of the slag with graphite is better than that of silicon with graphite. The mass transfer coefficient for the systems was found to be in the range 1.2- 3.2x10^{-6} m/s. The highest value was obtained for the MgO containing slag. This could either be explained by the higher basicity of the slag and/or by the physical and chemical properties of MgO affecting the transfer of boron.

Miki et al. developed an expression for the activity coefficient of aluminum and magnesium in molten silicon at infinite dilution relative to the pure liquid state (Equation (2.34) and (2.35)) [20]. The equations are valid in the temperature range 1723-1848 K and 1698-1798 K, respectively. To determine the activity coefficient of aluminum, a molten silicon-aluminum alloy was equilibrated with a solid Al_2O_3-$Al_6Si_2O_{13}$ mixture. The activity coefficient of magnesium was found by equilibrating a magnesium silicon alloy with a MgO-SiO_2-Al_2O_3 slag doubly saturated with $MgSiO_3$ and SiO_2.

$$log\gamma^0_{Al(l)in\ Si} = -\frac{1570}{T} + 0.236 \quad (1723 \text{ to } 1848 \text{ K}) \tag{2.34}$$

$$log\gamma^0_{Mg(l)in\ Si} = -\frac{4900}{T} + 1.96 \ (1698\text{-}1798 \text{ K}) \tag{2.35}$$

Safarian et al. determined the activity coefficients for aluminum and magnesium in molten silicon from activity curves at 1414 ˚C [21]. The activity coefficients for dilute solutions are listed in Table 2.1.

Table 2.1: Activity coefficients of Al and Mg in liquid Si at 1414 ˚C

	γ_i^0
Al	0.370
Mg	0.0498

2.2 Vacuum refining

The basic principle of vacuum refining is to use the difference in the vapor pressure of the liquid components at elevated temperatures [2]. Removal of boron through vacuum refining is a challenge as pure boron has a lower vapor pressure compared to silicon. The criterion for refining of an element from liquid silicon through vacuum refining is expressed in Equation (2.36):

$$\frac{P_i}{P_{Si}} > \frac{N_i}{N_{Si}} \tag{2.36}$$

where P_i and P_{si} represent the partial pressure of the impurity and silicon, respectively, in the gas phase. N_i and N_{Si} are their molar fractions in the melt [2]. The partial pressures can be found from Equation (2.37):

$$P_i = a_i P_i^0 \tag{2.37}$$

Where P_i^0 is the standard vapor pressure and a_i is the activity given by Equation (2.38):

$$a_i = \gamma_i N_i \tag{2.38}$$

Here γ_i is the activity coefficient [22]. Some reactions may be too slow for practical purposes, and the kinetics should therefore also be considered in addition to a thermodynamic evaluation of the process. The fundamental criterion for refining is expressed in Equation (2.39) [23]:

$$\frac{n_i}{n_b} > \frac{N_i}{N_b} \tag{2.39}$$

Where n_i is the impurity evaporation rate and n_b the solvent evaporation rate. N_i and N_b are their respective concentrations in the bulk liquid metal. Based on Equation (2.39), Olette developed the volatility criterion in Equation (2.40) for silicon containing impurity *i* [24];

$$\alpha = \gamma_i^0 \frac{P_i^0}{P_{Si}^0} \sqrt{\frac{M_{Si}}{M_i}} > 1 \quad (2.40)$$

Where M_{Si} (kg/mol) and M_i (kg/mol) represent the atomic weight of Si and the impurity. The magnitude of this expression reflects the purification driving force. The elimination of impurities in vacuum melting is generally observed to follow first order kinetics for metals and metallic elements [25]. The overall mass transport rate can therefore be expressed by Equation (2.41);

$$-\frac{d[wt\%B]}{dt} = k\frac{A}{V}[wt\%B] \quad (2.41)$$

Here A (m^2) is the surface area and V (m^3) is the liquid Si volume. Integration of Equation (2.41) gives equation (2.42);

$$[wt\%B] = [wt\%B]_{initial}\, e^{-\frac{kA}{V}t} \quad (2.42)$$

2.3 Removal of boron from the slag by evaporation

Conventional slag purification methods for removal of boron are expensive and produce a lot of waste material [2]. In addition, removal of boron from silicon in its elemental form by vacuum refining is impossible. None of the methods mentioned above are optimal for obtaining solar grade silicon alone, but a combination of them may constitute a simpler and cheaper alternative.

2.3.1 Evaporation of boron as volatile species

When boron enters the slag phase it will be oxidized. However, evaporation of boron oxides are not thermodynamic favorable [26]. Boron hydrides such as HBO, BHO_2 and $B_3H_3O_3$ are previously reported to have higher vapor pressures than the boron oxides, a hydrogen atmosphere may therefore improve the vaporization of boron from the slag [27]. For HBO the reaction can be written as:

$$B_2O_3 + 2H_2\,(g) = 2HBO\,(g) + H_2O\,(g) \quad (2.43)$$

If boron can be evaporated from the slag as boron hydrides less slag will be needed for refining and a higher refining rate will be obtained. In turn the cost of the process will be reduced as well as the waste slag after refining.

2.3.2 Literature: Evaporation of boron in hydrogen atmosphere

To date no published literature on boron removal from slag by H_2 exists, but there are a number of publications regarding boron evaporation directly from the silicon melt. In these cases boron

has to be oxidized at the melt surface by an oxidizing gas before it can evaporate. In the following a review of some of these articles will be shown.

In our previous unpublished study we found that boron could not be removed from the $CaO\text{-}SiO_2$ slag by evaporation in an inert atmosphere due to the low vapor pressure of boron oxides [26]. When refining the slag in a pure hydrogen atmosphere the boron content in the slag was reduced by 22.4% after 1.5 hour refining time at 1600˚C, the initial boron content of the slag was 88 ppm.

Nakamura et al. studied evaporation of boron from silicon by a steam-added plasma melting method [28]. The amount of silicon melted varied between 0.6 and 300 kg, and a silica crucible was used. The temperature of the silicon melt was 1873-1973 K, except for the 300 kg experiment where the temperature was 1823-1873 K. The initial boron content in the silicon was 5-10 mass ppm.

They found the boron content to decrease linearly with time to less than 0.1 ppm when the added gas contained 4.3-4.6 vol% H_2O and 50.4- 50.6 vol% H_2 (Figure 2.19). Furthermore, they found the boron removal rate to increase as the hydrogen content in the gas increased (Figure 2.20).

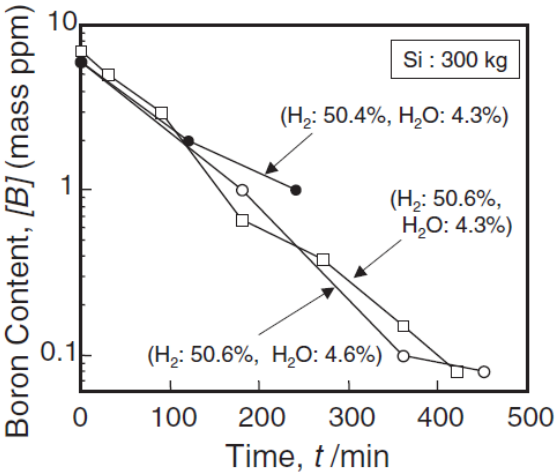

Figure 2.19: Boron content as a function of time [28]

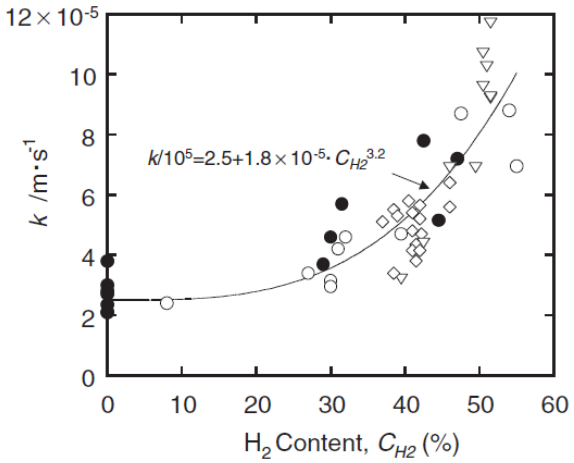

Figure 2.20: The effect of H_2 content in the added gas on the boron removal rate [28]

Wu et al. demonstrated that the boron content in metallurgical grade silicon could be effectively reduced by oxidizing refining in a $H_2O\text{-}O_2$ atmosphere [27]. Based on thermodynamic calculations they found the partial pressure of gaseous boron hydrides to be 10^5-10^{10} times the gaseous boron oxides in the temperature range 1685-2500 K. The gaseous boron hydrides were found to mainly be in the form of $B_3H_3O_6$ and BHO_2, but also BH_3O_3, BHO, BH_2O_2 and $B_2H_4O_4$. Except for BHO, the partial pressure of all the species was found to decrease with increasing temperature. Experimentally metallurgical grade silicon was refined in an electric arc furnace in an $Ar\text{-}H_2O\text{-}O_2$ atmosphere. The boron content was reduced from $18x10^{-6}$ to $2x10^{-6}$ after 10 minutes of refining as shown in Figure 2.21.

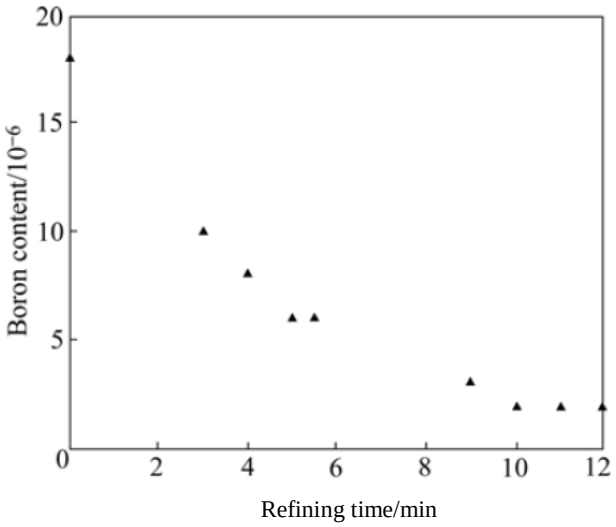

Figure 2.21: Boron content in MG-Si with increasing refining time [27]

Evaporation of boron in hydrogen atmosphere has also been investigated by Nordstrand et al. [29]. They investigated boron removal by treating the surface of a silicon melt with moist hydrogen. The initial boron concentration in silicon was about 130 ppm. Three different series of experiments were performed. In each of their experiments one of the following parameters were altered; the H_2O vol% in the gas, the temperature or the H_2 content in the gas. All the experiments lasted for 4.5 hours. They concluded that the rate of boron removal in the form of boron hydrates increased with decreasing temperature between 1450-1600˚C. Furthermore, a H_2 vol% of 50 was found to give the highest possible boron removal rate. Increasing the H_2 content above this level resulted in an excess amount of H_2. In Figure 2.22 it is shown that the boron concentration could be reduced to well below 1 ppm after 4.5 hours refining time when the water content was 3.2% and the vol% H_2 was at least 50. For the experiment performed with 100 vol% H_2 and no water, the boron removal rate was found to be slow. The silicon loss in the experiments was found to be about 10%.

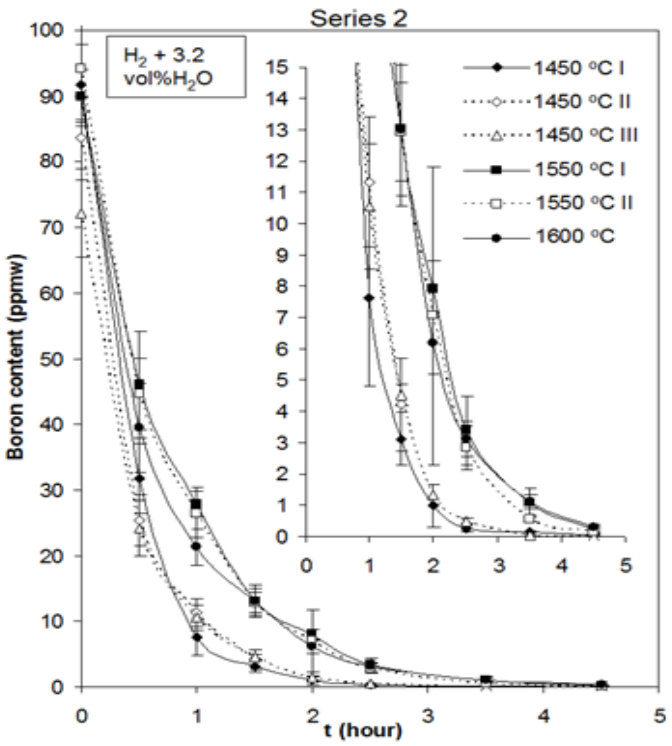

Figure 2.22: Boron content as a function of time for different temperatures [29]

Nishimoto et al. investigated boron removal by slag end Cl_2 gas treatment [30]. In the experiments slag with a composition of 55 wt% CaO and 45 wt% SiO_2 was melted together with silicon containing approximately 300 mass ppm boron. The melting took place in a graphite crucible at 1600˚C in a resistance furnace. The atmosphere used was high purity argon. For the experiments where Cl_2 gas was supplied, the gas was introduced at 1823 K for a predetermined time. Cl_2 gas was also injected into a mixture of silicon and slag after equilibrium was attained.

For the metal-slag system the reaction kinetics was analyzed. The reaction kinetics was found to follow a first order rate law, and was controlled by mass transfer of boron in the slag. The mass-transfer coefficient for the slag was found to be $1.4x10^{-6}$ m/s. In Figure 2.23a and 2.23b the results from the Cl_2 gas treatment is shown. The boron concentration in the slag was reduced by 21% after 2 h, while it remained unchanged for silicon. When Cl_2 gas was injected into a mixture of silicon and slag after equilibrium was attained, the boron content in the slag was reduced, but still the content in silicon did not decrease. An explanation for this could be that the composition of the slag was changed by chlorination and therefore the activity of borate in the slag was changed.

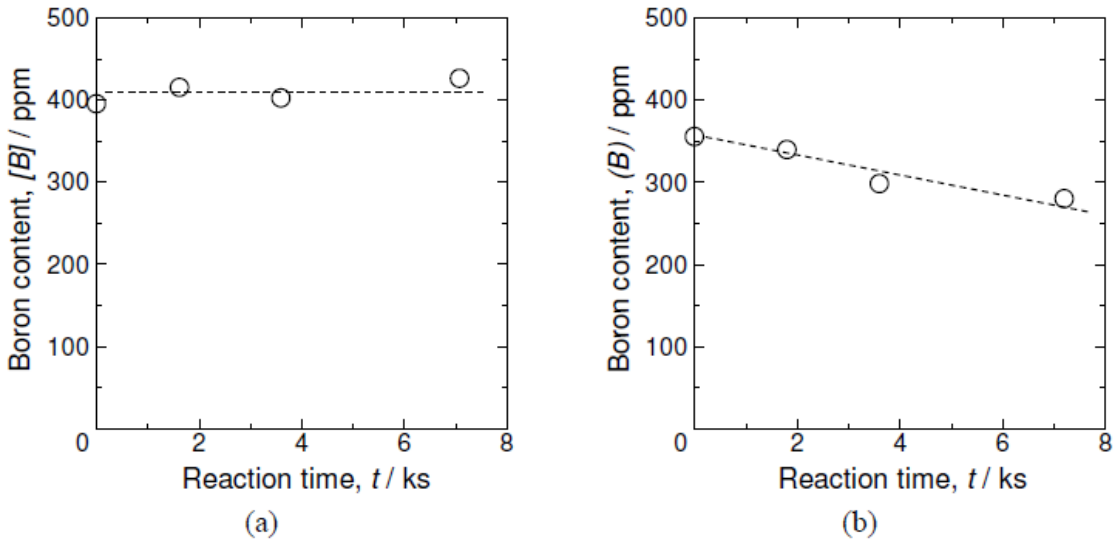

Figure 2.23: Boron content as a function of time when blowing Cl_2 gas at 1823 K on a) silicon and b) slag [30]

3. Experimental

In this report we want to explore ways of improving the method of slag refining. First, we want to measure the distribution- and mass transfer coefficient of boron for slag systems which previously have been little investigated. In addition we want to measure the activity coefficients of aluminum and magnesium in silicon. Second, we want to explore the possibility of evaporating boron from slag with the use of hydrogen gas.

The distribution- and mass transfer coefficient of boron was measured for two different slag systems. For each system the coefficients were measured as a function of time, while the temperature was held constant at 1600 ˚C. In all, 12 experiments were performed.

Boron evaporation in hydrogen atmosphere was investigated for a $CaO\text{-}SiO_2$ slag. In the experiments three parameters were varied, namely temperature, time and the slag/silicon mass ratio. In all, 14 experiments were performed.

3.1 Distribution of boron between slag and silicon

3.1.1 Preparation of slags

Four different slags with the following compositions were weighted out:

1. $Al_2O_3\text{-}MgO\text{-}SiO_2$ (18%-18%-64%)
2. $Al_2O_3\text{-}MgO\text{-}SiO_2$ (27%-23%-50%)
3. $CaO\text{-}SiO_2\text{-}TiO_2$ (39%-43%-18%)
4. $CaO\text{-}SiO_2\text{-}TiO_2$ (24%-27%-49%)

The purity of the different oxides is tabulated in Table 3.1.

Table 3.1: Purity of oxides

	Al_2O_3	MgO	SiO_2	CaO	TiO_2
Purity (%)	99.50	99.50	99.90	99.90	99.95

The compositions of the two $Al_2O_3\text{-}MgO\text{-}SiO_2$ slags are marked in the phase diagram in Figure 3.1, while the compositions of the two $CaO\text{-}SiO_2\text{-}TiO_2$ slags are marked in Figure 3.2. The compositions in the two phase diagrams were chosen so the melting temperatures of the slags were well below the refining temperature of 1600˚C.

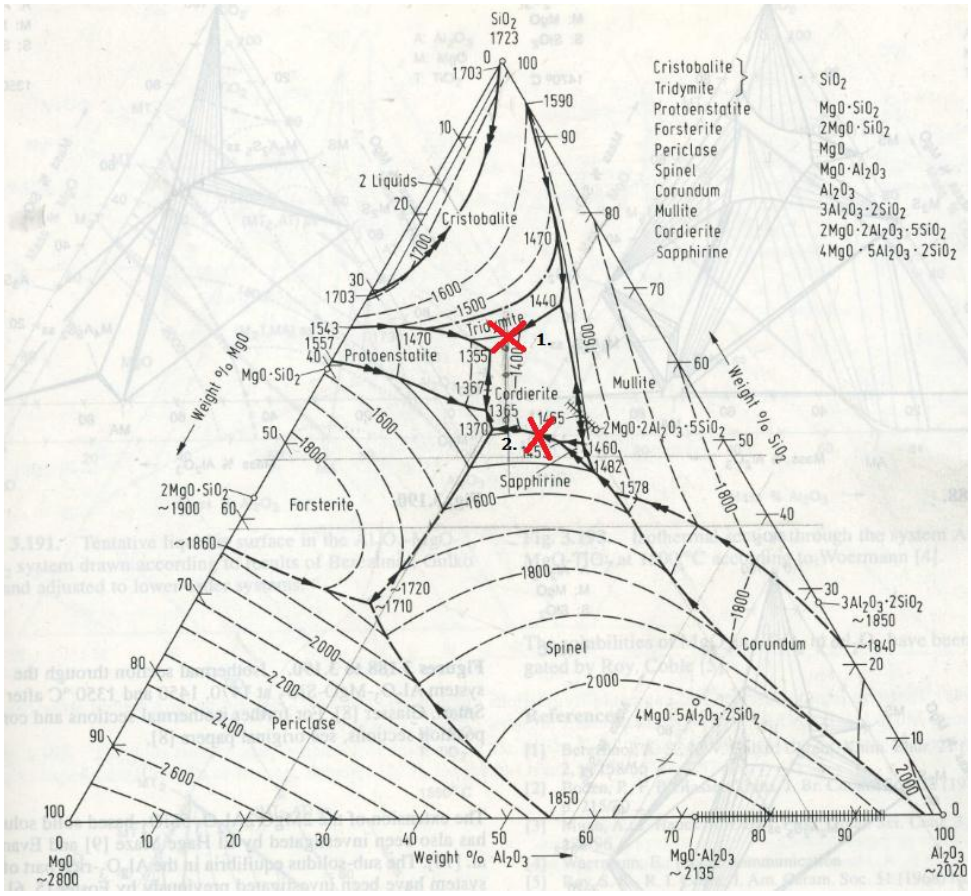

Figure 3.1: Al_2O_3-MgO-SiO_2 phase diagram, the composition of slag 1 and 2 is shown in the diagram [6]

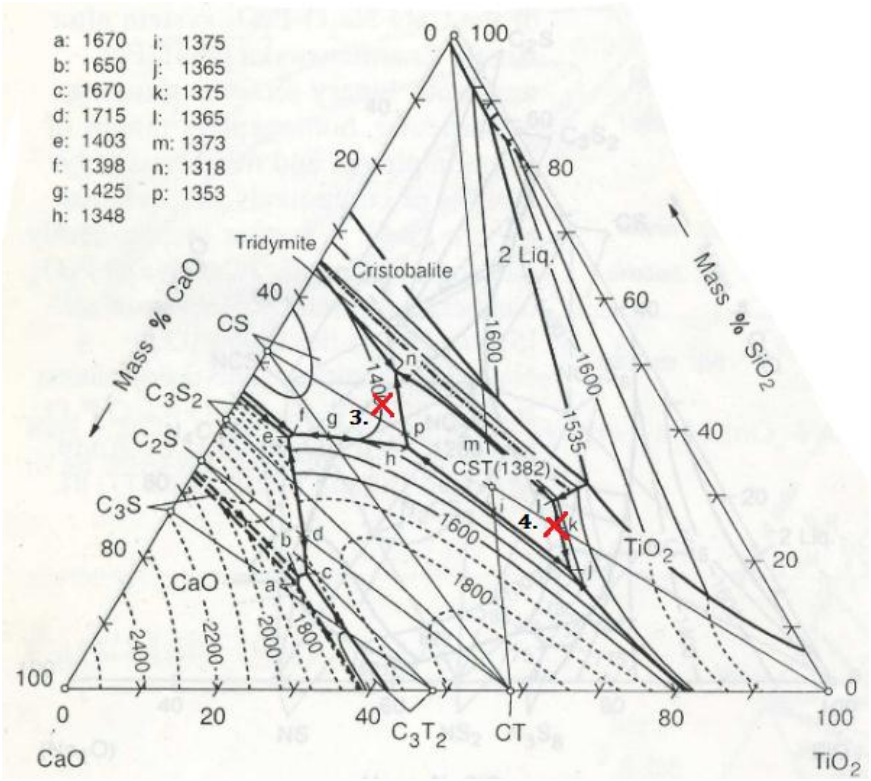

Figure 3.2: Al_2O_3-MgO-SiO_2 phase diagram, the composition of slag 3 and 4 is shown in the diagram [6]

To ensure proper mixing of the oxides in each slag, they were first mixed by hand, and then melted in a vacuum induction furnace to form a homogeneous mass. The melt was further poured into a casting mold. After melting the slag was crushed down to fine powder by a Herzog HSM 100 vibratory disc mill to a particle size of 150 μm. About 100 ppm of boron was added to the slag, before it was melted and crushed down to powder for two more times.

The casting process could be observed through a window in the vacuum induction furnace. The slag was observed to be very viscous when pouring the first Al_2O_3-MgO-SiO_2 (18%-18%-64%) slag into the casting mold, most of the slag therefore remained in the crucible when trying to pour it in the mold. In Figure 3.3 a viscosity diagram for the Al_2O_3-MgO-SiO_2 system at 1600˚C is shown. The viscosity of the first slag is marked "1" in the diagram. From the diagram the viscosity of the slag was found to be more than 50 poise. Based on the experimental observation and the position in the diagram in Figure 3.3 this slag was not used in further experiments. The mass transport of boron is most likely to be very slow at this high viscosity. The viscosity of the second Al_2O_3-MgO-SiO_2 slag marked "2" in Figure 3.3 this slag had a viscosity of about 15 poise which is also relatively high.

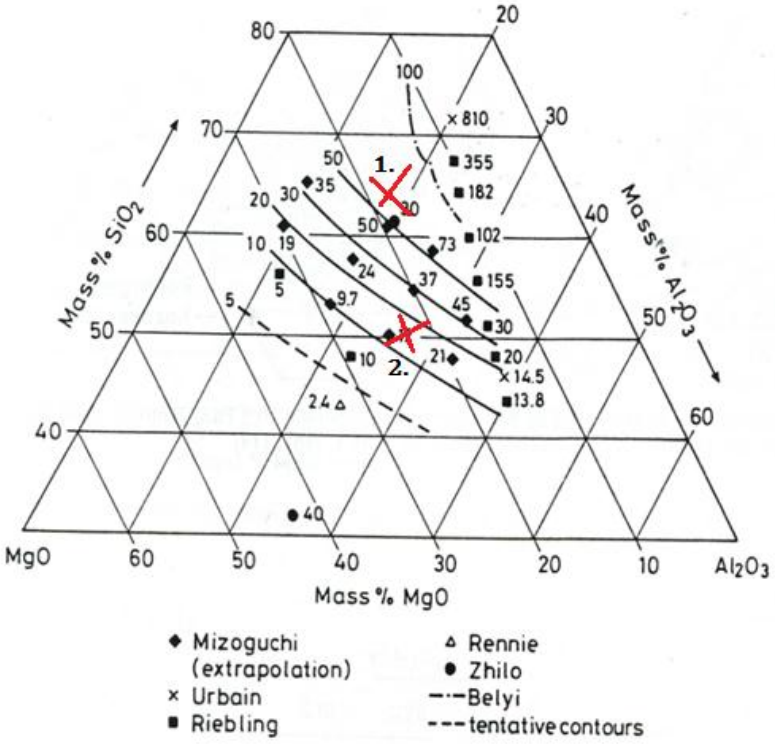

Figure 3.3: Viscosity of the Al_2O_3-MgO-SiO_2 slag at 1600 ˚C. The viscosities of slag 1 and 2 are drawn in the diagram

The viscosities of the two CaO-SiO_2-TiO_2 slags are shown in Figure 3.4 at 1600˚C. Slag 3 had a viscosity of 2.5 poise, while slag 4 had a viscosity of about 1.5 poise.

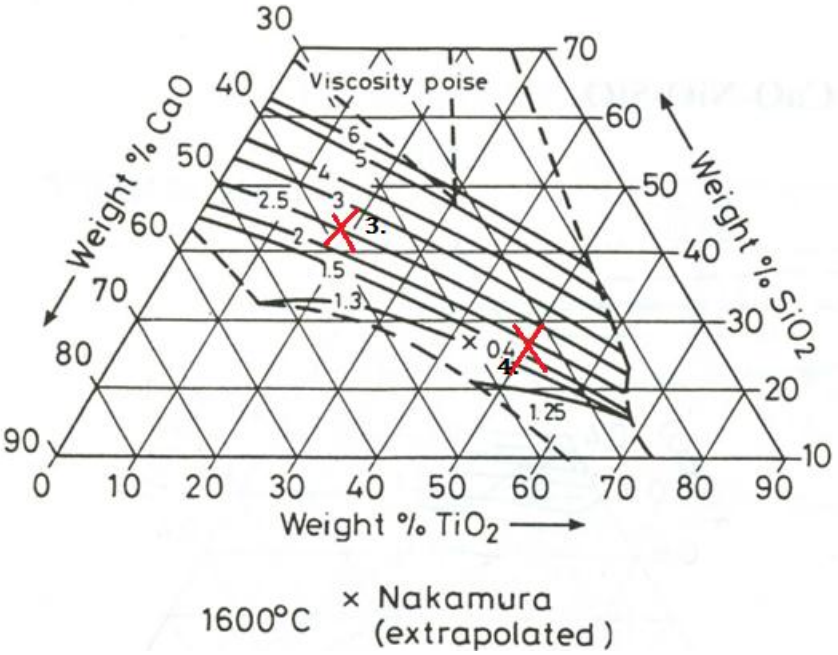

Figure 3.4: Viscosity of the CaO-SiO_2-TiO_2 slag at 1600˚C. The viscosities of slag 3 and 4 are drawn in the diagram.

3.1.2 Experimental procedure

A graphite heat resistance tube furnace was used for refining (Figure 3.5). A B-type thermocouple was used to measure the temperature. The crucible was made from graphite and had a height of 5.4 cm and a diameter of 4.0 cm. Figure 3.6 is a sketch of the inside of the furnace.

Figure 3.5: Graphite heat resistance tube furnace [32]

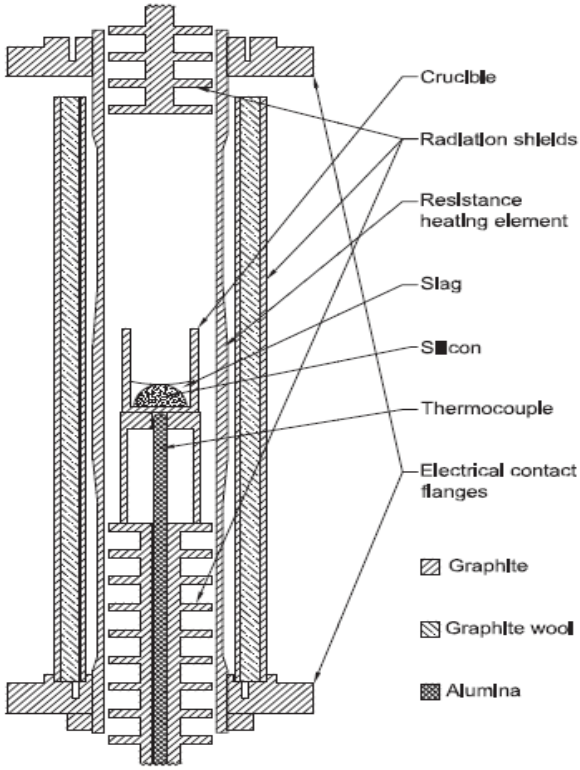

Figure 3.6: Sketch of the inside of the furnace [33]

Before heating, the furnace was emptied for air until a pressure of 0.1 Bar was obtained. Then argon gas was injected to atmospheric pressure to prevent entry of oxygen during the experiment. During the experiments a constant argon flow of about 0.13 l/min was injected from the bottom of the furnace, through the furnace and out on the top. Since silicon does not initially wet carbon materials, fifteen grams of electronic grade silicon was pre melted in a crucible. Molten silicon will then react with carbon to form a SiC layer at the interface between the two phases [34]. This prevents silicon to float up during refining, due to the different densities of slag and silicon, and a straight interface is attained between metal and slag during refining. After pre-melting fifteen grams of slag was added to the crucible. Each of the three slags was melted at 1600 ˚C for 3, 6 and 9 hours. After melting slag and silicon were carefully separated from the crucible and from each other. Any residuals of graphite on the slag or the silicon were polished away by a Dremel polisher. In Figure 3.7a one of the $CaO\text{-}SiO_2\text{-}TiO_2$ samples is shown after the crucible has been removed. In Figure 3.7b the sample is shown after slag and silicon has been separated from each other.

(a) **(b)**

Figure 3.7: $CaO\text{-}SiO_2\text{-}TiO_2$ and silicon after melting. a) A straight interface can be seen between slag and silicon b) Slag and silicon after being separated.

As seen in the pictures the chosen method of pre melting silicon to obtain a straight interface was quite successful.

For each experiment the whole sample was crushed. Three parallels were taken out from all the 26 samples to be analyzed by high resolution Inductively Coupled Plasma Mass Spectrometry (ICP-MS). For determination of the SiO_2 and CaO content in the slag, X-ray fluorescence (XRF) was used.

To confirm the equilibrium distribution of boron between slag and silicon, experiments were also performed where boron was initially added to silicon instead of the slag. One experiment was performed for each of the three systems.

3.1.3 Estimation of mass transfer coefficient

A metal-slag mass transfer coefficient, *k*, was estimated for each of the three systems. To find *k*, Equation (2.33) was used, written in the form as shown in Equation (3.1)

$$\frac{[\%B]-[\%B]_\infty}{[\%B]_{in}-[\%B]_\infty} = \exp(-k't) \quad (3.1)$$

Where k' can be expressed by Equation (3.2):

$$k' = \frac{kA}{V} \quad (3.2)$$

here A represents the reaction area and V is volume of the melt. In the experiments performed, A was estimated using the inner diameter of the crucible and the volume was found by multiplying the area with the height of the melt. The following numbers were used for the three systems:

A = 8.04 cm^2
h = 1.5 cm
V = 12.06 cm^3

The value of $[\%B]_\infty$ was found experimentally for the different systems. By using the solver tool in Excel, the *k* value that gave the smallest deviation between the experimental and the calculated boron concentration in silicon was found. An example is shown for the Al_2O_3-MgO-SiO_2 system:

$[\%B]_{in}$= 0 ppm
$[\%B]_\infty$ = 48 ppm

Table 3.2: Estimation of *k* for the Al_2O_3-MgO-SiO_2 (27%-23%-50%) system

t (h)	Experimental B (ppm)	Calculated B (ppm)	Deviation $(B_{Exp} - B_{Calc})^2$
0	0	0	0
3	41.8	38.7	9.49
6	44.9	46.2	1.71
9	47.7	47.7	0.00220
		Sum	11.19

k' = 1.52x10^{-4} 1/s
k = 2.28x10^{-6} m/s

For the calculations of *k* for the two CaO-SiO_2-TiO_2 slags see *Appendix I.*

3.1.4 Experimental plan

In Table 3.3 an overview of the experiments is shown. All the experiments were carried out at 1600˚C, with equal amounts of slag and silicon (15 g). In experiment 1-9, boron was initially added to the slag phase. One experiment was repeated for each system where boron was initially added to the silicon phase, these are experiment 10-12.

Table 3.3: Experiments performed for determination of the distribution coefficient of boron.

Experiment no.	Slag	Composition	Time (h)	$(B)_{in}$ (ppm)	$[B]_{in}$ (ppm)
1	Al_2O_3-MgO-SiO_2	27%-23%-50%	3	139.4	0
2			6	139.4	0
3			9	139.4	0
4	CaO-SiO_2-TiO_2	39%-43%-18%	3	82.4	0
5			6	82.4	0
6			9	82.4	0
7	CaO-SiO_2-TiO_2	24%-27%-49%	3	79.1	0
8			6	79.1	0
9			8	79.1	0
10	Al_2O_3-MgO-SiO_2	27%-23%-50%	6	0	92.3
11	CaO-SiO_2-TiO_2	39%-43%-18%	3	0	92.3
12	CaO-SiO_2-TiO_2	24%-27%-49%	3	0	92.3

3.2 Evaporation of boron in hydrogen atmosphere

3.2.1 Preparation of slag

CaO-SiO_2 slag with a CaO/SiO_2 mass ratio of about 1.2 was weighted out. The same procedure as described in 3.1.1 was followed for homogenization of the slag.

3.2.2 Experimental procedure

The same furnace was used as described in 3.1.2. In addition to pure argon gas a mixture of 50% argon and 50% hydrogen was injected from the top of the furnace and purged on the sample surface with a flow rate of about 0.5 l/min. The diameter of the injection tube was 7 mm. Three series of experiments were performed. In series 1 and 2 slag with an initial boron concentration of about 100 ppm was refined. In series 3, slag without boron was melted together with pre melted electronic grade silicon doped with about 100 ppm of boron. Graphite crucibles were used in all the experiments. The experimental series are summarized in Table 3.4.

Table 3.4: Experimental series performed in hydrogen atmosphere

	Variable	Temperature (˚C)	Refining time (h)	Amount slag/silicon (g)
Series 1	Temperature	1500, 1550, 1600	3	15g/0g
Series 2	Time	1600	0-6	15g/0g
Series 3	Amount of slag	1600	3	3.8g/15g, 7.5g/15g, 11.3g/15g, 15g/15g, 22.5g/15g

3.2.3 Experimental plan

In Table 3.5 an overview over all the experiments is shown. In Series 1 and 2 slag with a CaO/SiO_2 mass ratio of 1.21 was used. In Series 3 the CaO/SiO_2 mass ratio was 1.25.

Table 3.5: Experiments performed in hydrogen atmosphere

Experiment no.	Series	Temp. (˚C)	Time (h)	Slag/silicon (g)	$(B)_{in}$ (ppm)	$[B]_{in}$ (ppm)
13	1	1500	3	15 g/0 g	84.5	-
14	1	1550	3	15 g/0 g	84.5	-
15	1	1600	3	15 g/0 g	84.5	-
16	2	1600	0.1	15 g/0 g	84.5	-
17	2	1600	1	15 g/0 g	84.5	-
18	2	1600	2	15 g/0 g	84.5	-
19	2	1600	3	15 g/0 g	84.5	-
20	2	1600	4	15 g/0 g	84.5	-
21	2	1600	5	15 g/0 g	84.5	-
22	2	1600	6	15 g/0 g	84.5	-
23	3	1600	3	3.8 g/15 g	0	92.3
24	3	1600	3	7.5 g/15 g	0	92.3
25	3	1600	3	11.3 g/15 g	0	92.3
26	3	1600	3	15 g/15 g	0	92.3
27	3	1600	3	22.5 g/15 g	0	92.3

3.3 Temperature profile

The temperature profile of the furnace is shown in Figure 3.8. The figure shows the temperature in the furnace as a function of the distance from the bottom radiation shield, as shown in Figure 3.6.

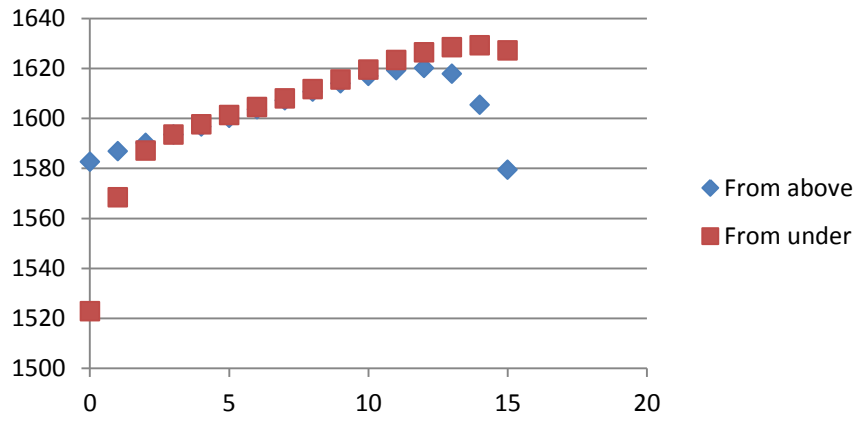

Figure 3.8: Temperature profile of the graphite heat resistance furnace [35]

The samples in experiment 1-27 were placed 4 cm above the bottom radiation shield, at this position the temperature was found to be 1598˚C from Figure 3.8. The crucible height was 5.4 cm; the temperature gradient in the crucible area was therefore 3.3˚C/cm.

3.4 Analysis techniques

3.4.1 ICP-MS

Inductively Coupled Plasma Mass Spectrometry (ICP-MS) is an analytical technique used for determination of element concentrations. In ICP-MS a high temperature ICP source is combined with a mass spectrometer. The elements in the sample are converted to ions by the ICP source and the ions are further separated by mass and then detected by the mass spectrometer. The plasma ion source (Argon) has a temperature of about 6 000-10 000 K, and the samples are almost completely ionized. When the ions reach the mass spectrometer they are separated by their mass to charge ratio (m/e). Only a single mass to charge ratio is allowed to pass through the detector at a given time period [36].

The ICP-MS technique can be used for determination of the concentration of most of the elements in the periodic table. The detection limit for the different elements is shown in Figure 3.9. For boron this is in the range 0.1-1 ppb. The ions formed by the ICP source are typically positively charged as M^+ or M^{2+}. Elements preferring to ionize with a negative charge such as Cl, I and F are therefore very difficult to detect by the ICP-MS instrument. Furthermore the sample has to be in solution. A solid sample, such as slag, must therefore be dissolved in acid or acid mixtures before it can be analyzed. The main advantages of the ICP-MS are the simple sample introduction, sensitivity and the high speed of analysis [36].

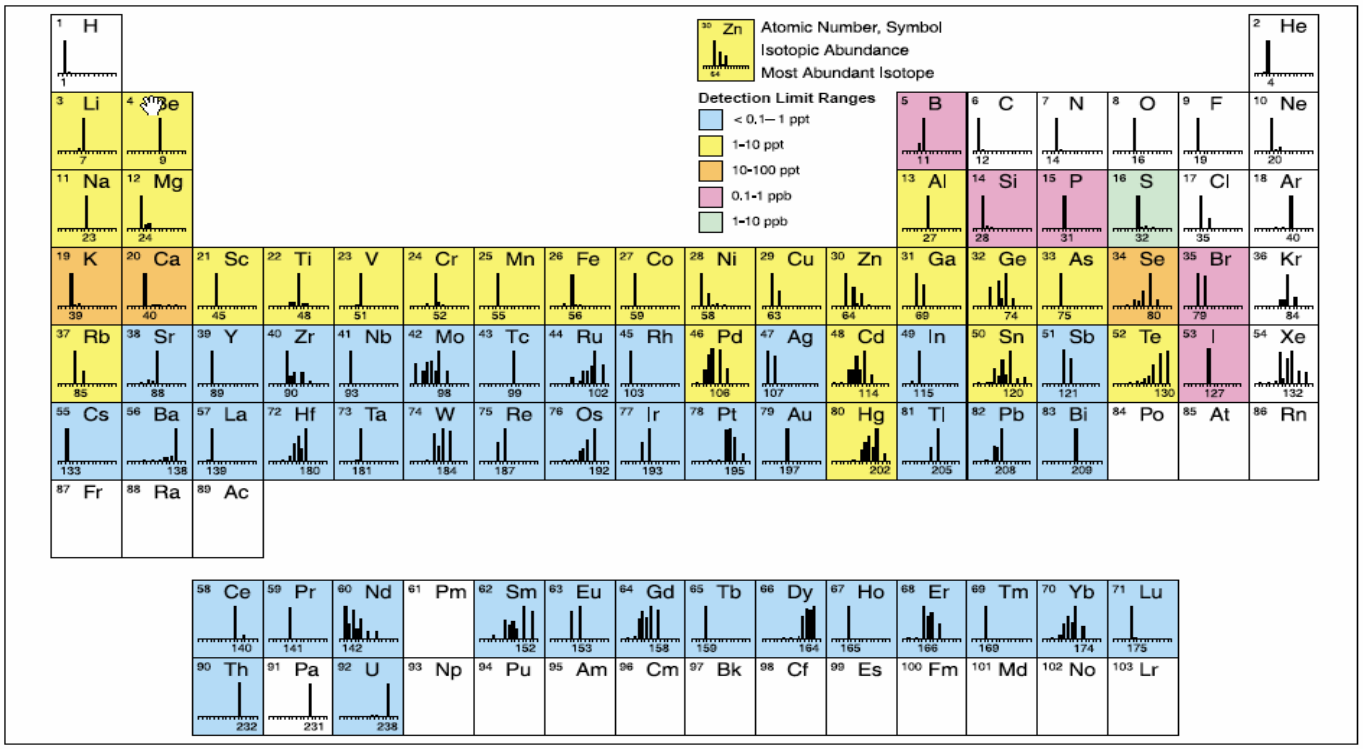

Figure 3.9: Elements that can be detected by ICP-MS and approximate detection limits [36]

3.4.2 XRF

X-ray fluorescence (XRF) is typically used for bulk analysis of larger fractions of geological materials. The method is based on the behavior of atoms when they are exposed to radiation. The atoms in the sample are excited by bombarding it with high energy x-rays. When the excited electrons fall back to its ground state radiation is emitted and the radiation is characteristic for the atom present. Fluorescence is a phenomenon where absorption of radiation of a specific energy is followed by re-emission of radiation with lower energy. The resulting fluorescent x-ray can be used for determination of the elements present in the sample. The abundance of an element in the sample is determined by the intensity of the energy detected.

The XRF spectrometer is easy to use, the preparation of samples is relatively simple and inexpensive, and the technique is therefore used in a wide range of applications. Although XRF has the ability to detect x-rays from most of the elements, the detection is limited when it comes to precise and accurate measure the abundance of elements with Z<11. Furthermore, the method is limited when it comes to distinguish between different isotopes of an element [37].

4. Results

4.1 Distribution of boron between slag and silicon

The distribution coefficient of boron was measured for three different systems. Three experiments were performed with 1 slag composed of Al_2O_3-MgO-SiO_2 (experiment 1-3) and 2 slags composed of CaO-SiO_2-TiO_2 (experiment 4-6 and 7-9), respectively. For each of the experiments 1-9 boron was initially added to the slag phase. One additional experiment was performed for each system where boron initially was added to the silicon phase (experiment 10-12).

4.1.1 Al_2O_3-MgO-SiO_2

The composition of the Al_2O_3-MgO-SiO_2 slag was determined by X-ray fluorescence (XRF). In Table 4.1 the initial slag composition and the composition in experiment 1-3 after 3, 6 and 9 hours, respectively, are shown. We notice that only a small change in the slag composition after 9 hours has occurred.

Table 4.1: Composition of the Al_2O_3-MgO-SiO_2 slag analyzed by XRF

	Initially (%)	**3h (%)**	**6h (%)**	**9h (%)**
Al_2O_3	27.3	27.5	28.2	28.8
MgO	22.7	22.8	23.1	23.4
SiO_2	50.0	49.7	48.7	47.9

The boron content in both silicon and slag was analyzed by High resolution ICP-MS. In Figure 4.1 the boron concentration in silicon and slag is plotted as a function of time for experiment 1-3. The curve tends to be flat after 3 hours which indicates that the system is close to equilibrium with respect to boron.

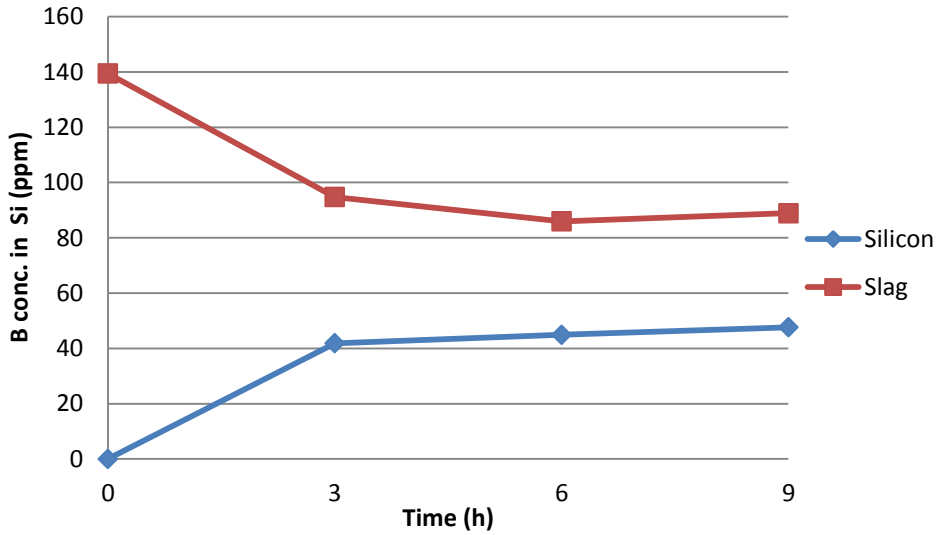

Figure 4.1: Boron concentration in silicon and Al_2O_3-MgO-SiO_2 slag as a function of time

In Figure 4.2, the distribution of boron between metal and slag found from Equation 2.1 is plotted as a function of time. After 9 hours the distribution coefficient of boron was found to be 1.9.

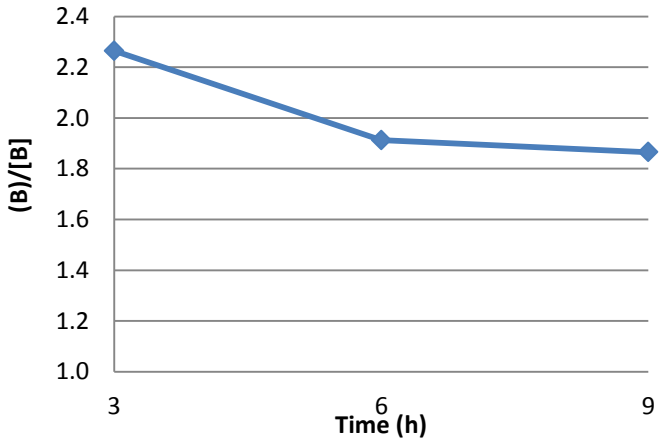

Figure 4.2: The distribution of boron between silicon and Al_2O_3-MgO-SiO_2 slag after 3, 6 and 9 hours

In Figure 4.3 the concentration of boron in silicon found experimentally is plotted together with the calculated values. The mass transfer coefficient, *k*, of the Al_2O_3-MgO-SiO_2 system was estimated using Equation (3.1) and the method of least squares. The calculations was shown under 3.1.3, based on these *k* was found to be 2.3×10^{-6} m/s.

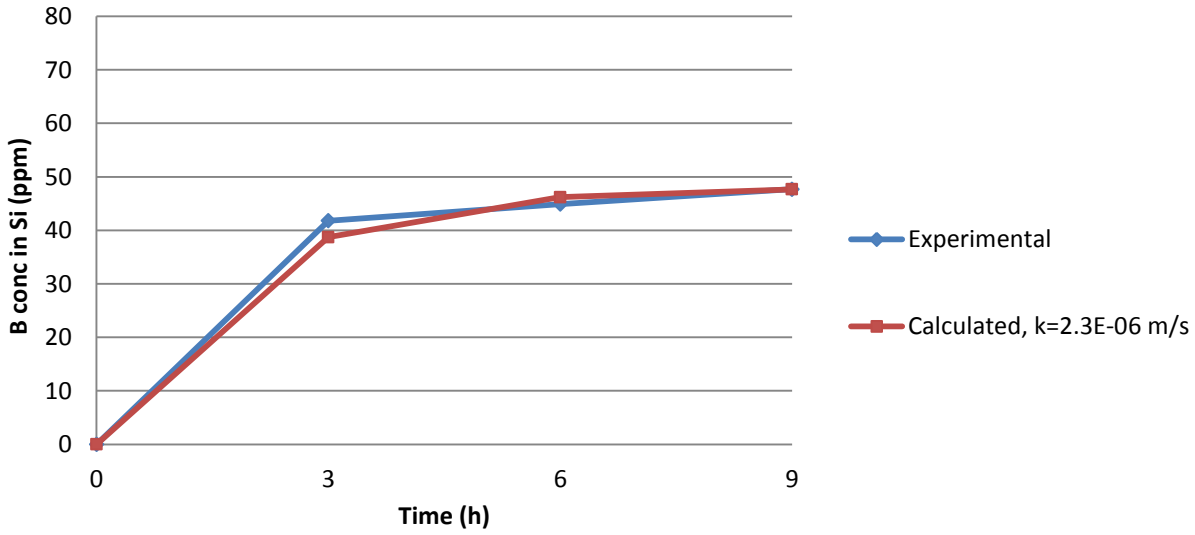

Figure 4.3: Boron content in silicon as a function of time found experimentally and calculated using k=2.3x10^{-6} m/s

In Table 4.2 the concentration of Al and Mg in silicon after 9 hours is shown. The concentrations were found by High resolution ICP-MS. The reduction of Al_2O_3 and MgO is described by Equation (4.1) and (4.2):

$$4Al + 3SiO_2 = 2Al_2O_3 + 3\,Si \tag{4.1}$$

$$2Mg + SiO_2 = 2MgO + Si \tag{4.2}$$

From the Slag Atlas the activity of SiO_2, Al_2O_3 and MgO in the slag at 1600 ˚C was found to be 0.68, 0.5 and 0.14, respectively [6]. In Equation (2.8) the activity was expressed by the molar fraction of the respective substances, x_i, and the activity coefficient, γ_i. Based on Equation (2.8), and the equilibrium constants, K, to the reactions in Equation (4.1) and (4.2), we can find an expression for the activity coefficients γ_{Al} and γ_{Mg} in silicon:

$$\gamma_{Al} = \sqrt[4]{\frac{a_{Al_2O_3}^2 a_{Si}^3}{K_1 a_{SiO_2}^3}} \frac{1}{x_{Al}} \tag{4.3}$$

$$\gamma_{Mg} = \sqrt{\frac{a_{MgO}^2 a_{Si}}{K_2 a_{SiO_2}}} \frac{1}{x_{Mg}} \tag{4.4}$$

The equilibrium constants, K_1 and K_2 were found from the thermodynamic software Fact Sage [38]. In Equation (4.3) and (4.4) x_{Al} and x_{Mg} is the molar fraction of Al and Mg in silicon at equilibrium. Due to the small impurity concentrations in Si, the activity of Si is assumed to be

unity. It is also assumed that coexisting magnesium in silicon does not affect the activity coefficient of aluminum and vice versa. The results are shown in Table 4.2.

Table 4.2: Content of Al and Mg in silicon after 9 hours analyzed by ICP-MS, and activity coefficients at 1600 ˚C

	Content	γ_i
Al	0.35%	0.60
Mg	0.24%	0.50

In figure 4.4 the aluminum and magnesium concentration in silicon is shown after 3, 6 and 9 hours. The figure shows a continuous increase in the Al and Mg content in Si with increasing refining time.

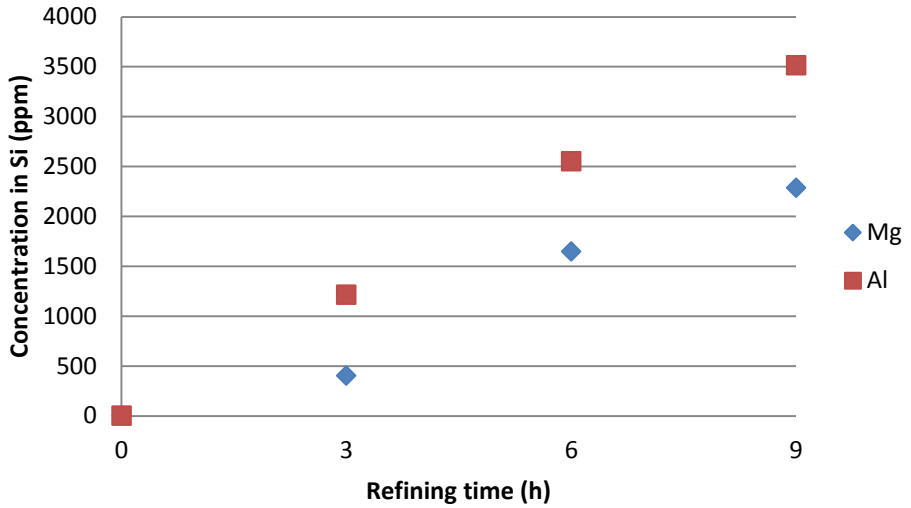

Figure 4.4: Al and Mg concentration in Si

4.1.2 CaO-SiO_2-TiO_2

Experiments were performed for two different compositions of the CaO-SiO_2-TiO_2 slag:

- Slag 1: CaO-SiO_2-TiO_2 (38.8 %, 42.6%, 18.6%)
- Slag 2: CaO-SiO_2-TiO_2 (24.0 %, 26.6%, 49.4%)

Slag 1:

The results from the XRF-analysis of the slag in experiment 4-6 are shown in Table 4.3.

Table 4.3: Composition of the CaO-SiO_2-TiO_2 slag (Slag 1) analyzed by XRF

	Initially (%)	3h (%)	6h (%)	9h (%)
CaO	38.8	41.8	44.0	46.1
SiO_2	42.6	58.0	55.9	53.8
TiO_2	18.6	0.3	0.2	0.1

After 3 hours there was almost no TiO_2 left in the slag, and consequently only the binary CaO-SiO_2 slag remains. Also the CaO/SiO_2 mass ratio changed during the experiments. Titanium oxide is reduced after Equation (4.5):

$$TiO_2 + Si = SiO_2 + Ti \quad (4.5)$$

From Equation (4.5) it is shown that the concentration of SiO_2 in the slag increases as TiO_2 is reduced. SiO_2 can react with silicon under the formation of SiO gas, as shown in Equation (4.6):

$$SiO_2 + Si = 2SiO\ (g) \quad (4.6)$$

In Table 4.4 the Ti content in silicon after 3, 6 and 9 hours is listed. We notice that we have a large increase in the Ti content in silicon.

Table 4.4: Ti concentration in silicon after 3, 6 and 9 hours (Slag1) analyzed by ICP-MS

	3h	**6h**	**9h**
Ti	9.6 wt%	9.7 wt%	10.7 wt%

In Figure 4.5 the change in boron concentration with time is plotted for slag and silicon, respectively, in experiment 4-6. The curve for the boron concentration in both slag and silicon tends to be horizontal after 3 hours which indicates that the system has reached equilibrium. Since most of TiO_2 has been reduced within 3 hours as previously shown, the slag phase in Figure 4.5 can be considered as the binary CaO-SiO_2 slag system. Furthermore, Table 4.4 shows the Ti concentration in silicon to be about 11%. Therefore, the system in Figure 4.5 can be regarded as a CaO-SiO_2 slag in equilibrium with silicon containing approximately 11% titanium after 3 hours.

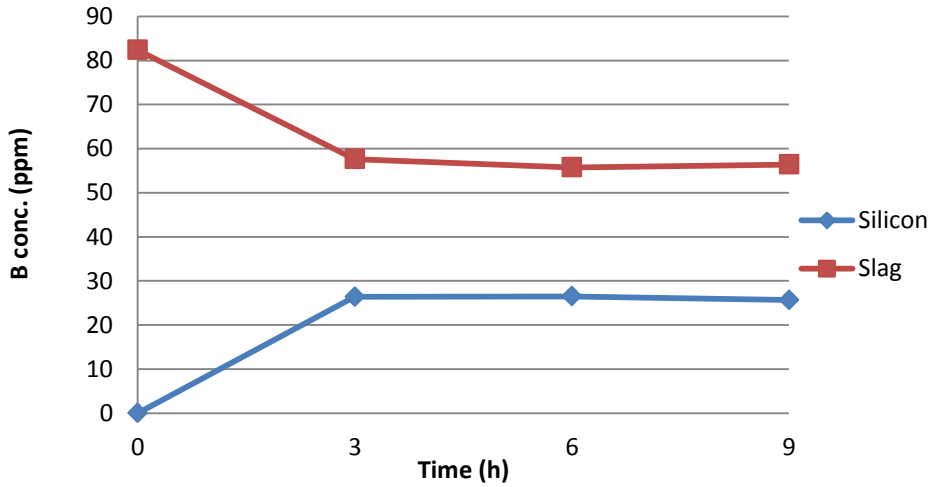

Figure 4.5: Amount of B in the initial CaO-SiO_2-TiO_2 slag, and in the CaO-SiO_2 slag in equilibrium with Si + 11 % Ti

Figure 4.6 shows the corresponding distribution coefficient of boron. After 9 hours the distribution coefficient was found to be 2.2.

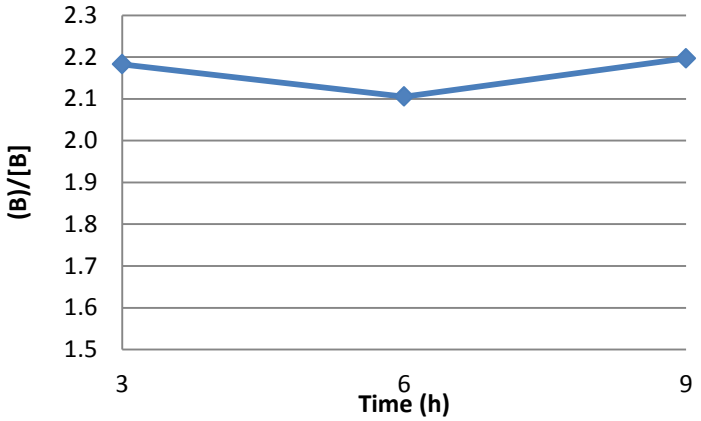

Figure 4.6: The distribution of boron between Si + 11 % Ti and CaO-SiO_2 slag after 3, 6 and 9 hours

The L_B values in Figure 4.6 were obtained for a system containing considerable amounts of Ti in silicon; the activity of silicon is therefore no longer unity for the system and the value of L_B can therefore not be directly compared to a CaO-SiO_2 –Si system. In Equation (2.11) an expression for the distribution coefficient of boron was derived. If the activity of silicon no longer is unity, L_B can be expressed by Equation (4.7):

$$L_B = \frac{K\gamma_B a_{SiO_2}^{3/4}}{\gamma_{BO_{1.5}} a_{Si}^{3/4}} k_{\%\rightarrow x} \tag{4.7}$$

If γ_B is assumed to be constant, a_{Si} will be the only changing parameter in L_B for a given slag composition and temperature. If the value of L_B in a CaO-SiO_2 – Si-Ti system is *x*, then L_B for the corresponding CaO-SiO_2 –Si system can be calculated from Equation (4.8):

$$L_B = x a_{Si}^{3/4} \tag{4.8}$$

The thermodynamic software FactSage was used to find the activity of silicon in the Si-Ti alloy. The activity of silicon containing 11 wt% Ti was found to be 0.97 at 1723 K, and the value of x was found to be 2.2 from Figure 4.6. The value of the corresponding CaO-SiO_2 - Si system is then 2.1, according to Equation (4.8).

The mass transfer coefficient for this system was found by using the same procedure as for the Al_2O_3-MgO-SiO_2 system. In Figure 4.7 the boron concentration in silicon found experimentally has been plotted together with the calculated values. In this case the value of *k* was found to be 5.2×10^{-6} m/s. For more details regarding the calculations see *Appendix I.*

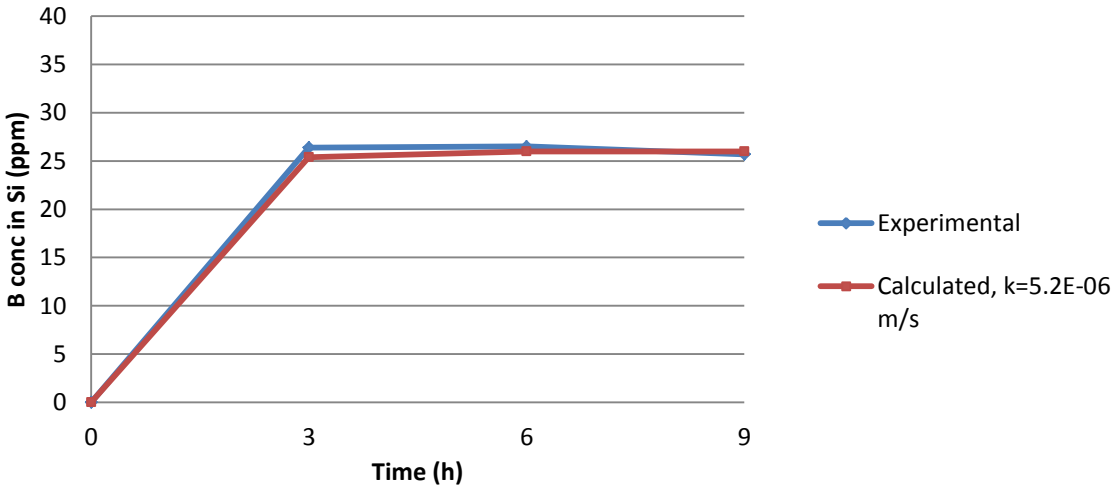

Figure 4.7: B content in Si as a function of time found experimentally and calculated using k=5.2x10^{-6} m/s

Slag 2:

The composition of the CaO-SiO_2-TiO_2 slag in experiment 7-9 found from XRF is shown in Table 4.5

Table 4.5: Composition of the CaO-SiO_2-TiO_2 slag after 3, 6 and 8 hours refining time (Slag 2), analyzed by XRF

	Initially (%)	3h (%)	6h (%)	8h (%)
CaO	24.0	24.7	26.5	29.6
SiO_2	26.6	50.4	52.6	65.8
TiO_2	49.4	24.9	20.9	4.6

Also in these experiments the TiO_2 concentration in the slag was considerably reduced. The concentration of SiO_2 was more than doubled as a result of oxidation of silicon after Equation 4.5. After 8 hours there was about 5 % TiO_2 left in the slag. In Table 4.6 the Ti concentrations in silicon after 3, 6 and 8 hours, respectively, are listed.

Table 4.6: Ti concentration in silicon after 3, 6 and 8 hours (Slag 2), analyzed by ICP-MS

	3h	6h	8h
Ti (µg/g)	12.6%	16.1%	21%

After 8 hours the silicon phase contained 21 % Ti. This phase was in equilibrium with a CaO-SiO_2-TiO_2 slag with the composition shown in Table 4.5. The change in boron concentration with time for the system is shown in Figure 4.8. Also this system seemed to approach equilibrium after 3 hours, but compared to Slag 1 the boron concentration in silicon was higher.

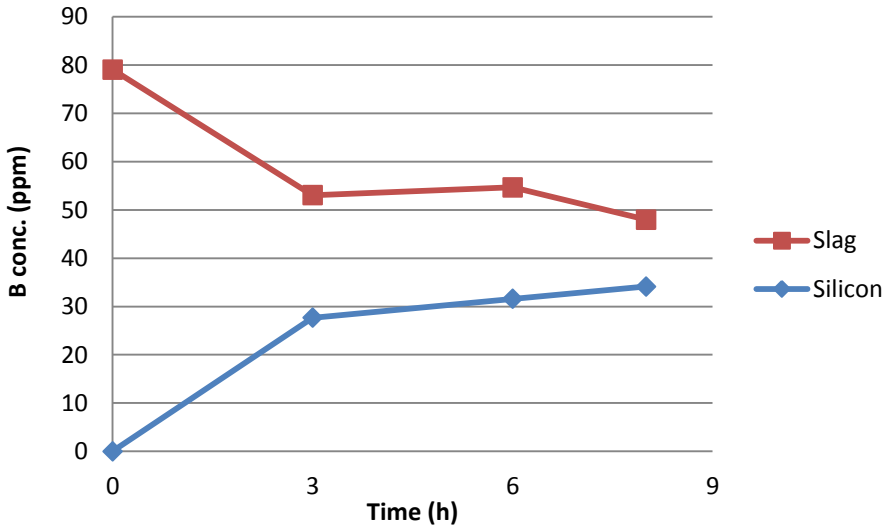

Figure 4.8: Boron concentration in the $CaO\text{-}SiO_2\text{-}TiO_2$ slag and Si+Ti as a function of time

The distribution coefficient of boron is plotted in Figure 4.9 as a function of time. After 8 hours refining time the distribution coefficient was found to be 1.4.

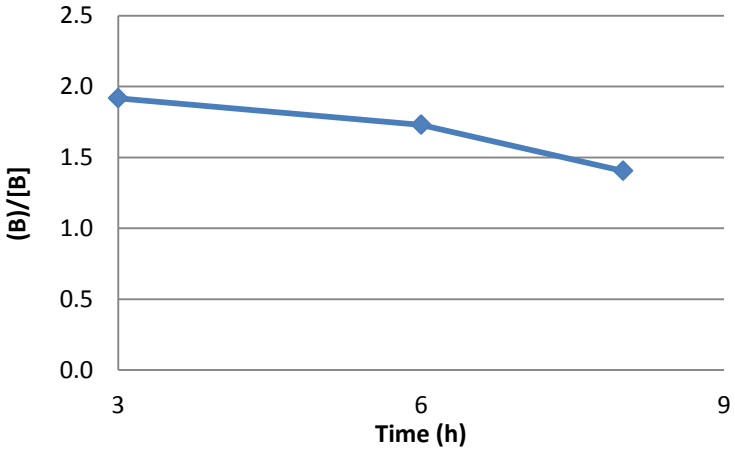

Figure 4.9: The distribution of boron between silicon and $CaO\text{-}SiO_2\text{-}TiO_2$ slag after 3, 6 and 8 hours

In Figure 4.10 the calculated and the experimental boron concentration in silicon is plotted as a function of time. The mass transfer coefficient for the system was found to be 2.0×10^{-6} m/s. For more details regarding the calculations see *Appendix I*.

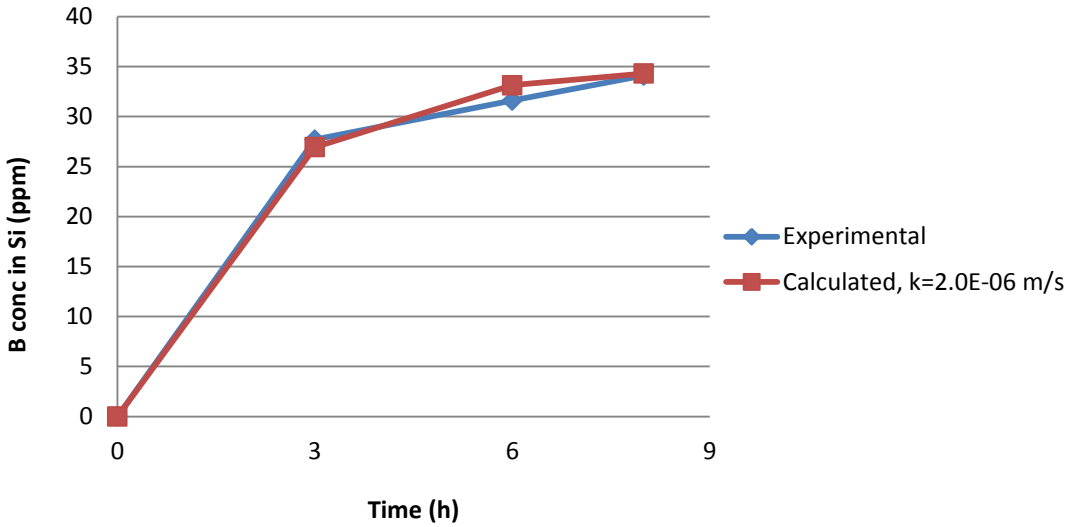

Figure 4.10: B content in Si as a function of time found experimentally and calculated using $k=1.8x10^{-6}$ m/s

4.1.3 Distribution coefficient: Boron in silicon

The distribution coefficient was also measured for the three system with boron initially added to the silicon phase. The refining time was 3 hours for the two $CaO\text{-}SiO_2\text{-}TiO_2$ slags and 6 hours for the $Al_2O_3\text{-}MgO\text{-}SiO_2$ slag. The L_B values found are listed in Table 4.7.

Table 4.7: Boron content in slag and Si (analyzed by ICP-MS) and L_B. Boron was initially added to Si

	(B) (ppm)	[B] (ppm)	L_B
$Al_2O_3\text{-}MgO\text{-}SiO_2$	109	60	1.8
$CaO\text{-}SiO_2\text{-}TiO_2$ (Slag 1)	57	28	2.0
$CaO\text{-}SiO_2\text{-}TiO_2$ (Slag 2)	49	34	1.4

4.2 Evaporation of boron in hydrogen atmosphere

Three series of experiments were performed. In Series 1 the effect of temperature on the boron evaporation rate was investigated (experiment 13-15), in Series 2 the rate of boron evaporation was investigated (experiment 16-22) and in Series 3 boron evaporation in a system containing both slag and silicon was investigated.

4.2.1 Observations

In Series 3 a lump of silicon was observed on the sample surface surrounded by slag. In Figure 4.11 this is shown for experiment 26, where equal amounts of slag and silicon were used. Figure 4.12 shows a cross section of the crucible in experiment 25 after refining; we can see that that the silicon lump constitutes a three phase silicon-slag-silicon area.

Figure 4.11: Experiment 26 after refining (Slag/Si = 1)

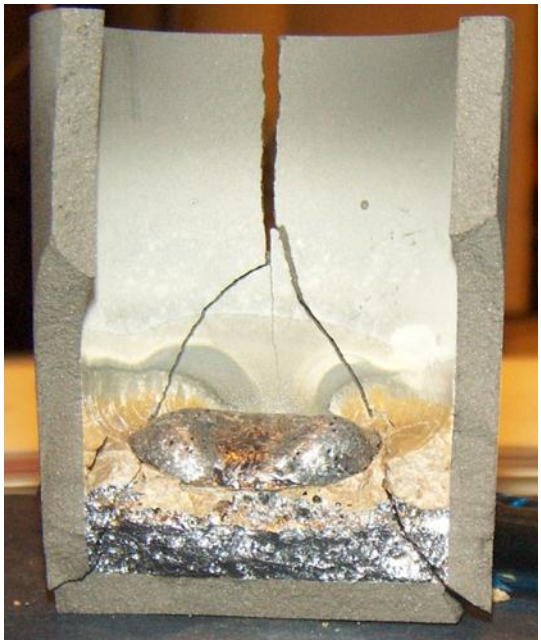

Figure 4.12: Cross section of experiment 25 (Slag/Si =0.75)

4.2.2 Series 1

The effect of temperature on boron evaporation from $CaO\text{-}SiO_2$ slag was investigated through experiment 13-15, a silicon phase was not involved in the experiments. The refining time was 3 hours and the initial boron concentration in the slag was 84.5 ppm. The results are shown in Table 4.8.

Table 4.8: Effect of temperature on boron evaporation

Experiment no.	Temperature (˚C)	B concentration (ppm)	Evaporated Boron (g)	Evaporated boron (%)
13	1500	66.8	0.00027	21
14	1550	60.8	0.00036	28
15	1600	62.3	0.00033	26

From Table 4.8 we notice the differences between the remaining boron concentrations in the slag after refining at different temperatures to be small. Although the boron concentration in silicon at the higher temperatures are slightly lower than at 1500˚C.

4.2.3 Series 2

The effect of refining time was investigated at 1600˚C through experiment 16-22, a silicon phase was not involved in the experiments. The results are shown in Figure 4.13. The figure shows that the boron concentration in the $CaO\text{-}SiO_2$ slag decreases with increasing refining time in a linear manner indicating that boron evaporates from the system.

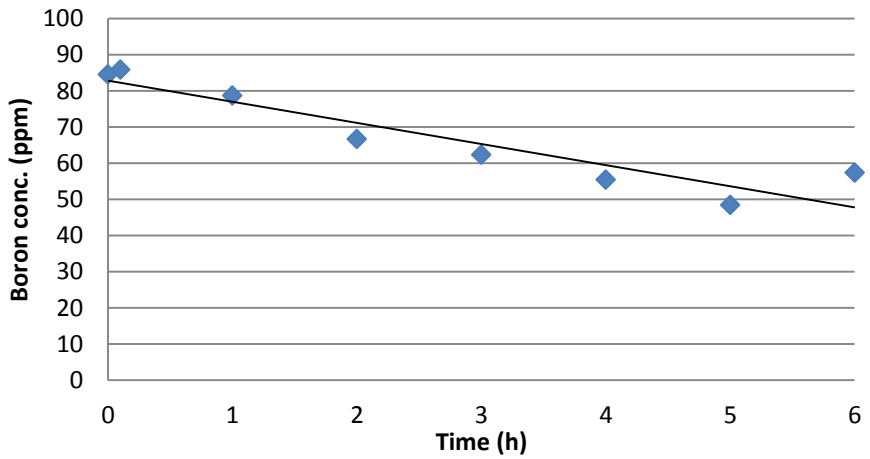

Figure 4.13: Boron concentration in slag as a function of time

In Table 4.9 the amount of evaporated boron after 1-6 hours found from Figure 4.13 is shown.

Table 4.9: The amount of evaporated boron from the slag after 1-6 hours

Experiment no.	Refining time (h)	Evaporated boron (g)	Evaporated boron (%)
17	1	0.00009	7
18	2	0.00027	21
19	3	0.00033	26
10	4	0.00044	35
21	5	0.00054	43
22	6	0.00041	32

The evaporation rate of boron can be found from Equation (2.32), in Figure 4.14 $Ln(B)/(B)_0$ is plotted as a function of the refining time (A/V*t). The value of A/V is the same as in Equation (3.2). The value of the mass transfer coefficient, *k*, is therefore the negative value of the slope in Figure 4.14.

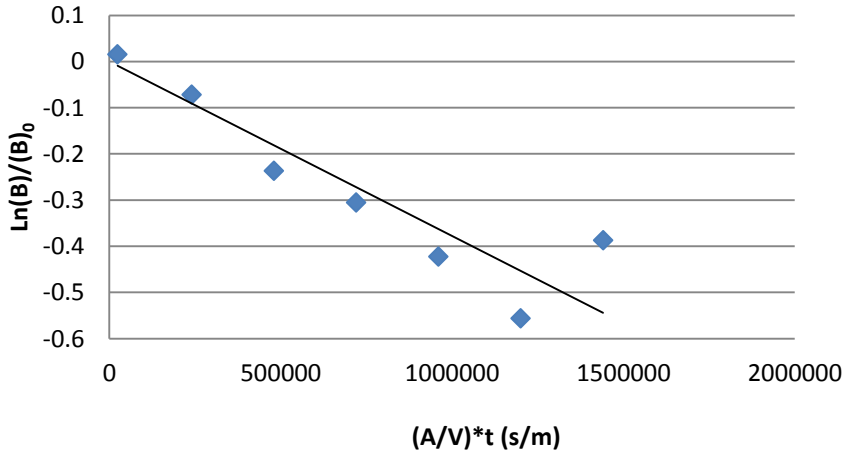

Figure 4.14: The logarithm of the boron content, $(B)/(B)_0$,as a function of (A/V)*t

In Figure 4.14 the points follows a linear trend which means that the boron evaporation follows first order kinetics. The mass transfer coefficient *k* was found from the slope of the trend line giving a value of $4*10^{-7}$ m/s.

In Table 4.10 the change in slag composition for the CaO-SiO_2 slag is shown after 3 and 6 hours.

Table 4.10: Slag composition after 0, 3 and 6 hours, respectively.

	Initial	**3h**	**6h**
CaO	54.8	57.5	60.5
SiO_2	45.2	42.5	39.5
CaO/SiO_2	1.21	1.35	1.53

The CaO/SiO_2 mass ratio increases with increasing time, which could be explained by the formation of SiO gas after Equation (4.9):

$$2SiO_2 + SiC = 3SiO(g) + CO(g) \quad (4.9)$$

4.2.4 Series 3

The effect of varying the slag/metal mass ratio of a system containing boron doped silicon and CaO-SiO_2 slag was investigated through experiment 23-27. The initial boron concentration in silicon was 92.3 ppm, the refining time was 3 hours and the temperature was 1600˚C. In Figure 4.15 the remaining boron concentration in silicon and slag, respectively, as a function of the slag/silicon mass ratio is shown.

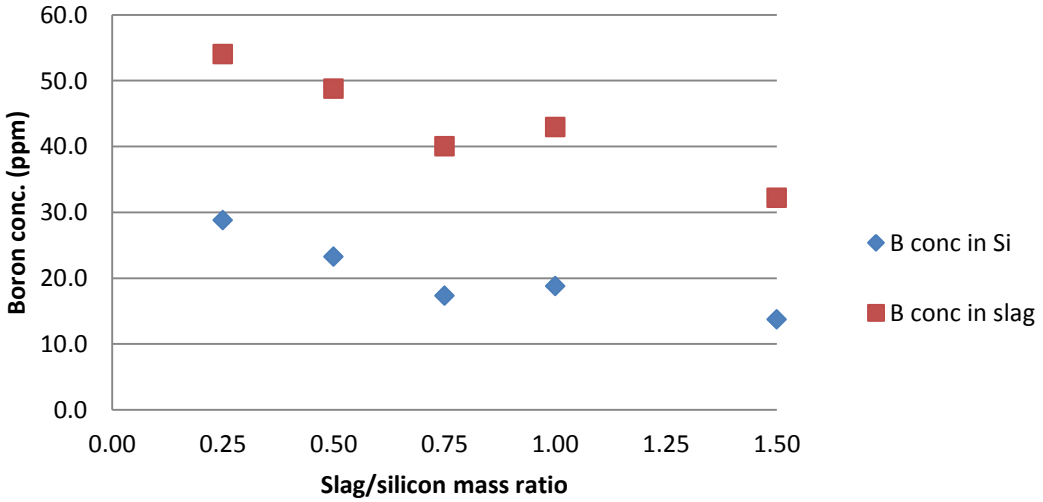

Figure 4.15: Boron concentration in silicon and slag as a function of the mass ratio of slag and silicon

In Figure 4.15 it is shown that amount of boron removed from silicon increases with increasing slag/silicon mass ratio. For a slag/silicon mass ratio of 1.5 the amount of boron in silicon is reduced from 92.3 ppm to 13.7 ppm after 3 hours.

The system contained 15 gram of boron doped electronic grade silicon. Since the initial boron concentration in silicon was 92.3 ppm, the initial amount of boron in the system was 0.00138 gram. The amount of evaporated boron can be calculated by subtracting the amount of remaining boron in silicon and slag from the initial value, the results are shown in Table 4.11.

Table 4.11: The amount of boron evaporated from the system after 3 hours for different slag/silicon mass ratios

Experiment no.	Slag/Si mass ratio	Evaporated boron (g)	Evaporated boron (%)
23	0.25	0.00075	54
24	0.5	0.00067	48
25	0.75	0.00068	49
26	1.0	0.00046	33
27	1.5	0.00045	32

In Table 4.11 a decreasing trend in the evaporation rate of boron with increasing slag/silicon mass ratio is shown. In Table 4.12 the relation between the evaporated amount of boron and the boron concentration in the slag has been compared using experiment 23 as a reference. The amount of evaporated boron is shown to increase with increasing boron concentration in the slag.

Table 4.12: Relation between the boron content in slag and the evaporated boron relative to experiment 23.

Experiment no.	B conc. in slag (% of reference)	Evaporated B (% of reference)
24	90	89
25	74	91
26	79	61
27	59	60

In Figure 4.16 the distribution coefficient of boron is shown for the $CaO\text{-}SiO_2$ – Si system. The evaporated boron was not taken into account in this figure. A small increase in L_B with increasing slag/silicon mass ratio was observed until a value of 2.3 was reached for a slag/silicon mass ratio of 0.75.

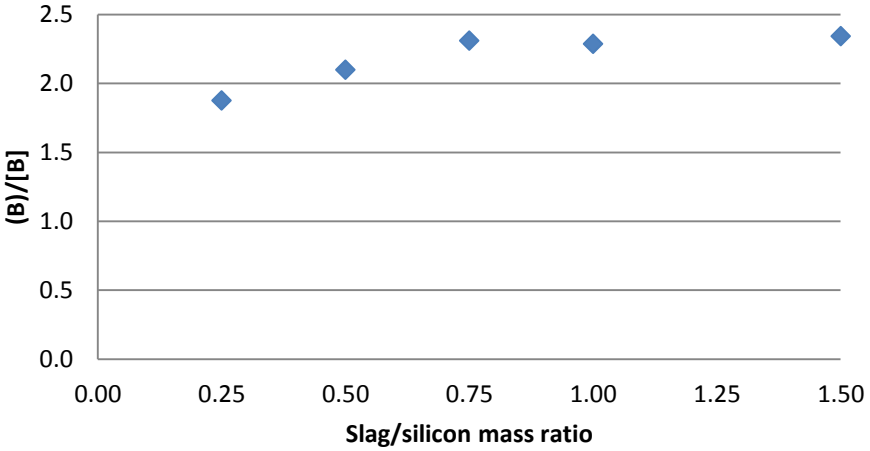

Figure 4.16: Distribution of boron between Si and CaO-SiO_2 slag

In Figure 4.17 the distribution coefficient of boron is shown after boron has evaporated from the slag. The amount of evaporated boron is added to the amount of boron in the slag and then divided by the amount of boron in silicon. A decreasing trend in the distribution coefficient of boron with increasing slag/silicon mass ratio is shown. The highest coefficient was obtained for a slag/silicon mass ratio of 0.25, and was found to be 8.8.

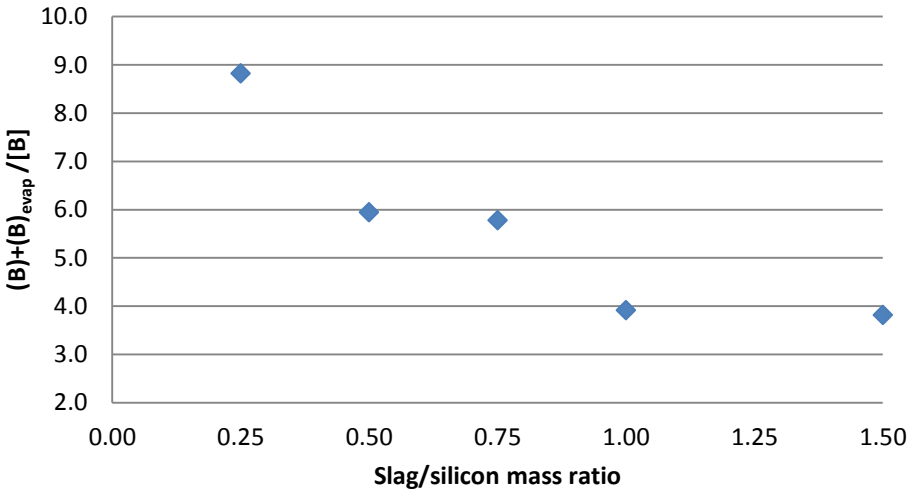

Figure 4.17: The distribution of boron between Si and CaO-SiO_2 slag when refined in hydrogen atmosphere

In Table 4.13 the change in slag composition after 3 hours is shown. After 3 there has only been a small change in the slag composition.

Table 4.13: Slag composition after 0 and 3 hours

	Initial	**3 h**
CaO	55.5	56.1
SiO_2	44.5	43.9
CaO/SiO_2	1.25	1.28

4.3 Uncertainty in analysis method

4.3.1 Reference material

The boron concentration in the reference material Diabase W-2 from United States Geological Survey was analyzed together with the slag samples. Diabase W-2 consist mainly of augite and plagioclase, but also smaller amounts of quartz, potassium feldspar, biotite and opaque minerals [39]. The reference material has a certified boron concentration of 12.0 ppm. For the boron concentration in silicon reference material 57b was used from the National Institute of Standards and Technology. This reference material consists of refined silicon with certified values of different elements [40]. The certified value of boron is 12.5 ppm. The results from the ICP-MS analysis are shown in Table 4.14-4.16. The reference materials in Table 4.14 were analyzed together with the samples in experiment 1-6.

Table 4.14.: Reference materials for experiment 1-6

	Analyzed (ppm)	Certified (ppm)	Deviation
Diabase W-2	10.9	12.0	-10.1%
NIST 57b	13.5	12.5	7.4%

The reference materials in Table 4.15 were analyzed together with the samples in experiment 7-9.

Table 4.15: Reference materials for experiment 7-9

	Analyzed (ppm)	Certified (ppm)	Deviation
Diabase W-2	11.9	12	-0.8 %
NIST 57b	11.6	12.5	-7.8%

In Table 4.16 the results for the reference materials analyzed together with the samples from experiment 10-27 are shown.

Table 4.16: Reference materials for experiment 10-27

	Analyzed (ppm)	Certified (ppm)	Deviation
Diabase W-2	12.1	12	0.8%
NIST 57b	12.0	12.5	4.2%

5. Discussion

In this section the findings for the refining properties of the Al_2O_3-MgO-SiO_2 and the CaO-SiO_2-TiO_2 slags, the activity coefficients of Al and Mg in silicon and slag refining in hydrogen atmosphere will be discussed separately. Then, sources of error and uncertainty will be evaluated. Finally, some of the practical implications from this study are mentioned.

5.1 Distribution of boron between slag and silicon

5.1.1 Al_2O_3-MgO-SiO_2

The system was found to be close to equilibrium with respect to boron after 3 hours. The distribution coefficient of boron (L_B) was found to be 1.9 after 9 hours and the mass transfer coefficient was estimated to be 2.3×10^{-6} m/s.

Distribution coefficient of boron

In Figure 4.1 it was shown that the change in boron concentration in slag and silicon after 3 hours was small, this means that the system is close to equilibrium with respect to boron after 3 hours. For the inverse experiment where boron initially was added to the silicon phase, a L_B value of 1.8 was found (Table 4.7). This is 0.1 less than what was found for the previous experiments, and might indicate that the system needs slightly more than 6 hours to reach equilibrium. On the other hand, these small differences might only be due to insignificant variations in the test sample etc. It seems reasonable to conclude that the distribution coefficient of boron in the Al_2O_3-MgO-SiO_2 system examined here is close to 1.9.

Johnston et al. found the value of L_B to range from 1 to 2 for the different compositions of a slag containing Al_2O_3-CaO-MgO-SiO_2 [16]. For a SiO_2/ Al_2O_3 ratio of 1.7 they found L_B to be about 1.4 (Figure 2.16b). This is the same SiO_2/ Al_2O_3 ratio as for the Al_2O_3-MgO-SiO_2 slag used in this study (see Table 4.1), but for this system L_B was higher. However, the differences in the slags make it difficult to compare the two systems.

Mass transfer of boron

The viscosity of the slag at 1600˚C was in Figure (3.3) found to be about 15 poise. At this high viscosity mixing in the slag will be a slow process. Despite this a relatively high mass transport of boron from slag to silicon was found during the three first hours as shown in Figure 4.3. In the calculations of *k* a straight reaction interface between metal and slag was assumed. In reality the silicon phase had a slightly concave-like shape which means that the estimated reaction area between metal and slag are somewhat smaller than the true area. In the experimental part k' was expressed by Equation (3.2), if the reaction interface has a concave shape the ratio *A/V* in Equation (3.2) will increase, and consequently the value of *k* will decrease. However, since the reaction interface was only weakly concave, the assumption of a straight interface should be quite

good. Most of the boron was transported from slag to silicon within the three first hours and a more precise *k* could therefore be found if additional experiments lasting for less than 3 hours had been performed. Furthermore, this would result in a steeper curve between 0 and 3 hours in Figure 4.3.

5.1.2 CaO-SiO_2-TiO_2 (Slag 1)

This system was found to reach equilibrium within 3 hours. The distribution coefficient of boron after 9 hours refining time was found to be 2.2, and the mass transfer coefficient of boron was estimated to be 5.2×10^{-6} m/s.

Distribution coefficient of boron

In Figure 4.5, the boron content in slag and silicon after 3, 6 and 9 hours, respectively, are plotted. The change in boron concentration in slag and silicon after 3 hours was negligible which indicates that equilibrium is reached after 3 hours refining time. In Table 4.3 the composition of the slag after 3, 6 and 9 hours, respectively, is shown. It is evident that TiO_2 is reduced as only a small fraction of the compound is left in the slag after 3 hours. As a consequence of the reduction of TiO_2 after Equation (4.5), the amount of SiO_2 in the slag initially increases. Furthermore, SiO_2 can react after Equation (4.6) under the formation of SiO gas. After 9 hours the slag had a CaO/SiO_2 mass ratio of 0.86, while the titanium content in silicon was about 11%. The distribution coefficient of boron for this system if no Ti had been present in the metal phase was estimated from Equation (5.1). The obtained value of L_B was 2.1.

$$L_B = \frac{K\gamma_B a_{SiO_2}^{3/4}}{\gamma_{BO_{1.5}} a_{Si}^{3/4}} k_{\%\rightarrow x} \tag{5.1}$$

Teixeira et al. found the distribution coefficient of boron to be close to 2.0 at a CaO/SiO_2 mass ratio of 0.86 and 1823 K [3]. Jakobsson et al found a value of about 2.3 at the same slag composition and 1873 K (Figure 2.17) [17]. These values are in good agreement with the L_B value found for the CaO-SiO_2 – Si system in our study.

The activity of silicon will decrease as more impurities are present in the melt. In turn this will lead to an increase in the value of L_B when assuming the activity coefficient of boron in silicon to be constant. If the amount of impurities in silicon becomes high enough the activity coefficient of boron will change due to changed interactions between the different species in the melt. The amount of Ti in Si was 11% which is quite high; a second order term therefore has to be added to the activity coefficient. The activity coefficient of boron in silicon can then be expressed as [41] :

$$ln\gamma_B = ln\gamma_B^0 + \varepsilon_B^{Ti} X_{Ti} + \rho_B^{Ti} X_{Ti}^2 \tag{5.2}$$

Here γ_B^0 is the activity coefficient of boron in silicon at infinite dilution, ε_B^{Ti} is the first order interaction coefficient, ρ_B^{Ti} is the second order interaction coefficient, and X_{Ti} is the molar fraction of Ti in silicon. In Equation (5.2) interactions from all other impurities than Ti on B are neglected. From Equation (5.2) a qualitative evaluation of γ_B can be made. If ε_B^{Ti} is negative, γ_B will decrease with increasing $X_{Ti,}$ even though ρ_B^{Ti} is positive. This means that L_B found for the $CaO\text{-}SiO_2$ – Si-Ti system from Equation (5.1) is a slightly higher than the true value. If ε_B^{Ti} is positive, the L_B is lower than the true value.

For the inverse experiment where boron initially was added to the silicon phase, a L_B of 2.0 after 3 hours refining was obtained. This is relatively close to the value of 2.2 obtained after 9 hours refining. The difference in L_B could be due to inhomogeneous samples, contaminations during preparation of the samples for analysis, or uncertainty in the analysis method. It seems reasonable to conclude that the system needs about 3 hours to reach equilibrium, and that the distribution coefficient of boron for the system is close to 2.2.

Mass transfer of boron

The mass transfer coefficient of boron for the slag, *k*, was in Figure 4.7 estimated to be 5.2×10^{-6} m/s which is more than two times higher than for the $Al_2O_3\text{-}MgO\text{-}SiO_2$ system. The viscosity of the slag used in this system was in Figure 3.4 found to be 3 poise which is considerable lower than the slag for the $Al_2O_3\text{-}MgO\text{-}SiO_2$ system which was 15 poise. This seems reasonable as the mass transfer of boron in the slag often is considered to be the rate limiting step.

Nishimoto et al. found the mass transfer coefficient of boron in a $CaO\text{-}SiO_2$ slag consisting of 55 wt% CaO and 45 wt% SiO_2 to be 1.4×10^{-6} m/s at 1600˚C [30]. At this slag composition the viscosity was slightly lower than for the slag used in this study. Despite this, the value of *k* estimated in our study was almost four times higher than the *k* value found by Nishimoto et al. Krystad et al. found the value of *k* to be 1.7×10^{-6} m/s for a slag consisting of 50% CaO and 50% SiO_2 which is close to the slag composition of 46% CaO and 54% SiO_2 in our study after 9 hours [19]. The mass transfer coefficients of boron found in the literature were generally smaller than the value found in our experiments although they are in the same order of magnitude. Again the estimation of a straight interphase between slag and silicon will result in a slightly higher mass transfer coefficient than for a concave interface although the effect is assumed to be small. However, differences between the studies in both the viscosity and the molecular structure of the slag and silicon phase, which influence the mass transfer rate of boron, may explain the different mass transfer coefficients found.

5.1.3 $CaO\text{-}SiO_2\text{-}TiO_2$ (Slag 2)

Also this system was found to approach equilibrium after 3 hours. The distribution coefficient of boron after 8 hours was found to be 1.4 while the mass transfer coefficient was estimated to be 2.0×10^{-6} m/s.

Distribution coefficient of boron

In Figure 4.8 the boron concentration in slag and silicon as a function of time was shown. After 3 hours the change in boron concentration per time declines indicating that the system approaches equilibrium, although this is not as evident as for Slag 1. The composition of the slag during refining is shown in Table 4.5. Since the initial TiO_2 content in the slag was 49% which is quite high, about 5% TiO_2 was still left in the slag after 8 hours. A large increase in the SiO_2 content in the slag after 8 hours can be observed, while the CaO content is only slightly increased. As previously mentioned this can be explained by the reduction of TiO_2 after Equation (4.5) under the formation of SiO_2. Due to the large amounts of SiO_2 produced, this will dominate over the amount of SiO gas produced from Equation (2). After 8 hours L_B for the system was found to be 1.4. However, this system was quite different from the initial system as the value of L_B at equilibrium will change as the slag composition changes. Furthermore, the Ti content in silicon increases during refining. It is therefore difficult to determine the time for equilibrium to be reached for this particular system.

For the inverse experiment with boron initially added to the silicon phase, a L_B of 1.4 was obtained after 3 hours refining (Table 4.7). This was the same value as obtained when boron was added to the slag phase after 8 hours. In Figure 4.8 the system had not reached this value after 3 hours, but again inhomogeneous samples, contaminations during sample preparation, and uncertainty in analysis method could potentially affect the experimental results.

Mass transfer of boron

The mass transfer coefficient of boron for the system, *k*, was estimated to be 2.0×10^{-6} m/s. The high SiO_2 content in the slag after 8 hours has a negative effect on the slag viscosity (Figure 3.4) which may explain the reduced value of *k* compared to Slag 1. However, the composition of Slag 2 was quite different from Slag 1 and comparing the two systems is therefore difficult.

5.2 Activity coefficient of Al and Mg in silicon

The activity coefficients of Al and Mg in Si at infinite dilution were found to be 0.6 and 0.5 respectively. The amount of aluminum and magnesium in silicon after 9 hours was 0.35 and 0.24 mass %, respectively (Table 4.2).

The initial silicon used in the experiments was very pure; it is therefore assumed that Al and Mg are the only impurities in the silicon melt. Due to the small concentration of the two impurities in silicon it is also assumed that the effect of coexistent impurities on the activity coefficients can be neglected. The activity coefficient of Al and Mg in Si is therefore the coefficients at infinite dilution. This means that the activity coefficient can be considered as a constant in the concentration range for a given temperature. In Table 5.1 the activity coefficients at infinity dilution in molten silicon found from our experiments are listed together with coefficients from

Miki et al. and Safarian et al. The temperature where the coefficients were found is stated in parenthesis.

Table 5.1: Activity coefficients of Al and Mg in molten silicon at infinity dilution

	Bjerke et al. [26]	**Miki et al. [20]**	**Safarian et al. [21]**
γ_{Al}^{0}	0.60 (1600˚C)	0.24 (1575˚C)	0.37 (1414˚C)
γ_{Mg}^{0}	0.50 (1600˚C)	0.17 (1525˚C)	0.050 (1414˚C)

We notice that the activity coefficients found in our study were higher than in the comparable studies. Except for the value of γ_{Mg}^{0} found by Safarian et al., the coefficients were in the same order of magnitude. The three different values of $\gamma_{Al}^{0}$and γ_{Mg}^{0} were all found at different temperatures. However the effect of the temperature should only have a small effect on the activity coefficients. If the system has not reached equilibrium with respect to aluminum or magnesium after 9 hours, the amount of these species in silicon used in the calculation of $\gamma_{Al}^{0}$and $\gamma_{Mg}^{0}$is too small. This means that X_{Al} and X_{Mg} in Equation 4.3 and 4.4 are smaller than the true values, and the calculated activity coefficients will become too large. In Figure 4.4 it is shown a continuously increase in the Al and Mg content in silicon with increasing refining time. No flattening of the curves in Figure 4.4 is observed, this indicates that the system has not reached equilibrium with respect to Al and Mg after 9 hours, and that the activity coefficients found in this work therefore are higher than the true values. The high viscosity of the slag can probably explain the slow mass transfer rates of Al and Mg in the system.

Interactions between impurities in Si can also influence the results. However, in the experiments above the concentration of Al and Mg in silicon was assumed to be so small that they did not interact with each other even though they were present in the same solution. In Equation 5.3 and 5.4 the activity coefficients of aluminum and magnesium, γ_{Al} and γ_{Mg}, are expressed in terms of interaction coefficients [42].

$$ln\gamma_{Al} = ln\gamma_{Al}^{0} + \varepsilon_{Al}^{Mg} X_{Mg} + \varepsilon_{Al}^{B} X_{B} \ldots \quad (5.3)$$

$$ln\gamma_{Mg} = ln\gamma_{Mg}^{0} + \varepsilon_{Mg}^{Al} X_{Al} + \varepsilon_{Mg}^{B} X_{B} \ldots \quad (5.4)$$

Where ε_{j}^{i} is the interaction coefficient of *i* on *j* in silicon, and X_i is the molar fraction of element *i* in the melt. From Equation (5.3) and (5.4) we can see that very small values of X_{Mg}, X_{Al} and X_B result in the activity coefficient to be equal to the activity coefficients at infinite dilution.

To illustrate the effect of the presence of a second dilute solute in a melt the activity coefficient of nitrogen in binary iron alloys at 1600˚C can be used as an example. In Figure 5.1 the logarithm

to the activity coefficient of nitrogen in liquid iron when impurity *i* is present, f_N^i , is shown as a function of the weight percent of element *i*.

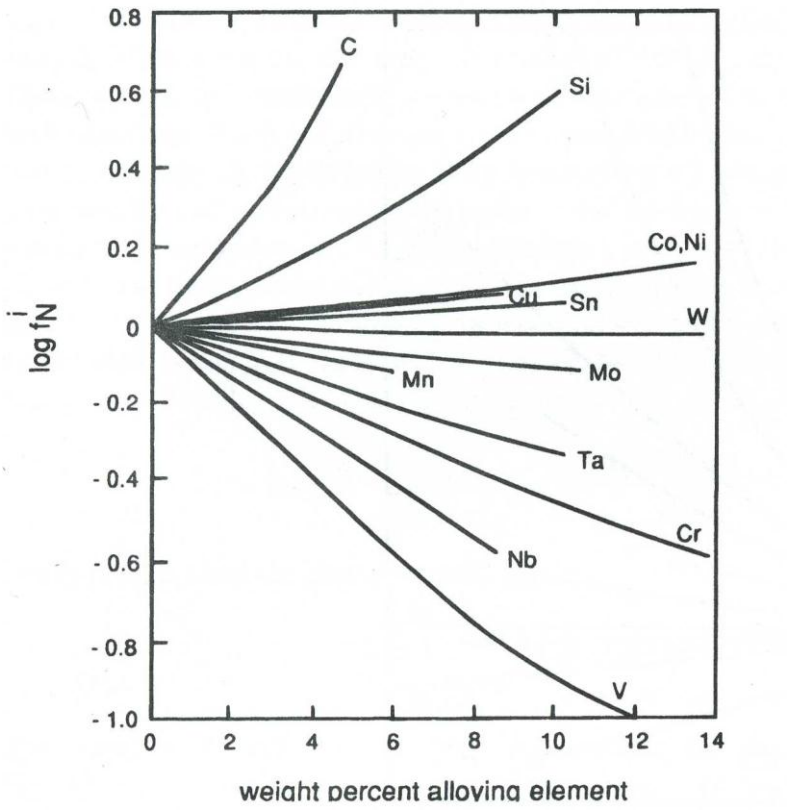

Figure 5.1: The influence of impurities in liquid iron on the activity coefficient of nitrogen [42]

The activity coefficient of nitrogen can then be written as:

$$logf_N = \sum_i logf_N^i \tag{5.5}$$

The two elements that give the largest influence on f_N in Figure 5.1 are carbon (C) and vanadium (V). If the weight percent of these two elements are 0.35 in two separate iron melts, which was the present weight percent of Al in silicon, the change in f_N will be approximately 0.096 and 0.077 for the melts containing C and V, respectively. Since these were the elements that gave the largest deviation from ideality in Figure 5.1, it can be assumed that the influence on the activity coefficients of Al and Mg, due to the coexistence of the two impurities, at least not are any larger. The presence of a second dilute solute in the melt will therefore result in a small change in the activity coefficient. However, the coefficients found in Table 5.1 will not change significantly as the effect is quite small. The activity coefficients of Al and Mg in silicon are dependent on several factors it is therefore many sources to uncertainty in both this study as well as other comparable studies. However, the main reason for the high activity coefficients found in this

study can be explained by the non-equilibrium conditions in the system with respect to Al and Mg.

5.3 Evaporation of boron in hydrogen atmosphere

5.3.1 Series 1

The effect of temperature on boron evaporation from slag was investigated in the temperature range 1500-1600˚C, a silicon phase was not involved in the experiments. The effect was found to be small although a slight increase in the boron evaporation rate was observed at the higher temperatures as shown in Table 4.8.

Effect of temperature

Since the viscosity of the slag decreases with increasing temperature according to Equation (2.12), an increased temperature should have a positive effect on the evaporation rate of boron, due to higher mass transport of boron from the bulk slag to the slag surface. Wu et al. found in a theoretical study that the partial pressure of the most common boron hydrides, except for BHO, decreased with increasing temperature [27]. The small effect of varying the temperature in this study may be due to the two effects canceling each other. Nordstrand et al. found that when boron was evaporated directly from a silicon melt, the boron removal rate increased with decreasing temperature in the temperature range 1450-1600˚C, which confirms the findings by Wu et al. [29]. However, it is not necessarily the same boron species that evaporates directly from silicon compared to those that evaporates from the slag. For instance, if BHO is the main specie evaporating from the slag, the evaporation rate of this specie will not change considerably in the investigated temperature range according to Wu et al. [27]. This may explain the temperature independence observed in this study.

5.3.2 Series 2

The effect of refining time on boron evaporation was in this second series investigated at 1600˚C. Neither in this series was a silicon phase involved in the experiments. The boron concentration in the slag was found to decrease with increasing refining time in a linear manner in the investigated concentration range. The evaporation rate of boron was found to follow first order kinetics and the mass transfer coefficient of boron was found to be $4*10^{-7}$ m/s.

Kinetics of boron removal from slag

The first order rate kinetics of boron removal is in agreement with previous studies on gaseous removal of boron [29]. The composition of the $CaO\text{-}SiO_2$ slag was shown in Table 4.10. Due to the formation of SiO gas as shown in Equation (4.9) the basicity of the slag increased from 1.21 to 1.53 during the 6 hours refining time. Since the amount of CaO increases relative to SiO_2, the system becomes more basic and will therefore have a lower viscosity. At the same time the oxygen partial pressure will be reduced and for a slag-metal system this means that oxidation of boron could be restricted. The evaporation rate of boron is rather constant throughout the 6 hours

refining time which indicated that variation in the slag basicity had no considerable influence on the evaporation rate of boron in the basicity range in this study. Neither did the reduced boron content in the slag with time seem to influence the evaporation rate considerably in the concentration range investigated. Since boron already is in an oxidized state in the slag phase, the effect of changing the slag basicity may influence the evaporation rate of boron if a metal phase is involved, due to change in the oxygen partial pressure.

5.3.3 Series 3

In Series 3 boron evaporation was investigated for a system containing both silicon and slag at 1600˚C. The effect of varying the slag/metal mass ratio was studied. The best refining effect was obtained for the system with the highest slag/metal mass ratio. However, it was observed that the rate of boron evaporation from the system increased with decreasing slag/metal mass ratio due to a higher boron concentration in the slag. The distribution coefficient of boron after 3 hours was close to 2.3. When accounting for the evaporated boron the distribution coefficient was in the range 3.8-8.8.

Reaction mechanism

When boron is transported from the metallic phase, through the slag phase and evaporated at the slag surface the transportation process can be simplified to follow four steps. First boron is transported through the bulk metal; this transport is caused by a combination of diffusion and convection. In the second step boron is oxidized at the metal-slag interface. Boron is oxidized by silica from the slag, and the reaction can be written as:

$$¾\ (SiO_2) + [B] = (BO_{1.5}) + ¾\ Si \qquad (5.6)$$

The rate of the reaction in Equation (5.6) is strongly dependent on temperature as shown in Equation (2.26). Since the temperature in the refining process is high it can be assumed that the oxidation reaction in Equation (5.6) not determines the refining rate of the process. Next boron is transported through the slag. The slag phase is often relatively viscous compared to silicon; transport of boron in the slag phase is therefore often considered as the rate determining step in slag refining [2]. In the experiments performed in this study H_2 gas was purged on the melt surface, causing good convection in the slag phase, and therefore enhanced boron transportation in the slag. At last boron is evaporated as boron hydrides at the slag surface. Exactly which boron compounds that evaporates is uncertain, but it has been reported in literature that HBO is the most volatile among the boron species [29]. The reaction for evaporation of HBO can be written as:

$$B_2O_3 + 2H_2\ (g) = 2HBO\ (g) + H_2O\ (g) \qquad (5.7)$$

The evaporation rate of boron from slag was in this study found to be $4*10^{-7}$ m/s, if it is assumed that this evaporation rate also applies to the system when a metal phase is involved, the

evaporation rate can be compared to the mass transfer coefficient of boron in the slag of $1.4x10^{-6}$ m/s reported by Nishimoto et al [30]. The mass transfer coefficient of boron in the $CaO-SiO_2$ slag in this study is probably higher due to forced convection in the melt caused by the gas purging. The boron mass transfer rate in the slag is more than three times higher than the evaporation rate of boron. It is therefore reasonable to assume that evaporation of boron is the rate limiting step in this process.

Distribution coefficient of boron

In Figure 4.16 the distribution coefficient of boron in the $CaO-SiO_2$ – Si system was shown at a CaO/SiO_2 mass ratio of 1.28 (Table 4.13). For a slag/metal mass ratio of 0.75 or more the value of L_B was found to be near 2.3. This value is close to the L_B found by Jakobsson et al. and indicates that boron has equilibrated between slag and silicon. For the two systems with a slag/silicon mass ratio of 0.25 and 0.50, the L_B values obtained was 1.9 and 2.1, respectively. Since the mass transfer rate of boron in the slag is more than 3 times faster than the evaporation rate, equilibrium with respect to boron between slag and metal should be reached. The deviation may be due to analytical errors.

The effect of hydrogen on slag refining

In Figure 4.17 L_B was found by adding the amount of evaporated boron to the amount of boron retained by the slag, and it was found that less slag resulted in higher L_B. This is a consequence of the higher evaporation rate of boron in systems with less slag. However, since the evaporation rate of boron was slow compared to the mass transfer rate of boron from slag to silicon, the best refining effect was obtained for the system with the highest amount of slag. The L_B for this system was found to be 3.8 which is higher than the L_B reported by Jakobsson et al. and Johnston et al. for the same slag composition [17] [16]. This means that the proposed effect of hydrogen is obtained; more boron is continuously transported from silicon to slag to compensate for the evaporated boron, and consequently a higher refining efficiency is obtained.

The effect of hydrogen on slag refining is illustrated in Figure 5.2. In the figure the boron concentration in silicon is plotted as a function of the slag/Si mass ratio. The amount of boron in silicon in conventional slag refining was calculated from Equation (2.1). The initial boron concentration in silicon and L_B used was 92.3 and 2.3, respectively. These are the same values as for the $CaO-SiO_2$ – Si system investigated in this study. The refining time in Figure 5.2 is 3 hours, which is the equilibration time for the slag. For more details regarding the calculations see *Appendix II*.

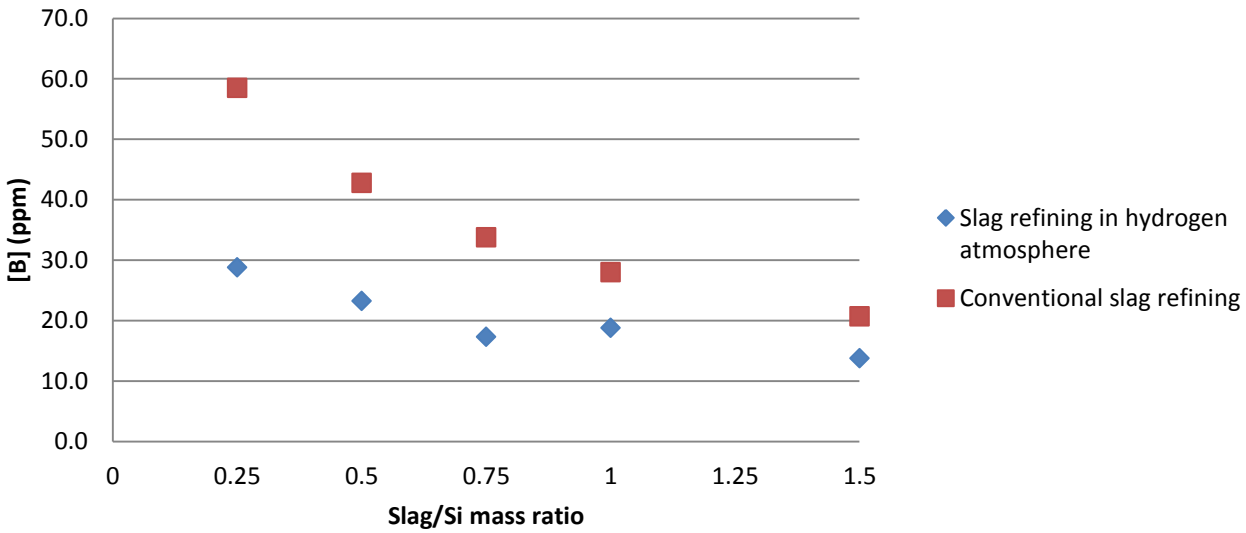

Figure 5.2: The amount of boron in silicon after 3 hours refining for conventional slag refining and slag refining in hydrogen atmosphere, respectively.

Figure 5.2 illustrates the increased refining effect by using hydrogen for this particular system. In the figure it is shown that the refining efficiency compared to conventional slag refining is increased by 51%, when the amount of slag is ¼ that of silicon. If the amount of slag is 1.5 times the amount of silicon the refining efficiency is increased by 34% with the use of hydrogen. The effect decreases with increasing slag/silicon mass ratio due to the lower boron concentration in the slag. This is reasonable since the evaporation rate of boron is expected to follow an exponential decrease according to Equation (2.32).

Comparison of the evaporation rate of boron in Series 2 and 3

In Table 5.2 the amount of boron evaporated after 3 hours in Series 2 (experiment 19) is shown together with the amount of boron evaporated after 3 hours in Series 3 (experiment 23-27).

Table 5.2: The amount of boron evaporated in Series 1 and 3 after 3 hours

Experiment no.	Slag/Si mass ratio	Evaporated boron (g)	Evaporated boron (%)
19	No silicon	0.00033	26
23	0.25	0.00075	54
24	0.5	0.00067	48
25	0.75	0.00068	49
26	1.0	0.00046	33
27	1.5	0.00045	32

In Series 2 26 % of the initial boron has evaporated after 3 hours. Since the boron concentration in the slag is higher for Series 2 than for Series 3 the evaporation rate of boron is also expected to be higher for Series 2. However, Series 3 was found to have the highest evaporation rate of boron. In Series 3 silicon was pre-melted in the crucible with the intention of obtaining a straight

interface between slag and metal. However, a lump of silicon was observed on the sample surface after refining as shown in Figure 4.11. The lump could be caused by a volume change during cooling, forcing silicon up through the slag phase. Alternatively the lump arises during refining. If the latter is the case, an explanation for the increased evaporation rate in Series 3 compared to Series 2 could be that boron evaporates directly from the hydrogen exposed silicon lump. The mass transfer coefficient of boron when evaporating from silicon with hydrogen as the only refining gas, is found by Nordstrand et al. to be $5.6x10^{-7}$ m/s at 1500˚C [29]. In Series 2 the mass transfer coefficient was found to be $4x10^{-7}$ m/s. Consequently the evaporation rate of boron from slag is 29% lower than from silicon. From Figure 4.11 it is estimated that the silicon lump covering approximately 30% of the sample surface. Since the evaporation rate of boron from silicon is higher than from the slag, this may explain the higher evaporation rate of boron in the experiments in Series 3. Why the silicon lump arises is uncertain, but it could be caused by the extra convection in the area right under the tube where gas was injected.

5.3.4 Method

In this study the amount of hydrogen used in the gas was 50%. Nordstrand et al. previously found this amount of hydrogen to be sufficient to obtain the highest possible removal rate at 1500˚C [29]. This applies to a system where boron is removed directly from silicon. Whether this also is true for the slag system is uncertain. In our previous unpublished study we found that the boron content in slag was reduced by 22.4% after 1.5 hours refining time in pure hydrogen [26]. In this study the boron content in the slag was reduced by 21% after 2 hours when the gas contained 50% hydrogen. This implies that the highest possible removal rate of boron is obtained for higher hydrogen content in the refining gas than 50%, but more experimental work should be performed to confirm this.

5.4 Sources of error and uncertainty

Errors in the obtained results can occur during the process of preparing the samples for analysis or due to uncertainty in the analysis method. After refining, slag and silicon were carefully separated from each other before they were crushed. The boron in the two phases is not necessarily homogeneously distributed and the whole sample was therefore crushed before parallels were taken out for analysis. Since the amount of boron in the samples is in the ppm range contamination should be avoided. Especially when the samples are weighted out for analysis in parallels of less than 50 mg, only a trace amount of boron can affect the results. The samples were dissolved in a mixture of HF and HNO_3 before analyses and contaminants in these solvents were identified through blank samples and subtracted from the sample results.

When we compare the amount of boron in slag and silicon after refining with the initial values in experiment 1-9, small deviations were found. On average the boron content in the system after refining deviates 3.1% from the initial boron content. In experiment 1-9 slag and silicon was melted in an inert atmosphere and boron will therefore not evaporate from the system [26], the

uncertainty in the analysis method could therefore be estimated to be 3.1%. In the experiments involving hydrogen it was assumed that the amount of evaporated boron was the initial amount of boron in the system minus the amount of boron in the slag and in silicon. Since an average deviation of 3.1% on the total boron content in the systems was found in experiment 1-9. It can be assumed that this also applies to experiment 13-27. However, a deviation of ± 3.1% will not have a significant effect on the results obtained in this study.

The analysis results for the reference materials Diabase W-2 and Nist 57b are shown in Table 4.16 - 4.18. The average deviation from the certified values was 5.2%, the value of 3.1% found above is therefore within the expected variation of the analysis method.

In experiment 4-6, shown in Figure 4.5, the boron content in both the slag and silicon phase was rather constant after 3, 6, and 9 hours, respectively. As we find almost exactly the same boron content in three independent attempts for both the slag and the silicon phase the reliability of the experiments and the corresponding results shown in Figure 4.1 and 4.8 is very good.

5.5 Practical implications of the study

The kinetic and thermodynamic properties of the Al_2O_3-MgO-SiO_2 slag evaluated in this thesis were shown to be in the same range as previous studies. The drawback with the Al_2O_3-MgO-SiO_2 slag is the high viscosity which limits the useful composition range of the slag. Furthermore, the high viscosity will also complicate the process of pouring the slag from the ladle in the refining process of silicon.

As most of the TiO_2 is reduced during the refining process makes it difficult to use this compound as a part of a slag for refining of silicon. The amount of Ti in metallurgical grade silicon is about 5 ppm, while the required Ti concentration in solar grade silicon is less than 0.1 ppm [2]. When using slags containing TiO_2, the amount of Ti supplied to silicon is significantly more than the initial amount in the metallurgical grade silicon, and removal of Ti will be resource demanding. Slags containing considerable amounts of Ti should therefore be avoided.

In this study the use of hydrogen was shown to increase the refining efficiency for all slag compositions evaluated. Ideally the evaporation rate of boron from the slag should be high enough to ensure that a minimal amount of slag is needed for refining. For all experiments performed so far, the evaporation rate of boron was found to be relatively low. Even though the evaporation rate of boron increases with decreasing amounts of slag, a long refining time will be needed to attain the target concentration of less than 0.3 ppm of boron in SoG-Si [2]. This study found the temperature to not have a significant effect on the evaporation rate of boron from slag in the temperature range 1500-1600˚C. If the refining process is carried out at 1500˚C instead of 1600˚C it will be less energy demanding as long as the refining rate of the system is attained. However, the experiments in this study did not involve a silicon phase and more experiments

should therefore be performed to see how the temperature affects the refining rate when a silicon phase also is a part of the system. The main advantage of evaporating boron from slag compared to direct boron evaporation from silicon is to prevent loss of silicon. In the experiments done by Nordstrand et al. on boron evaporation from silicon, the silicon loss was found to be about 10% [29]. In this study a more efficient slag refining method is proposed, but an even higher evaporation rate of boron is desired for the process before it will be of industrial interest.

6. Conclusions

The following main conclusions can be made from this master thesis:

- The distribution coefficients of boron (L_B) for the Al_2O_3-MgO-SiO_2 (29%-23%-48%) and the CaO-SiO_2 (46%-54%) – Si (11% Ti) systems were found to be 1.9 and 2.2, respectively. The corresponding mass transfer coefficients of boron were $2.3x10^{-6}$ and $5.2x10^{-6}$ m/s, respectively. Since the composition of the CaO-SiO_2-TiO_2 (24%-27%-49%) changed continuously during refining, a conclusion on the L_B for this system cannot be drawn.
- In this study the Al_2O_3-MgO.SiO_2 – Si system had not reached equilibrium with respect to aluminum and magnesium after 9 hours, and therefore no conclusions can be drawn regarding their respective activity coefficients in silicon.
- Boron can be evaporated from the CaO-SiO_2 slag when refined in an atmosphere containing 50% hydrogen, but the evaporation rate is low. The temperature was not found to significantly influence the evaporation rate of boron from the slag in the temperature range 1500-1600˚C.
- The evaporation rate of boron from the CaO-SiO_2 slag was in this study found to be $4x10^{-7}$ m/s.
- When slag refining was performed in a hydrogen atmosphere an increase in the refining efficiency compared to conventional slag refining was found. For the particular system investigated the increase was found to be in the range 34-51% depending on the slag/Si mass ratio.

References

1. Aasen, H. *Elkem Solar - Gorund-breaking technology for cost leadership*. [cited 2012 29/5]Available from: http://www.elkem.no/dav/9a385e0007.pdf.
2. Tangstad, M. and J. Safarian, *Compendium: New solar grade silicon production processes.* 2010: p. 65-91.
3. Teixeira, L.A.V., et al., *Behavior and State of Boron in CaO–SiO 2 Slags during Refining of Solar Grade Silicon.* ISIJ international, 2009. **49**(6): p. 777-782.
4. *Ellingham Diagrams*. [cited 2012 2/6] Available from: http://www.chem.ox.ac.uk/vrchemistry/o'hare/lecture3/ellingham.html.
5. Schei, A., J.K. Tuset, and H. Tveit, *High Silicon Alloys* 1998, Trondheim: Tapir akademisk forlag.
6. *Slag Atlas*, VDEh, Editor 1995, Verlag Stahleisen GmbH.
7. Hull, R., *Properties of crystalline silicon* 1999: The Institution of Electrical Engineers.
8. Keene, B.J. and K.C. Mills, *Densities of molten slags*, in *Slag atlas*, V.D.E. (VDEh), Editor 1995, Stahleisen: Düsseldorf. p. 326.
9. Helbæk, M. and S. Kjelstrup, *Fysikalsk kjemi*, 1999, Fagbokforlaget: Trondheim. p. 537-540.
10. Nakajima, K. and N. Usami, *Crystal Growth of Si for Solar Cells*, ed. Y. Kawazoe, et al.2009: Springer.
11. Olsen, S.E., T. Lindstad, and M. Tangstad, *Production of Manganese Ferroalloys* 2007, Trondheim: SINTEF and Tapir academic press.
12. Tangstad, M., *CaO and SiO2 phase Diagram*, R.S. refining, Editor 2011, Merete Tangstad: Lecture in TMT1, Fall 2011.
13. Nakajima, K. and N. Usami, *1.4.1.1 Slag refinging in a ladle*, in *Crystal Growth of Si for Solar Cells*2009, Springer. p. 8-11.
14. Engh, T.A., *Principles of metal refining*1992, New York: Oxford Science Publications.
15. *Chemical Kinetics*. [cited 2012 17/4] Available from: http://www.csus.edu/indiv/m/mackj/chem142/kinetics.pdf.
16. Johnston, M.D. and M. Barati, *Distribution of impurity elements in slag–silicon equilibria for oxidative refining of metallurgical silicon for solar cell applications.* Solar energy materials and solar cells, 2010. **94**(12): p. 2085-2090.
17. Jakobsson, L.K. and M. Tangstad, *Distribution of boron between silicon and calcium silicate slags*, 2012.
18. Luo, D., et al., *Removal of boron from metallurgical grade silicon by electromagnetic induction slag melting.* Transactions of Nonferrous Metals Society of China, 2011.
19. Krystad, E., S. Zhang, and G. Tranell. *The kinetics of boron removal during slag refining in the production of solar-grade silicon*. *TMS 2012*. 2012. Orlando, Florida, USA.
20. Miki, T., K. Morita, and N. Sano, *Thermodynamic Properties of Titanium and Iron in Molten Silicon.* Metallurgical and materials transactions, 1997. **28B**: p. 861-867.
21. Safarian, J. and M. Tangstad, *Vaccum refining of molten silicon.* Unpublished work.
22. Engh, T.A., *Principles of metal refining*, 1992, Oxford University Press: New York. p. 207-208.

23. Harris, R. and W.G. Davenport, *Vacuum distillation of liquid metals: Part 1, theory and experimental study.* Metallurgical and materials transactions, 1982: p. 581-588.
24. Olette, M., Physical Chemistry of Process Metallurgy Part 2, 1961: p. 1065-87.
25. Wang, Q., et al., *Investigation on the removal of phosphorus, aluminium, calcium, from metallurgical grade silicon using electron beam melting.* Journal of functional materials, 2010(2010-S1): p. 144.
26. Bjerke, H. and M. Tangstad, *Boron Evaporation from Calcium Silicate Slags*, 2011: Unpublished. p. 41, 46-47.
27. Wu, J.-j., et al., *Boron removal from metallurgical grade silicon by oxidizing refining.* Transactions of Nonferrous Metals Society of China, 2009. **19**(2): p. 463-467.
28. Nakamura, N., et al., *Boron Removal in Molten Silicon by a Steam-Added Plasma Melting Method.* Materials Transactions, 2004. **45**(3): p. 858-864.
29. Nordstrand, E.F. and M. Tangstad, *Removal of boron from silicon by moist hydrogen gas.* Unpublished data.
30. Nishimoto, H. and K. Morita, *The rate of boron elimination from molten silicon by slag and Cl2 gas treatment.* Materials Processing and enegy Materials TMS, 2011.
31. Safarian, J., *Vacuum induction furnace*, S.c.s.S.p.a. refining, Editor 2010: TMT10, Autumn semester 2010.
32. Richardsen, S., *Graphite resistance furnace*, 2011.
33. Jakobsson, L.K., *Inside of the furnace*.
34. Ciftja, A., T.A. Engh, and M. Tangstad, *Wetting Properties of Molten Silicon with Graphite Materials.* Metallurgical and materials transactions, 2010. **41A**: p. 3183-3195.
35. Jakobsson, L.K., *Temperature profile*, T-profile-0612, Editor 2012.
36. Wolf, R.E. *What is ICP-MS?... and more importantly, what can it do?* 2005 [cited 2011 19/12]; Available from: http://minerals.cr.usgs.gov/icpms/intro.html.
37. Wirth, K. and A. Barth. *X-Ray Fluorescence (XRF).* Available from: http://serc.carleton.edu/research_education/geochemsheets/techniques/XRF.html.
38. FactSage. *Fact-Web*. 2012 [cited 2012 23/5]; Available from: http://www.factsage.com/.
39. *United States Geological Survey, Certificate of analysis, Diabase W-2*. 2012 [cited 2012 24/5]; Available from: http://crustal.usgs.gov/geochemical_reference_standards/pdfs/diabase.pdf.
40. *Materials Details, SRM 57b - Sillicon Metal*. 2009 [cited 2012 29/5] Available from: https://www-s.nist.gov/srmors/view_detail.cfm?srm=57B.
41. Grande, T. and S. Stølen, *Chemical thermodynamics of materials*, ed. J.W.a. Sons 2008: John Wiley and Sons Ltd.
42. Gaskell, D.R., *Introduction to the thermodynamics of materials*. 4 ed, ed. R.H. Bedford 2003: Taylor and Francis.

Appendix I

A1 Estimation of mass transfer coefficient

The mass transfer coefficient of boron was calculated using Equation (3.1). The value of k' used in the calculations were the value that gave the smallest sum of $(B_{Exp} - B_{Calc})^2$, where B_{Exp} and B_{Calc} is the experimental and calculated boron concentration in silicon, respectively.

A.1.1 CaO-SiO_2-TiO_2 (39%-43%-18%)

$[\%B]_{in}$ = 0 ppm
$[\%B]_{\infty}$ = 26 ppm

Table A1.1: Estimation of *k* for the CaO-SiO_2-TiO_2 (39%-43%-18%) system

t (h)	Experimental B (ppm)	Calculated B (ppm)	Deviation $(B_{Exp} - B_{Calc})^2$
0	0	0	0
3	26.4	25.4	1.00
6	26.5	26.0	0.898
9	25.7	26.0	0.090
		Sum	1.36

k = 3.49x10^{-4} 1/s
k' = 5.23x10^{-6} m/s

A.1.2 CaO-SiO_2-TiO_2 (24%-27%-49%)

$[\%B]_{in}$ = 0 ppm
$[\%B]_{\infty}$ = 35 ppm

Table A1.2: Estimation of *k* for the CaO-SiO_2-TiO_2 (24%-27%-49%) system

t (h)	Experimental B (ppm)	Calculated B (ppm)	Deviation $(B_{Exp} - B_{Calc})^2$
0	0	0	0
3	27.7	26.9	0.575
6	31.6	33.1	2.39
9	34.1	34.3	0.0412
		Sum	3.00

k = 1.36x10^{-4} 1/s
k' = 2.04x10^{-6} m/s

Appendix II

A2 Calculation of the amount of boron in silicon

M_{sl} = the amount of slag (g)
M_{Si} = the amount of silicon (g)
B_{in} = the initial boron content in silicon (g)
(B) = boron concentration in slag (ppm)
[B] = boron concentration in silicon (ppm)
X = the amount of boron in the slag (g)

The distribution coefficient of boron is defined by Equation (A2.1):

$$L_B = \frac{(B)}{[B]} \quad \text{(A2.1)}$$

The concentration of boron in the slag can be found from Equation (A2.2):

$$(B) = \frac{X}{M_{Sl}} 10^6 \quad \text{(ppm)} \quad \text{(A2.2)}$$

The concentration of boron in silicon can be found from Equation (A2.3):

$$[B] = \frac{B_{in}-X}{M_{Si}} 10^6 \quad \text{(ppm)} \quad \text{(A2.3)}$$

By inserting (B) and [B] into the expression for L_B in Equation (A2.1), an expression for X can be found:

$$X = \frac{L_B M_{Sl} B_{in}}{M_{Si}+L_B M_{Sl}} \quad \text{(A2.4)}$$

The boron content in silicon at equilibrium, [B], can now be found from Equation (A2.3).

Appendix III

A3 Results from ICP-MS analysis

A3.1 Slag samples

The boron isotope B-11 was analyzed by ICP-MS. The analysis results for the slag samples are shown in Table A3.1 together with the relative standard deviation (RSD).

Table A3.1: ICP-MS results for slag samples

Reference material	Experiment no.	Refining time (h)	Slag	B-11 ppm	RSD, %
1	1	3	Al2O3-MgO-SiO2	94.9	1.2
1	1	3	Al2O3-MgO-SiO2	96.4	1.1
1	1	3	Al2O3-MgO-SiO2	92.9	2.4
1	2	6	Al2O3-MgO-SiO2	88.3	0.5
1	2	6	Al2O3-MgO-SiO2	78.7	2.0
1	2	6	Al2O3-MgO-SiO2	90.8	2.9
1	3	9	Al2O3-MgO-SiO2	85.2	2.0
1	3	9	Al2O3-MgO-SiO2	89.5	1.1
1	3	9	Al2O3-MgO-SiO2	92.0	2.1
1	4	3	CaO-SiO2-TiO2 slag 1	56.3	1.7
1	4	3	CaO-SiO2-TiO2 slag 1	59.1	1.3
1	4	3	CaO-SiO2-TiO2 slag 1	57.5	1.2
1	5	6	CaO-SiO2-TiO2 slag 1	57.3	1.4
1	5	6	CaO-SiO2-TiO2 slag 1	56.8	1.7
1	5	6	CaO-SiO2-TiO2 slag 1	53.1	1.8
1	6	9	CaO-SiO2-TiO2 slag 1	56.6	1.5
1	6	9	CaO-SiO2-TiO2 slag 1	54.6	2.3
1	6	9	CaO-SiO2-TiO2 slag 1	57.9	2.7
2	7	3	CaO-SiO2-TiO2 Slag 2	51.5	4.0
2	7	3	CaO-SiO2-TiO2 Slag 2	52.7	3.6
2	7	3	CaO-SiO2-TiO2 Slag 2	54.9	2.4
2	8	6	CaO-SiO2-TiO2 Slag 2	55.3	1.6
2	8	6	CaO-SiO2-TiO2 Slag 2	56.0	2.8
2	8	6	CaO-SiO2-TiO2 Slag 2	52.8	1.3
2	9	8	CaO-SiO2-TiO2 Slag 2	47.2	2.4
2	9	8	CaO-SiO2-TiO2 Slag 2	51.2	1.7
2	9	8	CaO-SiO2-TiO2 Slag 2	45.5	1.0
2		Initial slag	Al2O3-MgO-SiO2	134.2	1.4
2		Initial slag	Al2O3-MgO-SiO2	138.4	1.6

2		Initial slag	Al2O3-MgO-SiO2	145.6	0.8
2		Initial slag	CaO-SiO2-TiO2 Slagg 1	83.2	1.3
2		Initial slag	CaO-SiO2-TiO2 Slagg 1	84.3	2.5
2		Initial slag	CaO-SiO2-TiO2 Slagg 1	79.6	0.7
2		Initial slag	CaO-SiO2-TiO2 Slagg 2	82.3	3.3
2		Initial slag	CaO-SiO2-TiO2 Slagg 2	79.0	1.9
2		Initial slag	CaO-SiO2-TiO2 Slagg 2	75.9	1.5
3	10	6	Al2O3-MgO-SiO2	108.9	2.7
3	10	6	Al2O3-MgO-SiO2	111.3	2.6
3	10	6	Al2O3-MgO-SiO2	106.2	1.9
3	11	3	CaO-SiO2-TiO2 Slag 1	55.4	2.7
3	11	3	CaO-SiO2-TiO2 Slag 1	57.2	1.4
3	12	3	CaO-SiO2-TiO2 Slag 1	49.6	1.9
3	12	3	CaO-SiO2-TiO2 Slag 1	47.8	1.4
3	16	0	SiO2-CaO	87.3	2.7
3	16	0	SiO2-CaO	84.4	0.6
3	17	1	SiO2-CaO	76.3	1.8
3	17	1	SiO2-CaO	81.0	2.1
3	18	2	SiO2-CaO	66.3	2.6
3	18	2	SiO2-CaO	67.1	4.1
3	15, 19	3	SiO2-CaO	63.9	2.6
3	15, 19	3	SiO2-CaO	60.7	2.8
3	20	4	SiO2-CaO	55.0	2.7
3	20	4	SiO2-CaO	55.7	1.7
3	21	5	SiO2-CaO	49.3	2.4
3	21	5	SiO2-CaO	47.6	1.2
3	22	6	SiO2-CaO	56.7	1.9
3	22	6	SiO2-CaO	58.0	1.1
3	13	3	SiO2-CaO	67.4	0.6
3	13	3	SiO2-CaO	66.1	0.9
3	14	3	SiO2-CaO	61.9	1.2
3	14	3	SiO2-CaO	59.8	0.4
3	23	3	SiO2-CaO	52.8	2.5
3	23	3	SiO2-CaO	55.2	0.5
3	24	3	SiO2-CaO	49.2	1.6
3	24	3	SiO2-CaO	48.4	0.4
3	25	3	SiO2-CaO	40.4	3.5
3	25	3	SiO2-CaO	39.7	4.1
3	26	3	SiO2-CaO	40.5	4.0
3	26	3	SiO2-CaO	45.4	2.1
3	27	3	SiO2-CaO	34.1	3.2

3	27	3	SiO2-CaO	30.4	0.6
3		Initial slag	SiO2-CaO	83.8	2.4
3		Initial slag	SiO2-CaO	85.2	2.7

The analysis results for the slag reference material W-2 are shown in Table A3.2

Table A3.2: ICP-MS results for reference samples (W-2)

Ref no	Material	B-11 ppm	RSD, %
1	W-2	u20.98	4.0
1	W-2	11.34	2.3
1	W-2	10.52	1.5
2	W-2	12.55	3.0
2	W-2	11.50	2.1
2	W-2	11.56	1.4
3	W-2	13.1	4.1
3	W-2	11.1	3.4

A3.2 Silicon samples

The analysis results for the silicon samples are shown in Table A3.3.

Table A3.3: ICP-MS results for the silicon samples

Reference material	Experiment no.	Ref. time (h)	Material	B-11 (ppm)	RSD, %
1	1	3	Si	37.4	3.9
1	1	3	Si	42.4	2.6
1	1	3	Si	45.8	2.1
1	2	6	Si	41.4	0.7
1	2	6	Si	43.9	2.5
1	2	6	Si	49.5	1.3
1	3	9	Si	44.5	1.4
1	3	9	Si	44.1	2.4
1	3	9	Si	54.4	2.6
1	4	3	Si	26.7	1.6
1	4	3	Si	26.3	1.4
1	4	3	Si	26.2	1.3
1	5	6	Si	27.7	1.3
1	5	6	Si	26.3	0.7
1	5	6	Si	25.4	1.7

1	6	9	Si	24.6	1.9
1	6	9	Si	29.5	0.3
1	6	9	Si	22.8	2
2	7	3	Si	28.9	1.7
2	7	3	Si	25.9	4.0
2	7	3	Si	28.1	1.6
2	8	6	Si	31.1	3.0
2	8	6	Si	32.4	1.9
2	8	6	Si	31.2	1.7
2	9	8	Si	34.5	1.5
2	9	8	Si	33.8	1.3
2	9	8	Si	34.1	2.2
3	10	6	Si	58.7	2.5
3	10	6	Si	58.3	4.7
3	10	6	Si	63.4	2.5
3	11	3	Si	28.8	0.4
3	11	3	Si	29.0	3.1
3	11	3	Si	27.6	2.4
3	12	3	Si	38.8	1.1
3	12	3	Si	35.2	2.7
3	12	3	Si	29.0	2.0
3	23	3	Si	28.2	2.4
3	23	3	Si	30.7	2.9
3	23	3	Si	27.5	2.9
3	24	3	Si	22.3	2.9
3	24	3	Si	23.5	3.2
3	24	3	Si	23.9	0.9
3	25	3	Si	17.1	0.6
3	25	3	Si	16.7	2.0
3	25	3	Si	18.1	3.8
3	26	3	Si	19.5	1.5
3	26	3	Si	18.2	1.6
3	26	3	Si	18.6	2.0
3	27	3	Si	14.2	1.2
3	27	3	Si	13.4	3.6
3	27	3	Si	13.6	2.3
3	10-27		Initial Si	92.8	3.0
3	10-27		Initial Si	92.1	1.4
3	10-27		Initial Si	92.0	2.2

The analysis results for the silicon reference material NIST 57b are shown in Table A3.4

Table A3.4: ICP-MS results for reference samples (NIST 57b)

Reference no.	Material	B-11 ppm	RSD, %
1	NIST 57b	14.7	2.0
1	NIST 57b	12.6	1.2
1	NIST 57b	13.2	5.8
2	NIST 57b	10.7	2.3
2	NIST 57b	11.4	2.1
2	NIST 57b	12.8	2.7
3	NIST 57b	10.5	4.9
3	NIST 57b	13.0	4.3
3	NIST 57b	12.7	2.7

The concentration of the isotopes Mg-25 and Al-27 in silicon were analyzed by ICP-MS. The results are shown in Table A3.5 together with the relative standard deviation (RSD).

Table A3.5: ICP-MS results for amount of Mg and Al in silicon

Experiment no.	Refining time (h)	Mg -25 ppm	RSD, %	Al- 27 ppm	RSD, %
1	3	437	0.6	1346	3.9
1	3	377	4.0	1069	1.6
1	3	387	0.6	1219	4.3
2	6	1563	4.1	2441	3.4
2	6	1543	4.0	2491	2.7
2	6	1835	0.4	2716	1.8
3	9	2116	4.7	3309	3.7
3	9	1970	1.7	3232	2.0
3	9	2771	2.6	3999	3.3

Appendix IV

A5 Results from XRF analysis

The results from the XRF analysis for the CaO-$SiO_2$$TiO_2$ and the Al_2O_3-MgO-SiO_2 slags are shown in Table A5.1. The samples were analyzed with the instrument BRUKER S8 Tiger.

Table A5.1: XRF results for the CaO-$SiO_2$$TiO_2$ and the Al_2O_3-MgO-SiO_2 slags

	CaO-SiO_2-TiO_2 (Slag 1)				**CaO-SiO_2-TiO_2 (Slag 2)**				**Al_2O_3-MgO-SiO_2**			
	Initial	**3h**	**6h**	**9h**	**Initial**	**3h**	**6h**	**8h**	**Initial**	**3h**	**6h**	**9h**
Fe_2O_3 (%)	0.07	0.05	0.08	0.07	0.07	0.05	0.05	0.06	0.09	0.26	0.05	0.05
TiO_2 (%)	18.76	0.258	0.16	0.129	49.62	24.881	20.804	4.591	0.064	0.012	0.036	0.008
CaO (%)	39.08	41.89	44.3	46.52	24.11	24.65	26.44	29.35	0.31	0.31	0.33	0.35
K_2O (%)	0.006	0.005	0.004	0.005	0.004	0.003	0.003	0.004	0.009	0.006	0.007	0.005
P_2O_5 (%)	0.006	0.003	0.004	0.005	0.004	0.001	0.002	0	0	0	0	0
SiO_2 (%)	42.85	58.15	56.25	54.23	26.65	50.29	52.36	65.37	49.13	49.36	48.24	47.58
Al_2O_3 (%)	0.11	0.11	0.11	0.11	0.1	0.09	0.1	0.09	26.78	27.32	27.96	28.61
MgO (%)	0.01	0.02	0.02	0.03	0	0	0	0	22.3	22.59	22.84	23.23
Na_2O (%)	0	0	0	0	0	0	0	0	0	0	0	0
MnO (%)	0.004	0.003	0.003	0.003	0.004	0.003	0.004	0.003	0.005	0.003	0.001	0.001
Sum (%)	100.9	100.5	100.9	101.1	100.6	99.97	99.76	99.47	98.69	99.86	99.46	99.83
LOI (%) 950°C	-0.07	0.01	0.02	0.01	-0.03	-2.2	-1.91	-0.41	-0.02	-0.1	-0.03	-0.17
Sum (%)	100.7	100.3	100.7	100.88					98.21	99.27	99.04	99.42

The results from the XRF analysis for the CaO-SiO_2 slag used in Experiment 13-22 are shown in Table A5.2. The initial composition is shown together with the composition after 3 and 6 hours.

Table A5.2: XRF results for the CaO-SiO_2 slag used in Experiment 13-22

	Initial	**3h**	**6h**
Fe_2O_3 (%)	0.09	0.07	0.07
TiO_2 (%)	0.045	0.069	0.046
CaO (%)	55.03	57.67	60.98
K_2O (%)	0.007	0.005	0.005
P_2O_5 (%)	0.011	0.009	0.01
SiO_2 (%)	45.42	42.62	39.78
Al_2O_3 (%)	0.29	0.37	0.45
MgO (%)	0.31	0.29	0.25
Na_2O (%)	0	0	0
MnO (%)	0.006	0.004	0.004
Sum (%)	101.21	101.11	101.6
LOI (%) 950°C	0.1	0.17	-0.08

The analysis results for the $CaO\text{-}SiO_2$ slag used in Experiment 23-27 are shown in Table A5.3. The initial composition is shown together with the composition after 3 hours.

Table A5.3: XRF results for the $CaO\text{-}SiO_2$ slag used in Experiment 23-27

	Initial	**3h**
Fe_2O_3 (%)	0.11	0.08
TiO_2 (%)	0.021	0.03
CaO (%)	55.84	56.65
K_2O (%)	0.009	0.005
P_2O_5 (%)	0.012	0.008
SiO_2 (%)	44.8	44.31
Al_2O_3 (%)	0.31	0.34
MgO (%)	0.33	0.23
Na_2O (%)	0	0
MnO (%)	0.008	0.004
Sum (%)	101.44	101.66
LOI (%) 950°C	0.03	0.02